# Ichnology and geochemistry: an integrated approach to early marine diagenesis in the Arabian Gulf

by

Drew Brown

A thesis submitted in partial fulfillment of the requirements for the degree of

Master of Science

Department of Earth and Atmospheric Sciences

University of Alberta

## Abstract

Neoichnological studies in carbonate-dominated tropical latitudes are sparse. Moreso, the coupling of diagenetic research utilizing ichnology has been largely limited to ancient successions. This thesis combines geochemical analyses with modern ichnological observations to better understand the early marine formation of firmgrounds and hardgrounds in the Abu Dhabi coastal sabkha. First, characterization of infaunal behavior and animal spatial variability help determine study sites of interest within an intertidal zone (Al Qantur lagoon). There exists a relatively low complexity and diversity of burrowing morphologies in Abu Dhabi as attributed to heightened environmental stressors, such as salinity, heat, and subaerial exposure, as well as upward seepage of saline continental brines. Porewater analyses indicate a stabilization of salinity within burrows, suggesting the infauna irrigate their burrows to cope with increasing salinity. Crustacean burrows enhance solute advection in the lower intertidal zone by increasing substrate permeability, facilitating the penetration of seawaters to greater depths. Additionally, our research demonstrates that some examples of firmground and hardground features develop in the subsurface, which challenges traditional interpretations of hardground formation as cemented, exposed seafloors. Here, we present spatially-resolved geochemical analyses to better understand the underlying mechanisms promoting the formation, and resulting diagenetic processes, surrounding firmgrounds and hardgrounds in the Abu Dhabi coastal sabkha. Firmgrounds and hardgrounds both originate through early marine cementation, and microbial sediment cohesion. However, their compositions differ, with firmgrounds predominantly composed of peloids, and hardgrounds characterized by foraminifera and mollusc shells. Hardgrounds display dissolution textures, while firmgrounds remain less affected. Dissolution in Al Qantur lagoon is primarily driven by the advection of continental brines in the upper intertidal zone. Additionally, bioturbation plays a significant role in altering water and sediment chemistry, as crustacean activity spatially influences solute distributions, and prevents cementation.

The formation of firmgrounds and hardgrounds depends on a complex hydrological regime that transports solutes via marine and groundwater sources.

## Preface

Some of the research conducted for this thesis forms part of an international research collaboration, led by Dr. Hilary Corlett at Memorial University of Newfoundland, Professor Fiona Whitaker at the University of Bristol, with Professor Murray Gingras being the lead collaborator at the University of Alberta. Water chemistry data presented in this thesis was performed by Tom Kibblewhite from the University of Bristol, and Professor Fiona Whitaker. The ICP-MS data presented in chapter 3 was performed by myself, Daniella Gutierrez-Rueda and Professor Daniel Alessi at the University of Alberta. The DNA analysis presented in chapter 3 was performed by Jennifer Spence at the University of Alberta.

Chapter 2 of this thesis has been submitted for publication as D.G. Brown, H.J. Corlett, T. Kibblewhite, F. Whitaker, J.P. Zonneveld, and M.K. Gingras, "Neoichnology of a modern carbonate ramp intertidal zone and a comparison to clastic tidal flats" PALAIOS, *in review*. I was responsible for the data collection and analysis as well as the manuscript composition. The previously mentioned authors assisted with the data collection and contributed to manuscript edits. M.K. Gingras was the supervisory author and was involved with concept formation and manuscript composition.

## Acknowledgements

Firstly, thank you to my parents for supporting me throughout my life to strive for the things that bring me joy. You have continued to show me that with hard work and dedication, you can become successful both professionally and personally. Also, thank you so much to Katelin. You are my rock and have shaped me into a better man. Mom, dad, and Katelin, thank you for pushing me and believing in me.

Thank you to Hilary Corlett, Murray Gingras, Fiona Whitaker and J.P. Zonneveld. Hilary, I have greatly appreciated your attention to my growth in this part of my career. You are patient but encouraging, and your recognition of my work has meant so much to me during the stressful periods of this project. Even more so, I sincerely appreciate you taking the time out of your nights, weekends and days to talk to me and guide me when I am lost. Murray, thank you for shaping me into a better scientist and writer. I began this project unbelievably green, and your words of experience guided me greatly. I have taken "simple is better," and "make beautiful figures" to heart, and I hope it has shown. Fiona, thank you for leading me and teaching me even when you have a thousand things on your plate. You have taught me so much about the world of chemistry, and have lead by example with a unbelievable work ethic. J.P., thank you for your help during the curation of my first paper and following work. You introduced me to proper writing, proper etiquette, and how to make my science the best it can be. Your advice came at a time when I most needed it, and I really appreciate your help in shaping my early career. Most of all, thank you to you all for being my friend during this project.

Thank you to the IRG. You have become some of my best friends in life, and it will hurt so much to say bye to you all. I want to personally say thanks for not only being my friend, but for helping me grow as a scientist and answering my newbie questions. Particularly, thank you Scott Melnyk, Brette Harris and Baptiste Courtet.

Lastly, thank you to everyone who has helped with this project. Particularly, Tom Kibblewhite has been an outstanding resource and friend. Thank you to Daniella Gutierrez-Rueda, Jennifer Spence, Mark Labbe, Igor Jakab, Joel Pumple, Jordan Harvey, Adill, Anika, Rebecca Funk, Mohammad Al-Suwaidi, and the many friends who supported me along the way.

## Table of Contents

## List of Tables

## List of Figures

## Chapter 1: Introduction

The sabkha, or salt flat, is a depositional environment of great interest in the rock record, particularly because of the oil and gas reservoirs that tend to accompany sabkha deposits (Krumbein, 1985; Alsharhan & Kendall, 2002; Al Suwaidi et al. 2011). Indeed, some of the more famous producing plays are often characterized by sabkha environments, including the Western Canadian Sedimentary Basin, the Permian Basin in Texas, and the Arab Formation within the Middle East (Porter et al., 1982; Handford & Fredericks, 1980; Azer & Peebles, 1995). Modern analogues for sabkha environments can be found around the world, however the archetypal study area of the modern sabkha complex is in Abu Dhabi, UAE (Warren & Kendall, 1985; Lokier, 2013; Khan et al., 2016). Study of sabkha environments began in the 1950's, initially conducted by Dr. Douglas James Shearman and his students from the Imperial College of London (Curtis et al., 1963; Kendall & Skipwith, 1968; Butler, 1969; 1978). However, the seminal studies by Evans et al. (1964) and Evans et al. (1969) invited substantial research within the Arabian Gulf that is ongoing today. Notably, the evaporitic rich, supratidal area of the coastal sabkha complex received the most attention in early works, as oil bearing strata was most closely associated with a nodular anhydrite cap rock, and fenestral bindstones, which are currently observed in the landward portions of the coastal sabkha complex (Azer & Peebles, 1995; Marchionda et al., 2018). Additionally, dolomite in the sabkha is pervasive (Bontognali et al., 2010; Geske et al., 2015). Therefore, many previous works have tried to detail modern, dolomite precipitation utilizing the reflux-model, which is often attributed to evaporitic environments (McKenzie et al., 1980; Azer & Peebles, 1998; Saller & Henderson, 1998; Warren, 2000; Moore, 2001; Melim & Scholle, 2002). Other early research of the modern environment came from descriptions of the microbial mats in the upper intertidal zone (Kendall & Skipwith, 1968), and hardgrounds that were observed in tidal channels (Shinn, 1969). Research of the Abu Dhabi surface and subsurface environments continued, yet at a slower pace, into the '90s and '00s. From the mid-2000's to today, Dr. Stephen Lokier, Dr. Adrian Immenhauser, and colleagues, have become leading researchers in the Abu Dhabi coastal sabkha. Lokier and his colleagues have made great progress detailing previous sea level changes, anthropogenic influences, as well as revisiting many diagnostic features of the sabkha complex, such as the microbial mats, hardgrounds and intertidal zone accumulations (Lokier & Steuber, 2009; Lokier, 2013; Lokier et al., 2013; Lokier et al., 2015; Paul & Lokier, 2017). Immenhauser and his colleagues have become some of the leading researchers in carbonate diagenesis, especially for the Abu Dhabi locale. Particularly, their study of carbonate crystal growth and alteration in the Abu Dhabi intertidal zone has become a great resource for porewater behavior in hypersaline environments (Coimbra et al., 2009; Hippler et al., 2009 Christ et al., 2015; Immenhauser et al., 2017; Ge et al., 2020a; Ge et al. 2020b; Pedersen et al., 2021; Ge et al., 2023).

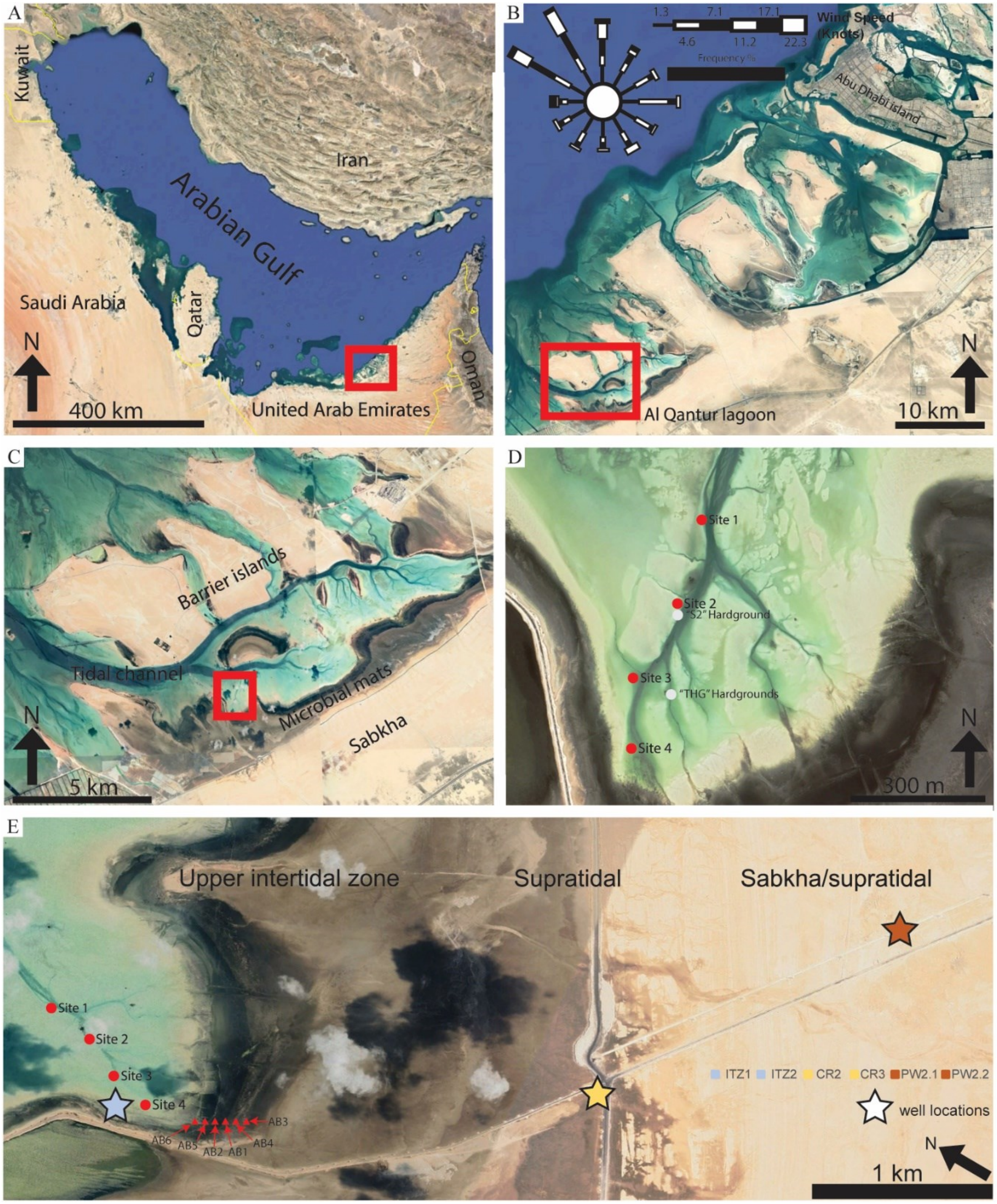


*Figure 1.1:* ***Geographical context of the study area****. Photos from Google Earth.* ***A****) Location of Al Qantur Lagoon study site (red box) on the coast of the United Arab Emirates, southern Arabian Gulf.* ***B****) Study site (red box) in relation to Abu Dhabi Island, with wind rose from El-Sayed (1999).* ***C****) Enlargement of study site showing environments from sabkha to barrier islands.* ***D****) Study site distribution across the intertidal zone and location of hardgrounds (Study sites shown by red dots, and hardgrounds shown by gray dots).* ***E****) Elongated view of the upper intertidal zone and supratidal sabkha depicting groundwater well location. Groundwater wells are represented by stars, and the study sites are presented by red dots. Additionally, microbial mat samples are represented by red triangles.*

## Study area

This study is based within the intertidal zone of the Abu Dhabi coast found on the southwest shoreline of the United Arab Emirates within the southern Arabian Gulf (Fig. 1.1A). One hundred kilometers southwest of Abu Dhabi exists a preserved section of coastline that encompasses the modern coastal sabkha (Fig. 1.1B). The study area occurs between a series of seaward, subtidal barrier islands, and landward, supratidal sabkha (Fig. 1.1C) in an area known as Al Qantur lagoon (Fig. 1.1D). Our study consists of a land-to-sea transect that extends from the lower extent of the upper intertidal zone into the upper section of the lower intertidal zone. Four sites subdivide the intertidal zone (Fig. 1.1D), where Site 1 is the most seaward, and Site 4 is the most landward. For the purposes of this study, Site's 1 & 2 are referred to as "distal," and Site's 3 & 4 are regarded as "proximal." Previously drilled groundwater wells were used for data collection ranging from the sabkha into the intertidal zone. Three well locations were identified, two in the intertidal zone, three in the supratidal, and two more landward into the sabkha (Fig. 1.1E). Approximate locations of microbial mat samples are denoted by red triangles in Figure 1.1E.

## Geological Background

The low-angle, homoclinal, carbonate ramp stretches from intercontinental dunes to the distal shelf. Late Pleistocene (19,000 yr. BP) to Holocene sea level changes in the Arabian Gulf are described by Evans et al. (1969), Lokier et al. (2015), and Paul & Lokier (2017). The majority of the Arabian Gulf's sedimentary basin were flooded during the first of two occurrences of transgression and stillstand phases that were identified between 12,000 yr BP and 5290–4570 yr BP (Lambeck 1996). A regression occurred from 1440-1170 yrs BP and was succeeded by the modern transgression (Lokier et al. 2015). Siliciclastic aeolian sand has been identified under the hardground base of the coastal complex succession (Evans et al., 1969; Paul & Lokier, 2017).

The Abu Dhabi carbonate ramp-sabkha complex is made up of a southern backshore, siliciclastic, terrestrial dune succession, a mixed carbonate-evaporite supratidal sabkha succession, a low-relief carbonate-dominated intertidal flat succession, and a northern carbonate lagoonal / barrier island complex succession (Paul and Lokier, 2017). A group of barrier islands to the north-northeast separates the intertidal zone from the open ocean (Fig. 1.1C). The intertidal zone is divided by primary tidal channels with tributaries, which transport water from Al Qantur lagoon to the Arabian Gulf.

With the exception of significant weather events (e.g. "the Shamal"), the middle-upper sabkha rarely experiences seawater submersion (Butler 1969; Kinsman 1969). Spring tides may reach the distal extent of the sabkha zone where it transitions into the upper intertidal zone (Lokier & Steuber 2009; Paul & Lokier 2017). Semi-diurnal tides occur in the intertidal zone (Paul & Lokier 2017). Despite the microtidal (0.5-2 m) tidal range, about 800 m of the tidal flats are exposed during spring tides due to the low relief of the ramp (Lokier & Steuber 2009). Winter lows of 7 °C and summer highs of 50 °C have both been reported (Lokier et al. 2013). High Mg/Ca ratios and high $Ca^{2+}$ and $Mg^{2+}$ concentrations can be found in the local seawater (Wood et al. 2002; Hippler et al. 2009; Pederson et al. 2021).

Firmgrounds are observed in the 5-15 cm depth of substrates in the middle to upper intertidal zone and are absent in the lower intertidal zone (Vallack, 2021). Firmgrounds in this locale are generally formed by partial lithification of carbonate sediments by early marine, phreatic cements and microbial binding (Folk & Lynch, 2001; Paul & Lokier, 2017; Ge et al., 2020a,b; Ge et al., 2023). A laterally extensive basal hardground extends from the lower intertidal zone into the supratidal sabkha and marks the base of the Abu Dhabi carbonate ramp-sabkha succession (Shinn 1969; Kirkham 1998; Paul & Lokier, 2017). The hardground base of Al Qantur lagoon is covered by approximately 20 to 50 cm of intertidal sediments composed of loose carbonate sand and shell fragments. A ~ 5 to 10 cm thick bioclastic accumulation overlies the entire intertidal basal hardground. A 50–200 m broad area of microbial mats exists in the upper intertidal zone (Kendall & Skipwith, 1968). The lower to middle intertidal zone is dominated by fine-grained (Wentworth-Udden scale), highly bioturbated carbonate sand composed of peloids, gastropods and bivalve shells.

## Rationale

The Arabian Gulf is one of the only modern sites for study of an inland sea and a carbonate ramp; an environment that was prominent in the past. The Arabian Gulf presents one of the leading research areas to analyze modern carbonate precipitation and alteration. Carbonate strata is notoriously difficult to interpret due to its susceptibility to diagenesis. Therefore, debunking the timing and reasons for precipitation and diagenesis of carbonates is a focus of many modern studies. Particularly, within the intertidal zone (Al Qantur lagoon) of the Abu Dhabi coastal sabkha, there occurs partially to fully lithified firmgrounds and hardgrounds. By studying these subsurface features, we may underline the mechanisms detailing precipitation and diagenesis in one locale. While these features have been recognized in previous studies (Immenhauser et al., 2017; Paul & Lokier, 2017; Ge et al., 2020a), their formation remains ambiguous. In particular, Ge et al. (2020a) recognized the formation of these features to be products of very specific chemical interactions between seawaters, porewaters and sediments. Yet, the delineation of primary chemical drivers demands further exploration, and it has become the goal of this thesis to describe those drivers in Al Qantur Lagoon, Abu Dhabi, UAE.

In attempting to understand firmground and hardground occurrence, three significant attributes of the chemical system have been recognized. The first observation being that bioturbation in this area has not been previously assessed. Secondly, the role bioturbation plays in diagenesis and hardground formation has been ignored, and third, a continental brine is recognized in Al Qantur lagoon and has likely contributed to the diagenesis observed in the sediments and hardgrounds. Exploring these findings with respect to the cryptic occurrence of firmgrounds and hardgrounds, are the leading motivations of this research.

Chapter 2 aims to characterize the bioturbation fabrics within Al Qantur lagoon using a neoichnological framework. Neoichnological studies connect modern infaunal behavior to observable environmental influences. These observations provide additional insight when interpreting animal traces in sedimentary strata. Previously, there have been no neoichnological studies of the Abu Dhabi intertidal zone despite an abundant infaunal community. Although ichnological characterization of temperate intertidal zones are numerous (e.g. Mangano & Buatois 2004a; Dashtgard & Gingras 2012; Desjardin et al. 2012; Zonneveld et al. 2014; Rodriguez-Tovar et al. 2014), the neoichnology of arid, carbonate-dominated coastal successions is not as well understood, with only a few significant studies published from such settings (Ekdale et al. 1984; Smith et al. 2000; Knaust et al. 2012; Kumar 2017).

Where burrowing organisms persist, sediment distributions and solute movement are inherently affected. Therefore, determining the spatial variability of bioturbate textures provides key insights to sediment and water interactions. Furthermore, linking infaunal bioturbation patterns and the carbonate sedimentology facilitates the interpretation of similar successions in the rock record. Chapter 2 of this thesis therefore aims to characterize the neoichnology and carbonate sedimentary fabrics of the Abu Dhabi carbonate ramp intertidal zone. In doing so, we provide the first neoichnologic description of the Abu Dhabi coastal sabkha, thereby addressing a current gap in research. Additionally, Chapter 2 will compare the findings to similar neoichnological studies of temperate to moderate, micro- to meso-tidal clastic intertidal zones. This will provide much needed assistance to the compilation of tidal flat ichnologic descriptions, as carbonate intertidal flats are not as well documented. Furthermore, this study emphasizes the necessity of combining ichnology with carbonate sedimentology and diagenesis.

Chapter 3 will focus on presenting spatially resolved geochemical analyses of both porewaters and sediments to determine the formation of early marine firmgrounds and hardgrounds in Al Qantur lagoon. Specifically, their formation is discussed in the context of the hydrologic regime, local microbial communities, geochemistry, and biogenic fabric. Early marine carbonate precipitation events are often attributed to ideal marine seawater chemistry (Shinn, 1969; Kennedy & Garrison, 1975), and more recently, biologic mediation (Dupraz & Visscher, 2005; Dupraz et al., 2009; Paul & Lokier, 2017; Pedersen et al., 2021; Ge et al., 2020b; Diaz & Eberli, 2022; Diaz et al., 2022), however some of their underlying drivers remain ambiguous. Examining the firmgrounds and hardgrounds found in the Abu Dhabi coastal sabkha can provide valuable insights into various aspects of the rapid cementation events that occur in modern marine carbonate deposition systems.

Hardgrounds are traditionally understood as an exposed seafloor that becomes lithified via early marine cementation from warm, tropical, $CaCO_3$ saturated waters (Garrison et al., 1969; Shinn, 1969; Dravis, 1979; Christ et al., 2015; Paul & Lokier, 2017; Ge et al., 2020a,b; Pedersen et al., 2021; Ge et al., 2023). Within stratigraphic sections, hardgrounds are understood as indicators of diminished or suspended sedimentation rates, and erosion at the sediment-water interface (Shinn, 1969; Kennedy & Garrison, 1975; Sarg, 1988; Christ et al., 2015). Nonetheless, recent investigations of the coastal lagoons and intertidal zones in Abu Dhabi have recorded the presence of firmgrounds and hardgrounds within the shallow subsurface or sediment column (Ge et al., 2020a; Pedersen et al., 2021; Vallack, 2021), challenging the conventional view of formation. To properly analyze the influencers driving firmground and hardground formation, we account for the hydrodynamics, chemical, physical, and biological processes that take place within Al Qantur lagoon. Particularly, utilizing the observations outlined in Chapter 2, we recognize how biogenic sedimentary structures are responsible for permeability variance, sediment mixing, and in some instances, preferential diagenetic alteration (Gingras et al., 2004; Meysman et al., 2006; Zorn, 2010; Corlett & Jones, 2012; Gingras et al., 2012; Baniak et al., 2022). The Al Qantur lagoonal substrates, whose fabrics are affected by bioturbation, also interact with twice-daily tides, advecting brines, and rarer meteoric input (Wood et al., 2002; Hippler et al., 2009; Lokier & Steuber, 2009; Pedersen et al., 2021). Chapter 3 emphasizes the importance of the upward-leaking continental brine and subsequent seawater mixing within the bioturbated sediment column in guiding carbonate precipitation and diagenesis. In doing so, Chapter 3 distinguishes firmgrounds from hardgrounds texturally, and discusses the diagenetic mechanisms within Al Qantur lagoon. This contributes to the ongoing discussion regarding the genesis of subsurface hardgrounds in the Arabian Gulf, underscoring the significance of recognizing analogous features in diverse carbonate settings.

## Terminology

The terminology used to describe early marine cementation features are variable and inconclusive. Particularly, the description of firmgrounds and hardgrounds changes based on the geological subdiscipline. Generally speaking, firmgrounds are sedimentary surfaces that are relatively compact and cohesive but not as hard or resistant as hardgrounds. Firmgrounds often consist of muddy to sandy-muddy sediments that become partially compacted. Hardgrounds are indurated and resistant. Hardgrounds typically form by marine cementation or via the growth of organisms like encrusting bryozoans, which contribute to the hardening of the surface. Ichnologists identify firmground and hardground features in the subsurface using observations of the burrowing and boring organisms are used. The *Glossifungites* and *Trytanites* ichnofacies are used to describe firmground and hardground trace fossils, respectively (Gingras et al. 2001; Furlong et al. 2015). Ichnologically, using the terminology "firmground" and "hardground" has implications for determining depositional setting. However, the firmgrounds and hardgrounds observed in this study are devoid in encrusting organisms and lack any distinct burrowing or boring structures. Therefore, it is difficult to apply the same methodology for this study. Rather, we describe these firmground and hardground features with a more simplistic sedimentological approach. Firmgrounds in Al Qantur lagoon are described as "partially lithified sediments" while hardgrounds are observed as "fully lithified." These descriptions more closely align with Christ et al. (2015), who describes a firmground as incipient minor seafloor lithification, and a hardground as a fully lithified seafloor.

## References

Al Suwaidi, A.S., Hami, M.E., Hagiwara, H., Aziz, S.K. and Al Habshi, A.R. (2010) Carbonates and evaporites of the Upper Jurassic Arab Formation, Abu Dhabi: a petroleum exploration challenge. *Quaternary carbonate and evaporite sedimentary facies and their ancient analogues*, 1st edn., *Wiley*, 421–429

Alsharhan, A. and Kendall, C. (2002) Holocene carbonate/evaporites of Abu Dhabi, and their Jurassic ancient analogs. *Earth Science Reviews*, 61, 187–202.

Azer, S.R. and Peebles, R.G. (1998) Sequence Stratigraphy of the Arab A to C Members and Hith Formation, Offshore Abu Dhabi. *GeoArabia*, 3, 251–268.

Baniak, G.M., La Croix, A.D. and Gingras, M.K. (2022) Recent advancements in characterizing permeability and porosity distributions in bioturbated flow media. *Earth-Science Reviews*, 232, 104162.

Bontognali, T.R.R., Vasconcelos, C., Warthmann, R.J., Bernasconi, S.M., Dupraz, C., Strohmenger, C.J. and McKENZIE, J.A. (2010) Dolomite formation within microbial mats in the coastal sabkha of Abu Dhabi (United Arab Emirates). *Sedimentology*, 57, 824–844.

Butler, G.P. (1969) Modern Evaporite Deposition and Geochemistry of Coexisting Brines, the Sabkha, Trucial Coast, Arabian Gulf. *Journal of Sedimentary Research*, 39, 70-89.

Christ, N., Immenhauser, A., Wood, R.A., Darwich, K. and Niedermayr, A. (2015) Petrography and environmental controls on the formation of Phanerozoic marine carbonate hardgrounds. *Earth-Science Reviews*, 151, 176–226.

Coimbra, R., Immenhauser, A. and Olóriz, F. (2009) Matrix micrite δ13C and δ18O reveals synsedimentary marine lithification in Upper Jurassic Ammonitico Rosso limestones (Betic Cordillera, SE Spain). *Sedimentary Geology*, 219, 332–348.

Corlett, H.J. and Jones, B. (2012) Petrographic and Geochemical Contrasts Between Calcite- and Dolomite-Filled Burrows In the Middle Devonian Lonely Bay Formation, Northwest Territories, Canada: Implications for Dolomite Formation In Paleozoic Burrows. *Journal of Sedimentary Research*, 82, 648–663.

Curtis, R., Evans, G., Kinsman, D.J.J. and Shearman, D.J. (1963) Association of Dolomite and Anhydrite in the Recent Sediments of the Persian Gulf. *Nature*, 197, 679–680.

Dashtgard, S.E. and Gingras, M.K. (2012) Marine Invertebrate Neoichnology. In: *Developments in Sedimentology*, *Elsevier*, 64, 273–295.

Desjardins, P.R., Buatois, L.A. and Mángano, M.G. (2012) Tidal Flats and Subtidal Sand Bodies. In: *Developments in Sedimentology*, *Elsevier*, 64, 529–561.

Diaz, M.R. and Eberli, G.P. (2022) Microbial contribution to early marine cementation. *Sedimentology*, 69, 798–822.

Diaz, M.R., Link to external site, this link will open in a new tab, Eberli, G.P. and Weger, R.J. (2023) Indigenous microbial communities as catalysts for early marine cements: An in vitro study. *The Depositional Record*, 9, 437–456.

Dravis, J. (1979) Rapid and widespread generation of Recent oolitic hardgrounds on a high energy Bahamian platform, Eleuthera Bank, Bahamas. *Journal of Sedimentary Research*, 49, 195–207.

Dupraz, C., Reid, R.P., Braissant, O., Decho, A.W., Norman, R.S. and Visscher, P.T. (2009) Processes of carbonate precipitation in modern microbial mats. *Earth-Science Reviews*, 96, 141–162.

Dupraz, C. and Visscher, P.T. (2005) Microbial lithification in marine stromatolites and hypersaline mats. *Trends in Microbiology*, 13, 429–438.

Ekdale, A.A., Bromley, R.G. and Pemberton, S.G. (1984) SEPM Short Course: Ichnology: The Use of Trace Fossils in Sedimentology and Stratigraphy.

Evans, G., Kendall, C.G.St.C. and Skipwith, P. (1964) Origin of the Coastal Flats, the Sabkha, of the Trucial Coast, Persian Gulf. *Nature*, 202, 759–761.

Evans, G., Schmidt, V., Bush, P. and Nelson, H. (1969) stratigraphy and geologic history of the sabkha, abu dhabi, persian gulf. *Sedimentology*, 12, 145–159.

Furlong, C.M., Gingras, M.K. and Zonneveld, J.P. (2015) Trypanites-Type Ichnofacies at the Bay of Fundy, Nova Scotia, Canada. *Palaios*, 30, 258-271.

Garrison, R.E., Luternauer, J.L., Grill, E.V., Macdonald, R.D. and Murray, J.W. (1969) Early Diagenetic Cementation of Recent Sands, Fraser River Delta, British Columbia. *Sedimentology*, 12, 27–46.

Ge, Y., Lokier, S.W., Hoffmann, R., Pederson, C.L., Neuser, R.D. and Immenhauser, A. (2020a) Composite micrite envelopes in the lagoon of Abu Dhabi and their application for the recognition of ancient firm- to hardgrounds. *Marine Geology*, 423, 106141.

Ge, Y., Pederson, C.L., Lokier, S.W., Strauss, H. and Immenhauser, A. (2023) Radiaxial fibrous calcite forms via early marine-diagenetic alteration of micritic magnesium calcite. *Sedimentology*, 70, 434–450.

Ge, Y., Pederson, C.L., Lokier, S.W., Traas, J.P., Nehrke, G., Neuser, R.D., Goetschl, K.E. and Immenhauser, A. (2020b) Late Holocene to Recent aragonite-cemented transgressive lag deposits in the Abu Dhabi lagoon and intertidal sabkha. *Sedimentology*, 67, 2426–2454.

Geske, A., Lokier, S., Dietzel, M., Richter, D.K., Buhl, D. and Immenhauser, A. (2015) Magnesium isotope composition of sabkha porewater and related (Sub-)Recent stoichiometric dolomites, Abu Dhabi (UAE). *Chemical Geology*, 393–394, 112–124.

Gingras, M.K., Baniak, Greg., Gordon, John., Hovikoski, Jussi., Konhauser, K.O., La Croix, Andrew., Lemiski, Ryan., Mendoza, Carl., Pemberton, S.G., Polo, Camilo. and Zonneveld, J.-Paul. (2012) Chapter 27 - Porosity and Permeability in Bioturbated Sediments. *Developments in Sedimentology*, 64, 837–868.

Gingras, M.K., Pemberton, S.G., Muelenbachs, K. and Machel, H. (2004) Conceptual models for burrow-related, selective dolomitization with textural and isotopic evidence from the Tyndall Stone, Canada. *Geobiology*, 2, 21–30.

Gingras, M.K., Pemberton, S.G. and Saunders, T. (2001) Bathymetry, sediment texture, and substrate cohesiveness; their impact on modern Glossifungites trace assemblages at Willapa Bay, Washington. *Palaeogeography, Palaeoclimatology, Palaeoecology*, *169*, 1-21.

Handford, C.R. and Fredericks, P.E. (1980) Facies patterns and depositional history of a Permian sabkha complex: Red Cave Formation, Texas Panhandle: The University of Texas at Austin, Bureau of Economic Geology, Geological Circular, 80, 38.

Hippler, D., Buhl, D., Witbaard, R., Richter, D.K. and Immenhauser, A. (2009) Towards a better understanding of magnesium-isotope ratios from marine skeletal carbonates. *Geochimica et Cosmochimica Acta*, 73, 6134–6146.

Immenhauser, A., Lokier, S., Kwiecien, O., Riechelmann, S. and Buhl, D. (2017) Recent carbonate firm-to hardgrounds in the Abu Dhabi lagoon: Environmental controls and petrography. *2017 EGU General Assembly*, 19, 6840

Kendall, C. and Skipwith, P. (1968) Recent Algal Mats of a Persian Gulf Lagoon: *Journal of Sedimentary Research*, 38, 1040-1058.

Kennedy, W.J. and Garrison, R.E. (1975) Morphology and genesis of nodular chalks and hardgrounds in the Upper Cretaceous of southern England. *Sedimentology*, 22, 311–386.

Khan, M.A., Boër, B., Ő̄zturk, M., Clüsener-Godt, M., Gul, B. and Breckle, S.-W. (2016) Sabkha Ecosystems: Volume V: The Americas. *Springer*, 441

Knaust, D., Curran, H.A. and Dronov, A.V. (2012) Chapter 23 - Shallow-Marine Carbonates. In: *Developments in Sedimentology*, 64, 705–750.

Krumbein, W.E. (1985) Applied and Economic Aspects of Sabkha Systems — Genesis of Salt, Ore and Hydrocarbon Deposits and Biotechnology. *Hypersaline Ecosystems: The Gavish Sabkha*, Berlin, Heidelberg, 53, 426–436.

Kumar, A. (2017) Recent biogenic traces from the coastal environments of the southern Red Sea coast of Saudi Arabia. *Arab J Geosci*, 10, 1-11.

Lokier, S. and Steuber, T. (2009) Large-scale intertidal polygonal features of the Abu Dhabi coastline. *Sedimentology*, 56, 609–621.

Lokier, S.W., Bateman, M.D., Larkin, N.R., Rye, P. and Stewart, J.R. (2015) Late Quaternary sea-level changes of the Persian Gulf. *Quaternary Research*, 84, 69–81.

Lokier, S.W., Knaf, A. and Kimiagar, S. (2013) A quantitative analysis of Recent arid coastal sedimentary facies from the Arabian Gulf Coastline of Abu Dhabi, United Arab Emirates. *Marine Geology*, 346, 141–152.

Lokier, S.W. (2013) Coastal Sabkha Preservation in the Arabian Gulf. *Geoheritage*, 5, 11–22.

Mángano, M.G. and Buatois, L.A. (2004) Ichnology of Carboniferous tide-influenced environments and tidal flat variability in the North American Midcontinent. *Geological Society, London, Special Publications*, 228, 157–178.

Marchionda, E., Deschamps, R., Cobianchi, M., Nader, F.H., Di Giulio, A., Morad, D.J., Al Darmaki, F. and Ceriani, A. (2018) Field-scale depositional evolution of the Upper Jurassic Arab Formation (onshore Abu Dhabi, UAE). *Marine and Petroleum Geology*, 89, 350–369.

McKenzie, J.A., Hsü, K.J. and Schneider, J.F. (1980) Movement of Subsurface Waters Under the Sabkha Abu Dhabi, UAE, and its Relation to Evaporative Dolomite Genesis. *SEPM Special Publication*, 28, 11-30

Melim, L.A. and Scholle, P.A. (2002) Dolomitization of the Capitan Formation forereef facies (Permian, west Texas and New Mexico): seepage reflux revisited. *Sedimentology*, 49, 1207–1227.

Meysman, F.J.R., Galaktionov, O.S., Gribsholt, B. and Middelburg, J.J. (2006) Bioirrigation in permeable sediments: Advective pore-water transport induced by burrow ventilation. *Limnology and Oceanography*, 51, 142–156.Moore, C.H. (ed) (2001) Chapter 6 - Evaporative Marine Diagenetic Environments. In: *Developments in Sedimentology*, *Elsevier*, 55, 145–183.

Paul, A. and Lokier, S.W. (2017) Holocene marine hardground formation in the Arabian Gulf: Shoreline stabilisation, sea level and early diagenesis in the coastal sabkha of Abu Dhabi. *Sedimentary Geology*, 352, 1–13.

Pederson, C.L., Ge, Y., Lokier, S.W., Swart, P.K., Vonhof, H., Strauss, H., Schurr, S., Fiorini, F., Riechelmann, S., Licha, T. and Immenhauser, A. (2021) Seawater chemistry of a modern subtropical 'epeiric' sea: Spatial variability and effects of organic decomposition. *Geochimica et Cosmochimica Acta*, 314, 159–177.

Porter, J.W., Price, R.A., McCrossan, R.G., Kent, P., Bott, M.H.P., McKenzie, D.P. and Williams, C.A. (1997) The Western Canada sedimentary basin. *Philosophical Transactions of the Royal Society of London. Series A, Mathematical and Physical Sciences*, 305, 169–192.

Rodríguez-Tovar, F.J., Seike, K. and Allen Curran, H. (2014) Characteristics, Distribution Patterns, and Implications for Ichnology of Modern Burrows of Uca (Leptuca) Speciosa, San Salvador Island, Bahamas. *Journal of Crustacean Biology*, 34, 565–572.

Saller, A.H. (1986) Radiaxial calcite in lower Miocene strata, subsurface Enewetak Atoll. *Journal of Sedimentary Research*, 56, 743–762.

Sarg, J.F. (1988) Carbonate sequence stratigraphy. Sea-level Changes: An Integral Approach. Wilgus, B.S.H.C.K., Kendall, C.G.S.C., Posamentier, H.W., Ross, C.A., van Wagoner, J.C. (Eds.), *SEPM Special Publication* 42, 155–181.

Shinn, E.A. (1969) Submarine Lithification of Holocene Carbonate Sediments in the Persian Gulf. *Sedimentology*, 12, 109–144.

Smith, C.R., A. Levin, L., Hoover, D.J., McMurtry, G. and Gage, J.D. (2000) Variations in bioturbation across the oxygen minimum zone in the northwest Arabian Sea. *Deep Sea Research Part II: Topical Studies in Oceanography*, 47, 227–257.

Vallack, H.L. (2021) Physical and biogeochemical drivers of Modern carbonate diagenesis in intertidal sediments of Abu Dhabi. Ph.D., University of Bristol

Warren, J. (2000) Dolomite: occurrence, evolution and economically important associations. *Earth-Science Reviews*, 52, 1–81.

Warren, J.K. and Kendall, C.G.ST.C. (1985) Comparison of Sequences Formed in Marine Sabkha (Subaerial) and Salina (Subaqueous) Settings—Modern and Ancient1. *AAPG Bulletin*, 69, 1013–1023.

Wood, W.W., Sanford, W.E. and Habshi, A.R.S.A. (2002) Source of solutes to the coastal sabkha of Abu Dhabi. *GSA Bulletin*, 114, 259–268.

Zonneveld, J.-P., Gingras, M.K., Hodgson, C.A., McHugh, L.P., Myers, R.A., Schoengut, J.A. and Wetthuhn, B. (2014) Biotic Segregation in an Upper Mesotidal Dissipative Ridge and Runnel Succession, West Salish Sea, Vancouver Island, British Columbia. *Experimental Approaches to Understanding Fossil Organisms: Lessons from the LivingSpringer Netherlands*, Dordrecht, 169–194.

Zorn, M.E., Gingras, M.K. and Pemberton, S.G. (2010) Variation in burrow-wall micromorphologies of select intertidal invertebrates along the pacific northwest coast, usa: behavioral and diagenetic implications. *PALAIOS*, 25, 59–72.

# Chapter 2: Neoichnology of a modern carbonate ramp intertidal zone and a comparison to clastic tidal flats

## INTRODUCTION

Neoichnology is the study of present-day animal-sediment interactions, aimed at understanding the environmental physico-chemical conditions associated with animal burrows and trails (eg. Mangano & Buatois 2004a, 2004b; Dashtgard & Gingras 2012; Desjardin et al. 2012; Pemberton et al. 2012; Kumar 2017). Neoichnological analyses provide a means of linking qualitative observations and quantitative data to modern environmental parameters, which provides an invaluable aid in interpreting sedimentary strata. Although ichnological characterization of temperate intertidal zones are numerous (e.g. Mangano & Buatois 2004a, 2004b; Dashtgard & Gingras 2012; Desjardin et al. 2012; Pemberton et al. 2012; Zonneveld et al. 2014; Rodriguez-Tovar et al. 2014; Kopcznski et al. 2017), the neoichnology of arid, carbonate-dominated coastal successions is not as well understood, with only a few significant ichnological studies published from such settings (Ekdale et al. 1984; Smith et al. 2000; Knaust et al. 2012; Kumar 2017).

The intertidal zone seaward of the Abu Dhabi coastal sabkha presents an ideal site for assessing the neoichnological attributes of an arid, carbonate intertidal environment. Although the Abu Dhabi coast is a harsh setting with high salinities and extreme temperatures, abundant burrowing organisms are present among thriving intertidal microbial mat communities. Following the pioneering research of Douglas James Shearman (Shearman 1963, 1978, 1980), numerous studies have focused on the sedimentology and stratigraphic architecture of Arabian Gulf Sabkha sub-environments (Evans et al. 1964; Evans 1966; Kendall & Skipwith 1968; Kendall et al. 2002; Alsharhan & Kendall 2003; Evans 2005; Lokier & Steuber 2009; Lokier et al. 2013; Paul & Lokier 2017; Ge et al.

2020a,b), whereas the ichnology of the Arabian Gulf coastal zone has enjoyed considerably less attention.

This paper characterizes the neoichnology and carbonate sedimentary fabrics of the Abu Dhabi carbonate ramp intertidal zone and compares the findings to studies of similar successions in different climatic zones (temperate-moderate, micro- to meso-tidal clastic intertidal zones). By distinguishing the animal-sediment interactions associated with different intertidal sub-environments, we can formulate an understanding of the factors causing these variances, particularly from the perspectives of environmental stress and resource availability. Furthermore, linking infaunal bioturbation patterns and the carbonate sedimentology facilitates the interpretation of similar successions in the rock record.

## METHODS

### Field Methods

Four sampling sites from the south-western margin of Al Qantur Lagoon were selected based on distinct differences in biogenic and physical sedimentary structures and macrofauna present at the surface. Together the four sites form a landward-basinward transect parallel to a first to second order tidal flat drainage channel (Fig. 1.1D). These four sites each represent a distinct component of the Al Qantur intertidal succession.

At each site a ~2 m wide field pit was dug to the depth of the associated hardground (typically 23 - 30 cm), in all cases ~30 m away from the western margin of the tidal channel (Fig. 1.1D). Pit walls were dug such that the largest wall was parallel to tidal channel flow. A large, flat spatula was used to carefully trim pit walls so that the visible face represented an undisturbed visual of physical and biogenic sedimentary structures. The field pits were the primary site for the physical descriptions of each study site and were also used for porewater extraction.

Surface waters were measured in the field using a Hach Portable Multi-Parameter Meter (Hach Company, Loveland, Colorado, USA) with Intellical probes recording oxidation redox potential (ORP/Redox; MTC101, accuracy ± 5 mV), specific electrical conductivity (SEC; CDC401, accuracy ± 0.5%) and temperature (accuracy ± 0.3 °C). These instruments were also used to measure groundwaters that are confined by the shallow (40-50 cm) hardground from two previously drilled groundwater wells (depth 3.5 and 6.8 m below sediment surface) adjacent to the study site (Figure 1.1), and to measure porewater samples in the field laboratory. Porewaters were extracted through Rhizon CCS porewater samplers (Rhizosphere Research Products) that consist of a hydrophilic porous tip (length 5 or 10 cm) with a pore size of 0.12–0.18 µm and into 60 ml syringes. At each study site Rhizons were inserted horizontally into the substrate at intervals of typically 2 cm in a vertical line from the shallow subsurface until insertion was impeded by either the upper surface of the hardground or a layer containing significant shell debris. Porewater samples were stored in the syringes they were collected in to avoid atmospheric exchange. Surface water samples were collected in HDPE bottles and filtered through Millex-GP PES Millipore Express membrane hydrophilic syringe filters with a pore size of 0.22 µm. All samples were collected during daylight hours (7:00 to 17:00) during spring tides (November, 2021). All water samples were refrigerated and returned to the field laboratory where porewater SEC and ORP were measured from an aliquot expressed from each syringe (allowing up to 1 hour for ORP measurements to stabilize) in isolation from atmospheric exchange.

Properties of waters within 2 cm of the sediment surface were monitored at each site from tidal inundation to drying. The tides in the area are mixed semi-diurnal and data was collected over the higher of the high waters, following exposure during preceding low tide (tidal minimum at midday). EXO1 sondes (Yellow Springs Incorporated, Ohio, USA) with calibrated conductivity/temperature, dissolved oxygen sensors were deployed at sites 1, 3 and 4, and a CT2X logger (Seametrics, Washington State, USA) with a calibrated conductivity/ temperature sensor was deployed at Site 2. Pressure measured at the sondes was corrected for barometric pressure change measured using a barologger (Solinst, Ontario, Canada) located 2 km away. Total dissolved solids (TDS) was calculated from Specific Electrical Conductivity using a site specific non-linear relationship based on analysis of 101 water samples from the study area (TDS (g/KgW) = 0.00296 x SEC + 0.518 x SEC (mS/cm)).

Coring was performed on undisturbed sediment on the west side of the field pits (distal from the tidal channel). At least two cores (Type I and Type II) were taken from each subject site. Type I core consisted of a 60 cm WaterMark Polycarbonate core barrel (7 cm internal diameter). Type II core used a 25 cm long PVC core barrel (10 cm internal diameter). Cores were pressed into the substrate by hand and hammer until reaching the hardground base, or until flush with the sediment surface. The Type I 60 cm Polycarbonate cores were sent to the University of Bristol, while the Type II 25 cm PVC cores were transported to the University of Alberta.

## Laboratory methods

The Type II cores were used for CT analyses using a Nikon XTH 225 ST Industrial CT Scanner (Nikon Corporation, Tokyo, Japan) at the Permafrost Archives Sciences (PACS) Lab at the University of Alberta. Results were enhanced using Adobe® Photoshop®. Using the curves and levels tools, CT images were contrasted so that the changes in sediment density were easily distinguishable. No other alterations to the photographs were made.

Grain size was determined by Dynamic Image Analysis using a CAMSIZER X2 with X-FALL module (Microtrac Retsch, Han/Düsseldorf, Germany) at the University of Bristol. The Type I core cases were carefully cut lengthwise on opposite sides without disturbing the sediment. Cores were split in half using either a taut steel wire or a knife and subsampled. Subsampled sediments were placed in an oven at 40-45°C overnight. Dried sediments were then removed of shell debris and individual grains were separated lightly with a mortar and pestle for analysis. Grain size is reported using the Wentworth-Udden scale (Fig. 2.1).

Microscope analysis of loose sediments was performed using a Tagarno Digital Microscope (TAGARNO, Horsens, Denmark) at the Digital Imaging Facility at the University of Alberta. A +25x, 26 mm lens was used to view individual carbonate sediment grains. Sediment was sampled directly from cores and placed on viewing panels under the microscope for imaging. Additional microscopic analysis of sediments was executed using the Zeiss Sigma 300 VP-FESEM scanning electron microscope (ZEISS Microscopy, Jena, Germany) at the University of Alberta SEM laboratory. Sediments were placed on low profile SEM pin mounts using an adhesive sticker, blasted with compressed air to remove excess debris and carbon coated.

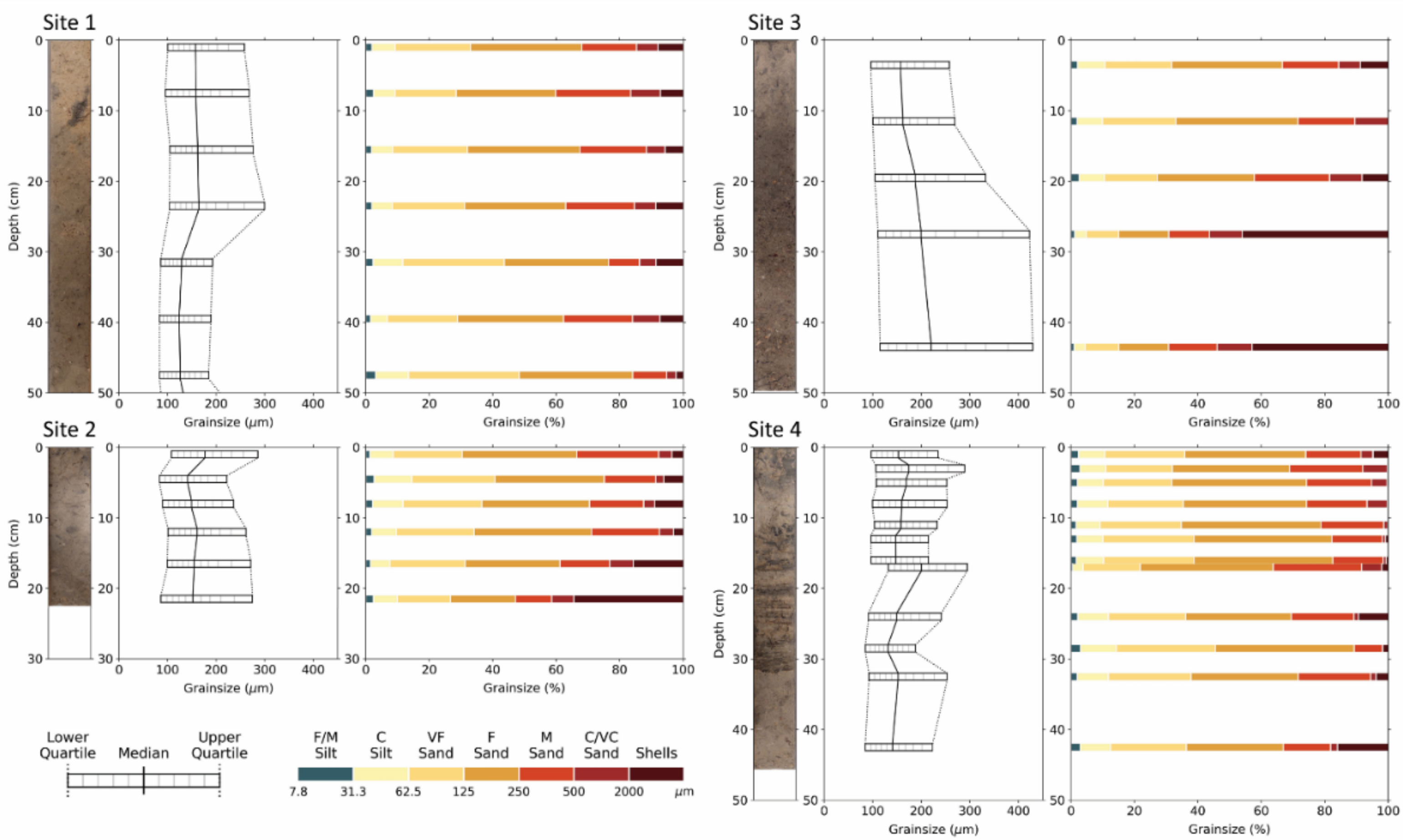


*Figure 2.1: **Grain size** determined from CamSizer and shell content with depth for each site data.*

## RESULTS

Sediment characterization was performed using core and field observations, grain size data, microscope and SEM. Grain size analysis is reported using the Udden-Wentworth scale (Fig. 2.1). Carbonate microfacies were described using Dunham's classification scheme (1962), with additions from Embry and Klovan's modification (1971). Dunham classifications provided in this study are for unlithified, loose sediments taken from study sites in the intertidal zone on the basis of the inferred texture they would resemble when lithified. To better understand the relationship between sedimentology and infaunal distributions, we conduct a microfacies analysis, which is summarized in Table 2.1.

*Table 2.1:* ***Carbonate microfacies of Al Qantur Lagoon****. The Bioturbated Peloidal Grainstone is typically observed in the shallow and middle depths (typically 1-25 cm) of cores and field pits and represents the area's typical intertidal sediment accumulation. Our classification of the Microbial Laminated Bindstone solely encompasses the layering of thin (1 mm) microbial mat communities and thin (1 mm) layers of fine-grained carbonate peloidal sand. This microfacies excludes thicker (1 cm +) layers of peloidal sand that may overlie individual units of the bindstone (such as at 7 - 12 cm depth, Fig. 2.5B). The Bioclastic Rudstone is observed in all core sections overlying the basal hardground. However, in this study's descriptions, it went unnoticed due to the presence of a hardground > 25cm depth, which the Type II core was unable to penetrate to.*

| Microfacies | Composition | Bioturbation | Accumulation | Additional Notes |
|---|---|---|---|---|
| Bioturbated Peloidal Grainstone | • Fine-grained sized carbonate sand consisting of peloidal grains<br>• Partially to fully coated in isopachous cements | • Heavily burrowed by worms and crustaceans | • Infaunal pellets (peloids), and carbonate sand accumulate together with deposited shells from local Mollusca and foraminifera.<br>• Subsequently disturbed by burrowing activities | • The archetypal intertidal sediment accumulation found at all study sites.<br>• Some observed *Miliolida* foraminifera<br>• Common shell debris consisit of *Cerithidea* sp. gastropods and *Brachiodontes* sp. bivalves |
| Microbial Laminated Bindstone | • Alternating, 1 mm thick, fine-grained carbonate sand interbedded between 1 mm thick microbial mats (herein termed bindstone).<br>• Thicker sections (≥1 cm) of carbonate sand interbedded between the bindstone layers are comparable to the Bioturbated Peloidal Grainstones | • Common worm burrowing<br>• Diminutive traces within buried microbial mat layers | • Microbial mat layers undergo obrution from tidal sediments and then re-establish themselves.<br>• Individual formation and morphology of microbial mats in the Abu Dhabi sabkha have been attributed to communities of Cyanobacteria, proteobacteria and other specialist bacterias (Serk, 2008; Hazzouri et al. 2022) | • Unique to Site 4<br>• The alternating succession of microbial mat and peloidal sand, together, assemble the microbial laminated bindstone<br>• Thick (1 cm +) bioturbated peloidal grainstone layers between bindstone layers are interpreted as older transgressional beds and storm deposits |
| Bioclastic Rudstone | • A shell debris framework supported by a fine-grained carbonate sand matrix<br>• Shell debris is dominantly composed of intact to partially fragmented *Cerithidea* sp., gastropods and disarticulated and fragmented *Brachidontes* sp. bivalves. | • Little to no bioturbation | • Shell debris from the local Mollusca consistently accumulates in dense concentrations above the hardground base that extends through the subsurface intertidal zone | • Observed in all core sections overlying the basal hardground<br>• Interpreted as a transgressive lag deposit |

## Bioturbation and sediment descriptions of Site 1

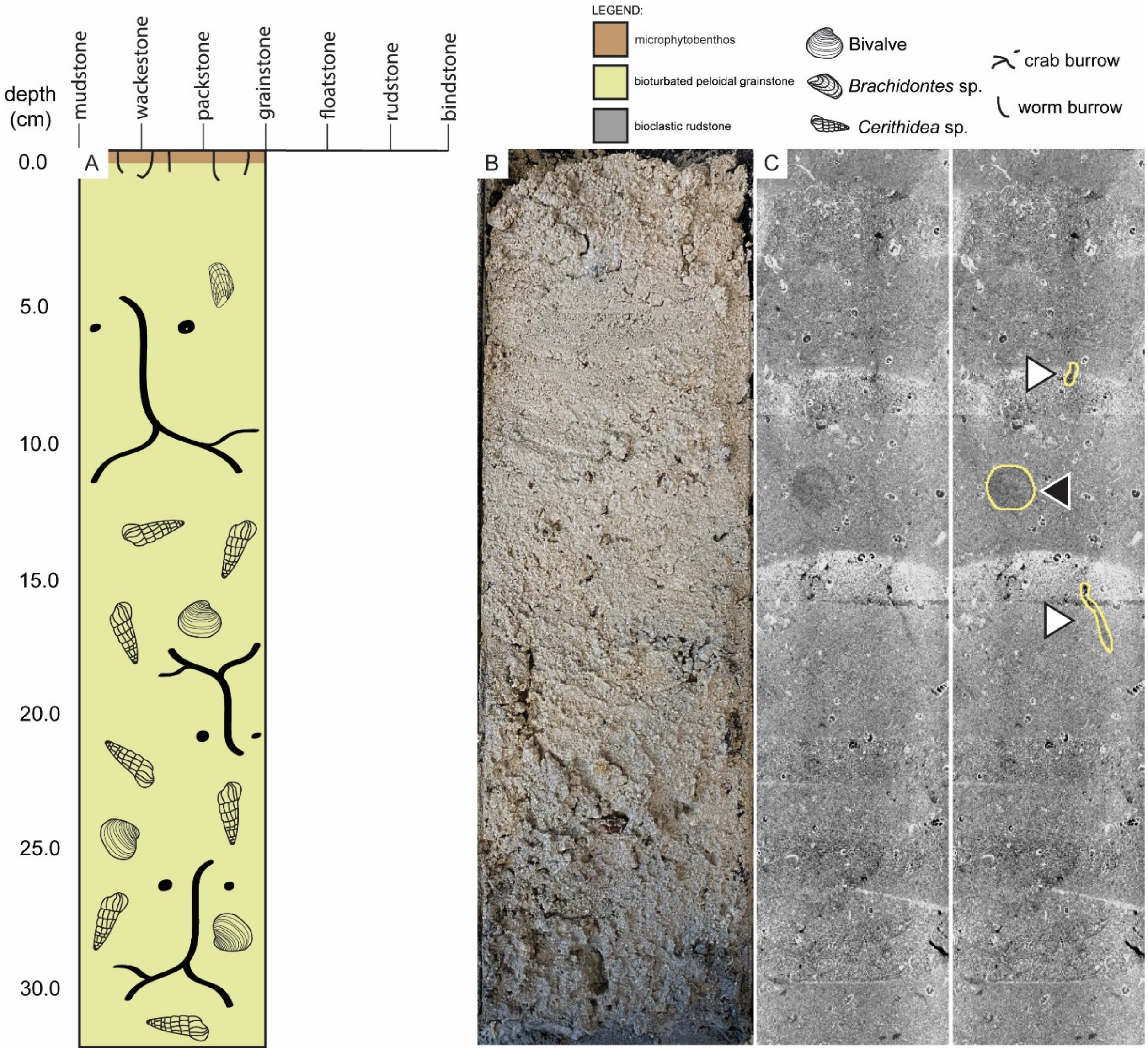


*Figure 2.2: **Site 1 comparison of carbonate lithologies to open core and CT**. **A**) Dunham, Embry & Klovan classified carbonate sedimentary log with associated bioclasts. **B**) Open face of sediment within Type II core after splitting. **C**) CT scans of the open face split core. Left-side image shows the blank scan while the right-side image displays the scan with highlighted animal traces.*

Site 1, within the lower intertidal zone is characterized by crustacean burrows in carbonate grainstone (Fig. 2.2). Site 1 sits at the highest relative position to the other study sites, and so flooding waters take longer to inundate the surface sediments. A hardground base 32 cm below the surface underlies the bioturbated peloidal grainstone layer. The grainstone is dominantly composed of peloidal grains with some mostly intact or partially fragmented *Cerithidea* sp. gastropods, rare bivalves, and foraminifera appearing in lesser amounts. The dominant grain size recorded at Site 1 is fine-grained.

Bioturbation intensity is high, and the sediment is massive in appearance. The high level of bioturbation is ascribed to vigorous mixing by intertidal crabs (*Ocypoda rtundata* & *Scopimera crabricauda*). Within the core/CT dataset, some crustacean burrows (black arrows, Fig. 2.2C) are visible. These burrows, exhibiting both vertical and horizontal, branching and unbranching patterns, reach a depth of 12 cm and have no lining. The diameter of these burrows is 4-20 mm. Within the core, two nereid burrows (white arrows, Fig. 2.2C) can be seen at depths of 7 cm and 16 cm. These worm burrows are horizontal, solitary, unlined, and less than 1.5 mm in diameter. Almost all burrows of the worms and crabs in this particular site are infilled.

# Bioturbation and sediment descriptions of Site 2

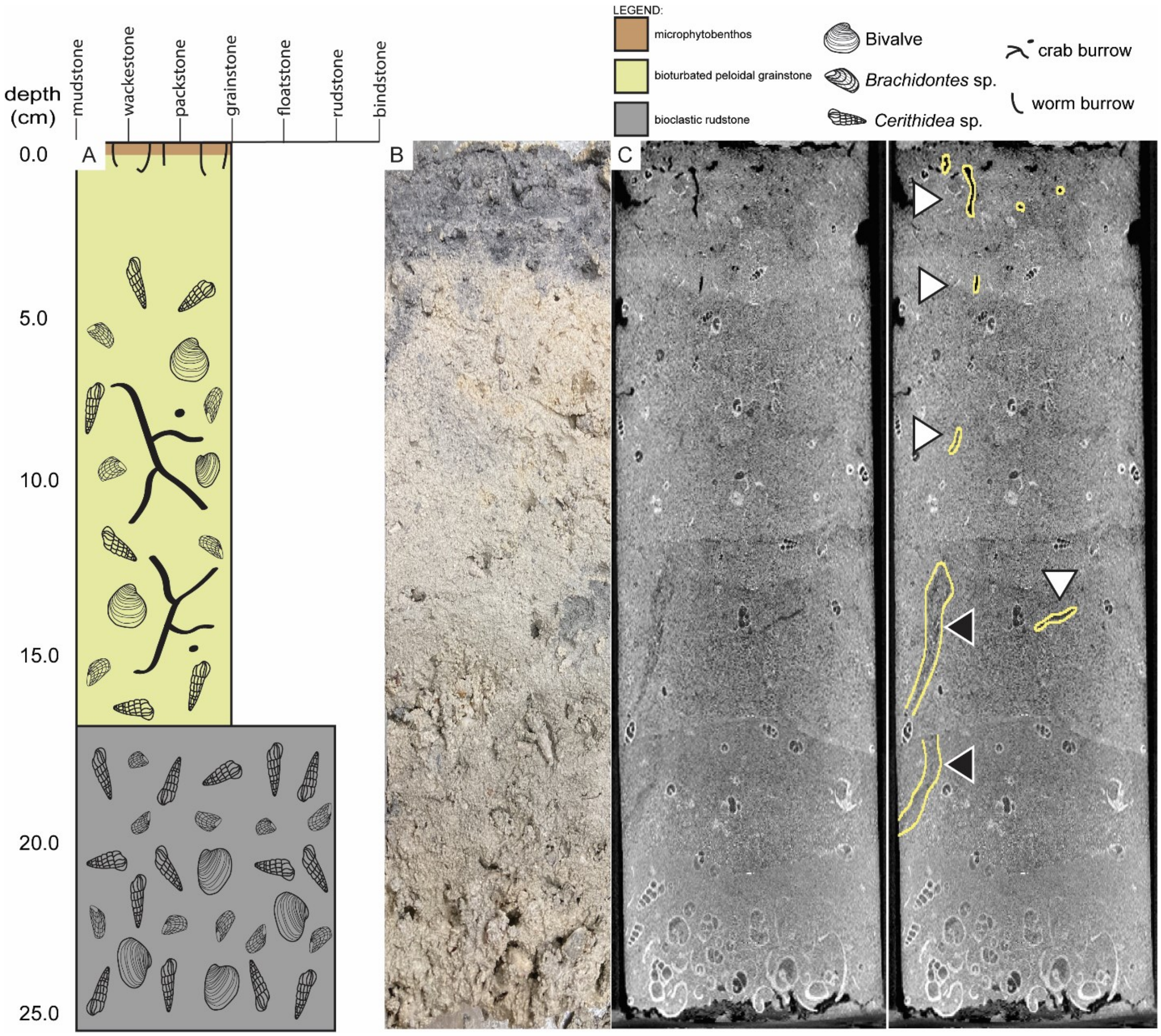


*Figure 2.3: **Site 2 comparison of carbonate lithologies to open core and CT**. **A**) Dunham, Embry & Klovan classified carbonate sedimentary log with associated bioclasts. **B**) Open face of sediment within Type II core after splitting. **C**) CT scans of the open face split core. Left-side image shows the blank scan while the right-side image displays the scan with highlighted animal traces.*

Site 2, within the lower part of the middle intertidal zone, features worm and crustacean burrows in dominantly carbonate grainstone (Fig. 2.3). A hardground base 25 cm below the surface underlies a bioclastic rudstone that is 8.5 cm thick. The bioclasts are composed of mostly intact or partially fragmented *Cerithidea* sp. gastropods and rare bivalves. A bioturbated peloidal grainstone, which overlies the bioclastic rudstone, is 16.5 cm thick. The grainstone consists of peloids and gastropod shells. The dominant grain size recorded at Site 2 is fine-grained.

Bioturbation intensity is high, and the sediment is predominantly massive in appearance, with rarer preserved burrows. Bioturbation is attributed to mixing of sediment by intertidal crabs (*Ocypoda rtundata* & *Scopimera crabricauda*) and nereid worms (*Nereis* sp.). Within the core/CT dataset, crustacean burrows (black arrows, Fig. 2.3C) are visible. These burrows, exhibiting vertical and horizontal, branching and unbranching patterns reach a depth of 20 cm and have no lining. The diameter of these burrows is 3-25 mm. Nereid burrows (white arrows, Fig. 2.3C) are vertical, solitary, unlined, <1 mm in diameter and reach to a depth of 14 cm. Nereid burrows <5 cm depth at this particular site are open, whereas all deeper burrows are infilled.

## Bioturbation and sediment descriptions of Site 3

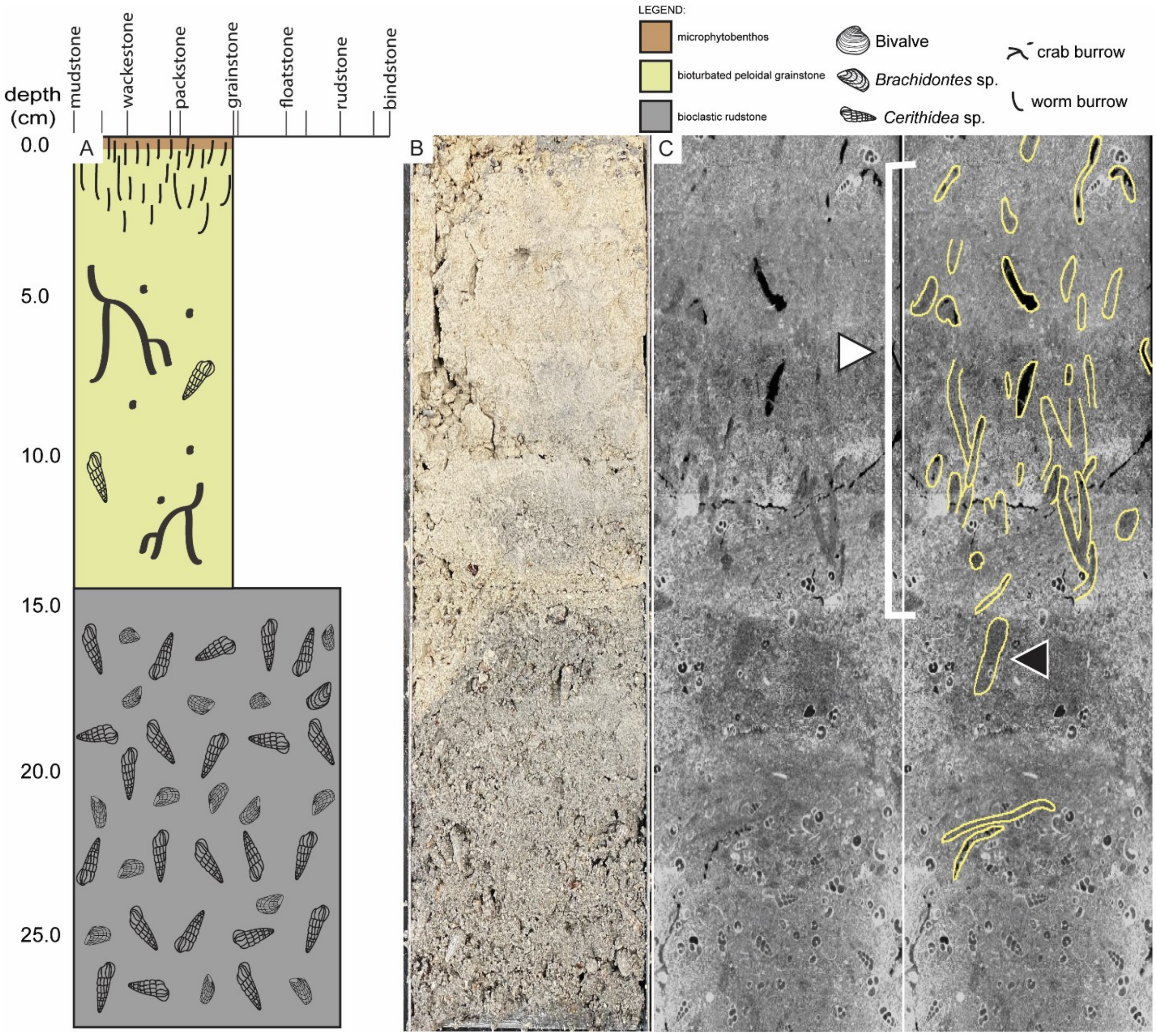


*Figure 2.4:* ***Site 3 comparison of carbonate lithologies to open core and CT**. **A**) Dunham, Embry & Klovan classified carbonate sedimentary log with associated bioclasts. **B**) Open face of sediment within Type II core after splitting. **C**) CT scans of the open face split core. Left-side image shows the blank scan while the right-side image displays the scan with highlighted animal traces.*

Site 3, in the upper part of the middle intertidal zone, features nereid burrows in carbonate grainstone (Fig. 2.4). Site 3 sits at a relatively lower elevation to the other study sites, and so tidal flood waters fill the study area quickly. A hardground base 27 cm below the surface underlies a bioclastic rudstone that is 13 cm thick. The bioclasts are predominately disarticulated and fragmented *Brachidontes* sp. bivalves and intact to partially fragmented *Cerithidea* sp. gastropods. The rudstone is overlain by a 14 cm thick layer of carbonate sand that is composed almost entirely of peloids. The dominant grain size recorded at Site 3 is fine-grained.

Bioturbation intensity is high, and the sediment is characterized by nereid burrows. Observed in the core/CT dataset, worm burrowing is more abundant in Site 3 than in the other sites, and is accredited to the polychaete worm *Nereis* sp.. Nereid burrows (white arrows, Fig. 2.4C), exhibiting branching and unbranching sections, reach a depth of 23 cm and are unlined. Worm burrow morphologies include Y-, J- and sub-helical shapes that have a maximum diameter of 3 mm, which is larger than other worm burrows in the intertidal zone. Potential arthropod burrows of unknown crustaceans (black arrows, Fig. 2.4C) exhibiting vertical and horizontal, branching and unbranching patterns, reach a depth of 15.5 cm and have no lining. Arthropod burrows are 3-15 mm in diameter. Closed (infilled) burrows occur at all depths, while open, non-filled burrows concentrate in the upper 15 cm of the core.

## Bioturbation and sediment descriptions of Site 4

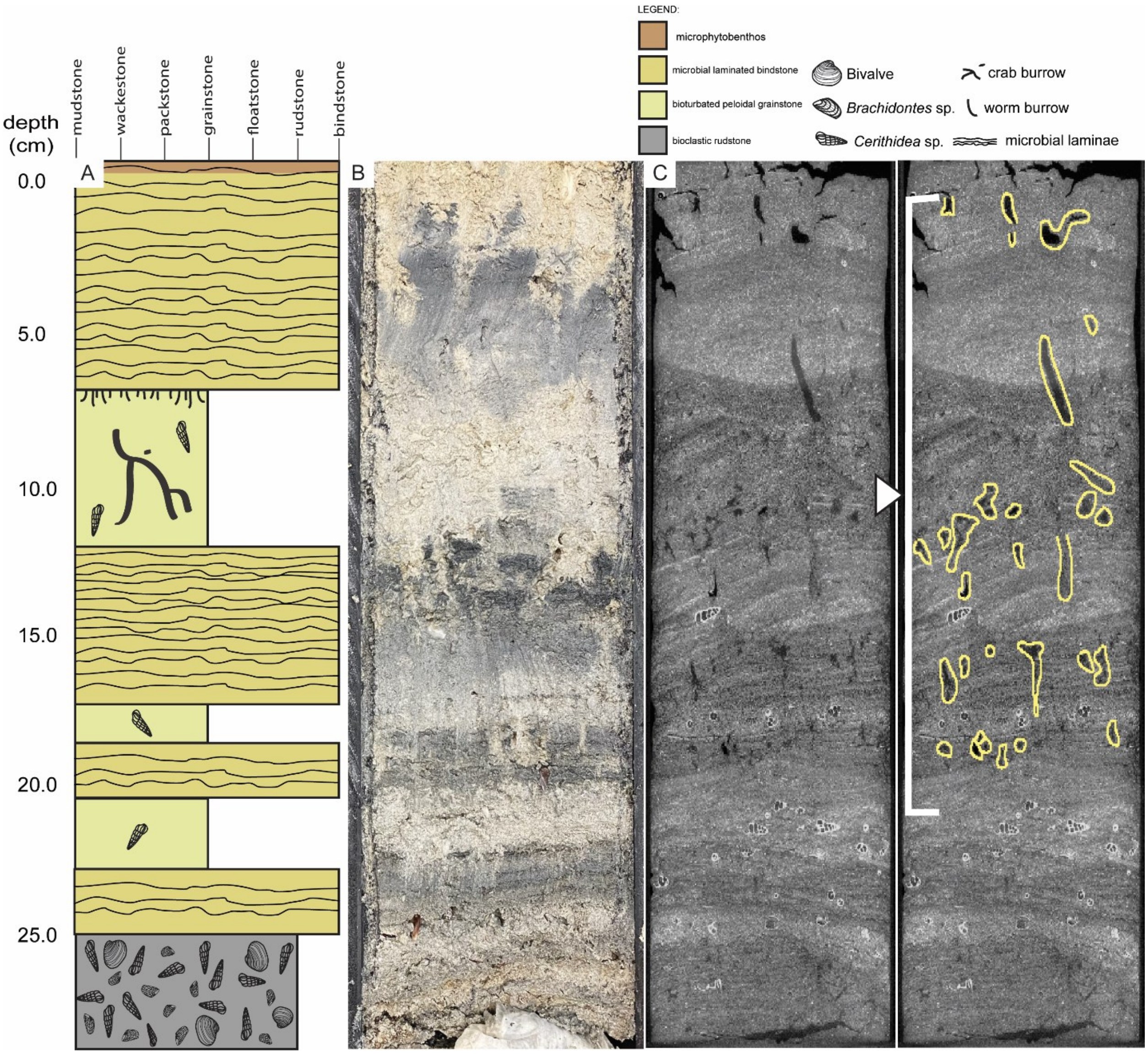


*Figure 2.5: **Site 4 comparison of carbonate lithologies to open core and CT**. **A**) Dunham, Embry & Klovan classified carbonate sedimentary log with associated bioclasts and microbial laminae. **B**) Open face of sediment within Type II core after splitting. **C**) CT scans of the open face split core. Left-side shows the blank scan while the right-side includes highlighted animal traces.*

Site 4, within the upper intertidal zone, features a microbial bindstone, characterized by biolaminae and worm burrows (Fig. 2.5). A hardground base 29 cm below the surface underlies a bioclastic rudstone that is 4 cm thick. Bioclasts are predominately intact or partially fragmented *Cerithidea* sp. gastropods and rare bivalves. The microbially laminated bindstone is made up of layers of 1 mm thick fine-grained carbonate sand that are interlaminated with 1 mm thick microbial mats. Grainstone layers between the microbially laminated bindstone consist predominantly of peloidal grains that are fully coated. Foraminifera and shell debris appear in lesser amounts. Several alternating layers of the microbially laminated bindstone and bioturbated peloidal grainstone overlie the bioclastic rudstone (Fig. 2.5B). The dominant grain size recorded at Site 4 is fine-grained.

Bioturbation intensity is reduced in this particular site. *Nereis* sp. burrows (white arrows, Fig. 2.5C) are the only traces observed in this section. These burrows, occurring as connected networks and isolated, individual burrows, exhibit I-, Y-, J- and sub-helical shapes that reach a depth of 20 cm. These burrows are unlined and predominantly less than 1 mm in diameter. Both open and infilled burrows are observed at all depths where bioturbation is observed. Where microbial laminae are present, traces become diminutive and isolated, whereas burrows in the carbonate sand are larger and connected.

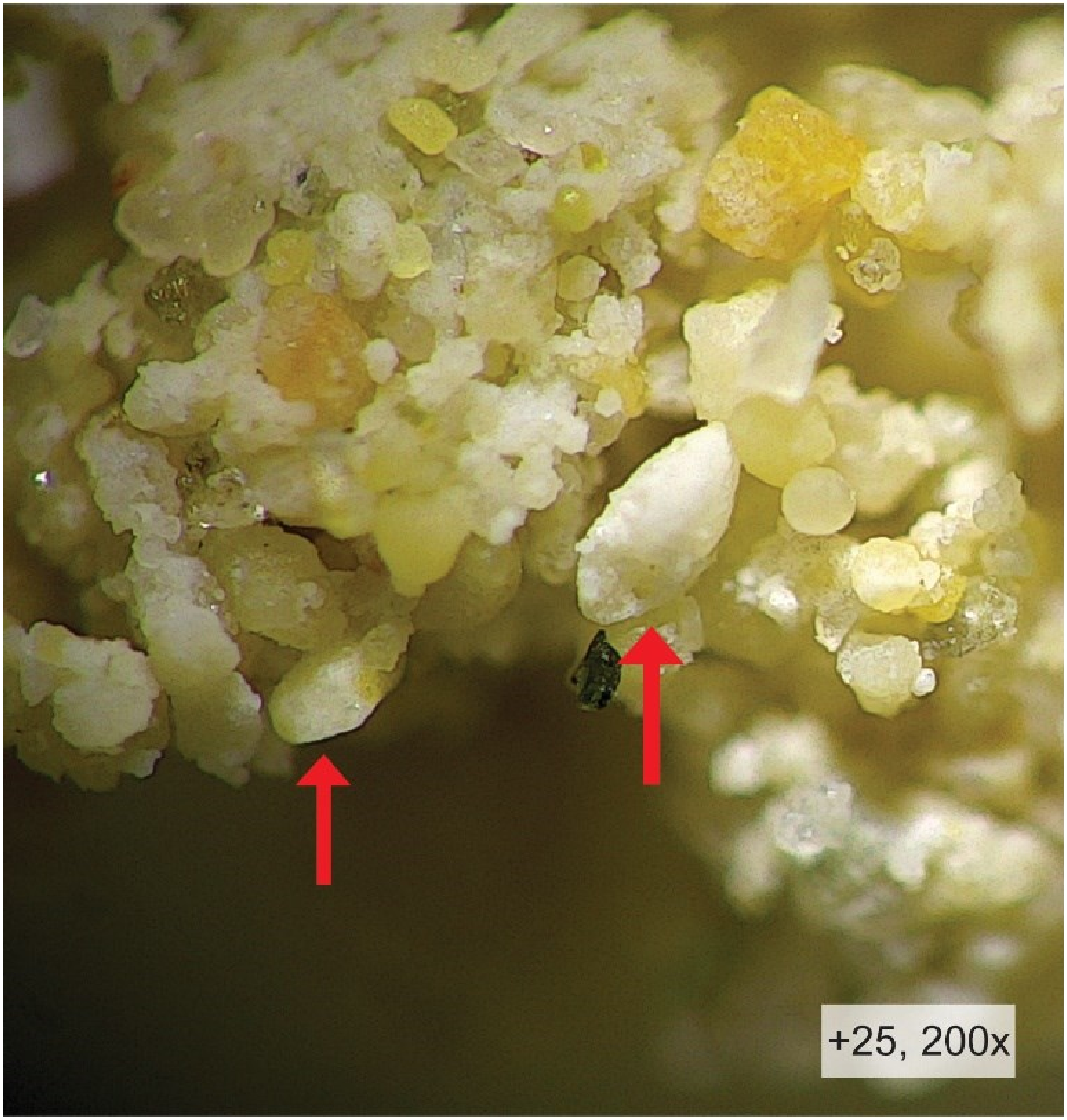


*Figure 2.6:* ***Microscope image of the microfacies "Bioturbated Peloidal Grainstone."*** *Note isopachous coatings on individual grains and arrows pointing to foraminifera. These two foraminifera are recognized under the order Miliolid, and are the most abundant occurring foraminifera, while at least three other unclassified species are recognized.*

## Intertidal allochems

Peloids are the dominant allochems found in intertidal sediments at all four sites. They are composed of fecal pellets and carbonate sand coated with isopachous cements that are occasionally micritized (Fig. 2.6). Foraminifera have been identified in the field and in core samples, but molluscan shells are the dominant bioclast in all sections of the intertidal zone. Both bivalves and gastropods occur, with gastropods occurring in higher quantities. In the field, mollusks were observed feeding on the surface of sediments. Five different shell species have been identified (Fig. 2.7). The skeletal concentrations observed in the field were classified using the biostratinomic classification system (Kidwell et al. 1986). Taxonomic composition is polytypic where intact *Cerithidea* sp. shells are the most abundant bioclast present in each core. *Brachiodontes* sp. frequently occur, but are seldom articulated or non-fragmented. Gastropod shells are largely oriented concordant with bedding. Bivalve shells are concave up, and typically bedding parallel. Bioclasts are matrix-supported, however stringers of shells occur in the middle depths of the substrates. The internal structure of bioclasts are simple. Species shown in Fig. 2.7 have been identified relying on the descriptions of the fauna of Abu Dhabi in Paul & Lokier (2017) and Grizzle et al. (2018) and typical soft sediment fauna (Grizzle et al. 2018; Smythe 1979). The common shell fragments discovered in the Al Qantur lagoon are described below.

## Recurring Mollusca genera

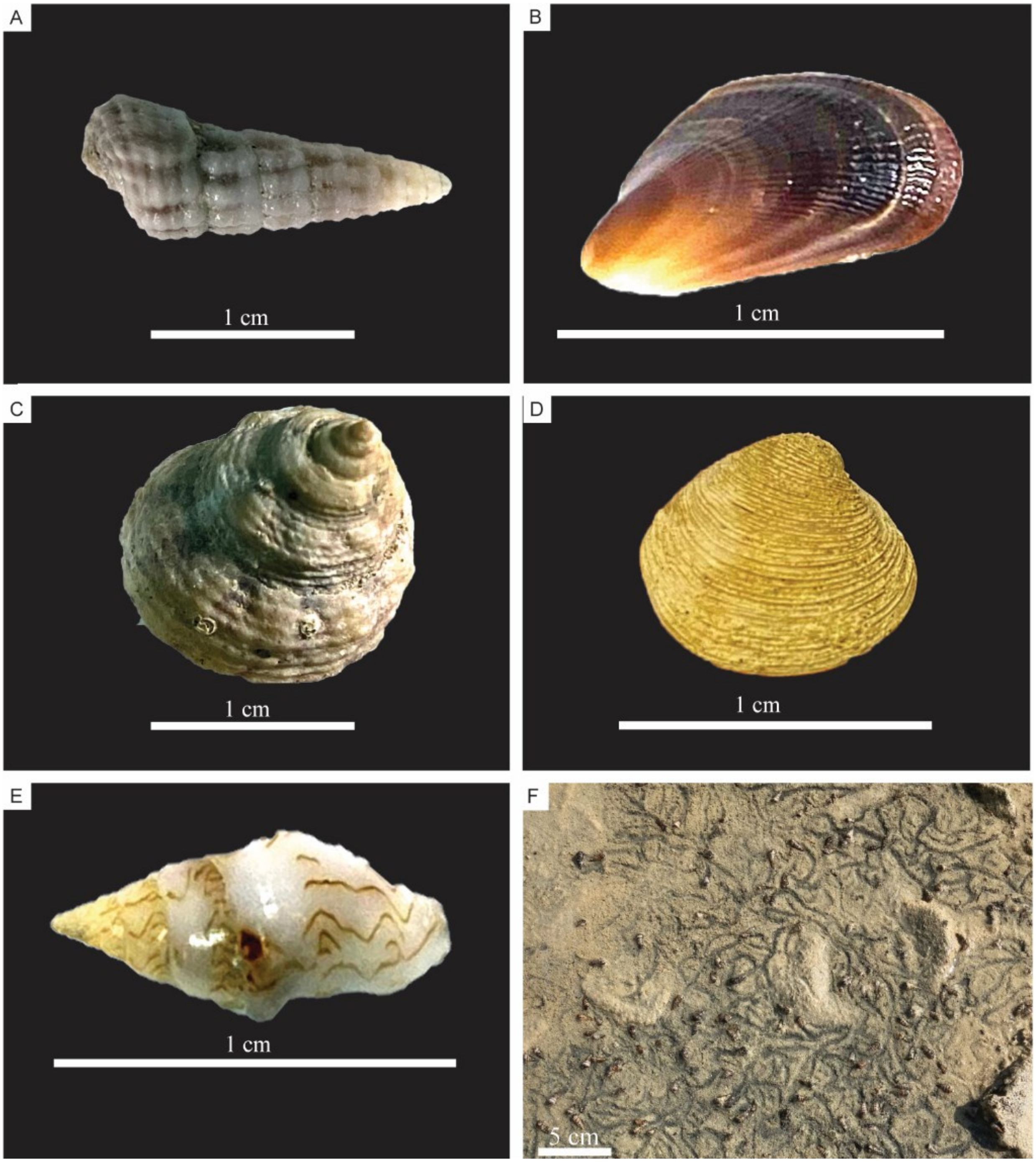


*Figure 2.7: **Sampled Mollusca shell species from field collections**. **A**)* Cerithidea *sp.* ***B**)* Brachiodontes *sp.* ***C**)* *?*Monodonta *sp. or ?*Clanculus *sp.* ***D**)* Circenita *sp.* ***E**)* Mitrella *sp.* ***F**) Surface grazing traces of gastropods during low tide.*

The intertidal zone hosts a diversity of mollusks, with select genera recurring in particular abundance in the substrates. Notable gastropod shells include intact to partially fragmented *Cerithidea* sp. (Fig. 2.7A), possibly intact *Monodonta* sp. or *Clanculus* sp. (Fig. 2.7C), and intact *Mitrella* sp. (Fig. 2.7E). Significant bivalve shells include fragmented, sometimes disarticulated or intact, *Brachidontes* sp. (Fig. 2.7B), and disarticulated or intact *Circenta* sp. (Fig. 2.7D).

Although the previously mentioned shells are the most prevalent in intertidal substrates, several other Mollusca have been identified in lesser amounts. These species include *Turritella* sp., *Modiolus* sp., possible *Strombus* sp., *Lunella coronate,* potential *Conomurex* sp., and possibly *Diodora* sp.. At least five other species have been recognized, but are not yet identified. Additionally, microborings have been observed on many of the bioclasts.

**Bioturbation Distribution**

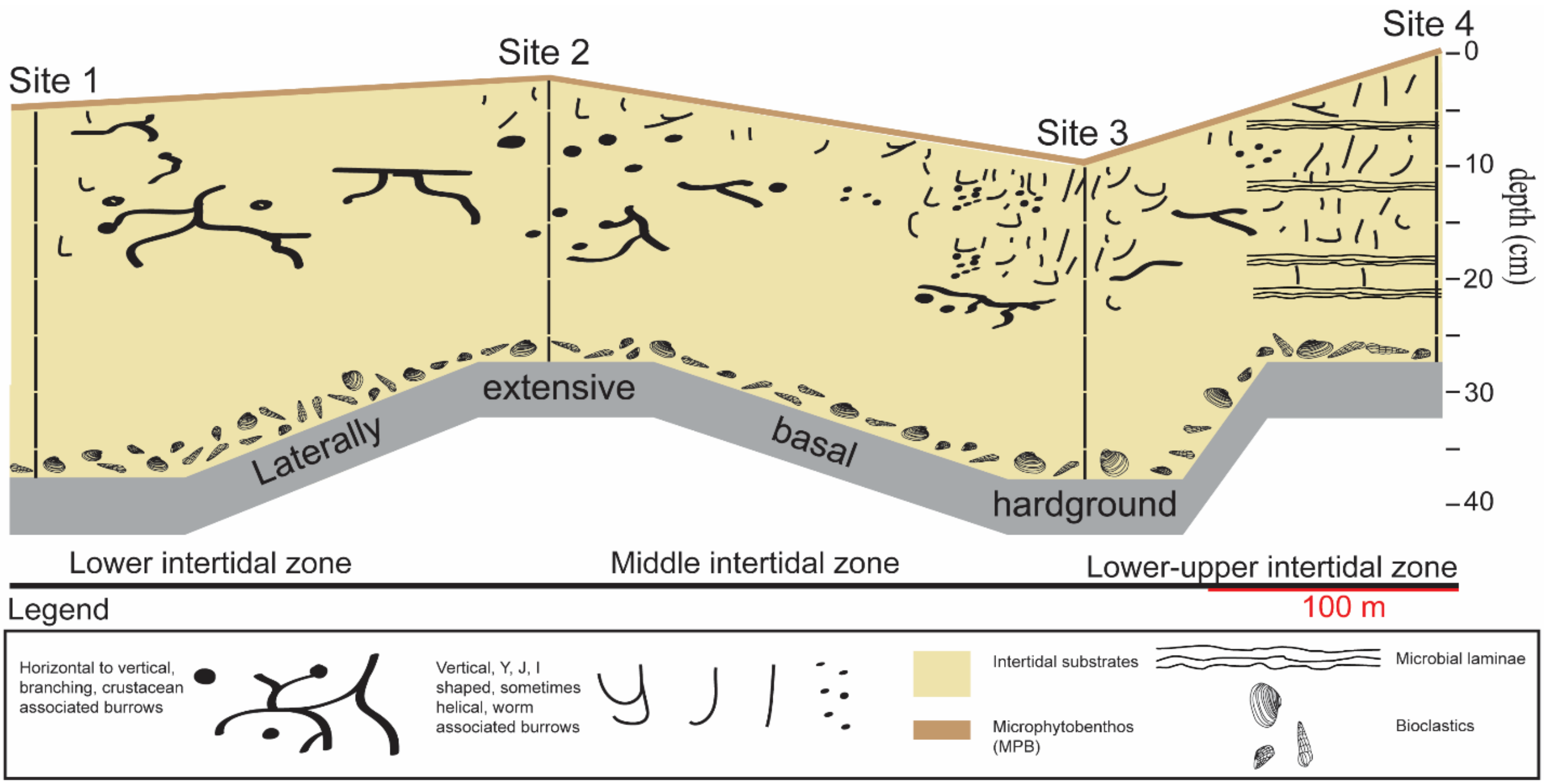


*Figure 2.8:* ***Profile showing position of sites within the intertidal zone, relative elevation, sediment and associated trace characteristics****. Upper intertidal, microbial mat and sabkha proximal portions of the ramp extend to the right, and seaward distal portions extend to the left. Note the change in trace type and trace abundance down ramp.*

Field observations indicate that both the ghost crab (*Ocypoda rtundata*) and the sand bubbler crab (*Scopimera crabricauda*) are abundant in the distal portions of our intertidal succession (Sites 1 and 2; see also John & George 2004). The polychaete worm *Nereis* sp., is predominately found within the proximal portions of the intertidal zone (Sites 3 & 4), and is notably abundant in Site 3. Nereid burrows are also observed in the distal Site 2, but in lesser amounts.

Observed burrows are generally of two types; those attributed to worms (primarily nereid polychaetes) and those attributed to crustaceans (ghost and bubbler crabs). Morphologically, worm-related burrows are typically small, <1-3 mm in diameter, and vertical (e.g., *skolithos*). The worms, *Nereis* sp., are mobile, and are both predatory and deposit feeders. Worm burrows are predominantly found in the upper 15 cm of our sections and are most abundant in Site 3. However, cryptobioturbation due to crustacean-associated bioturbation suggest that in distal parts of the intertidal zone the shallower-tiered nereid burrows are poorly preserved, or destroyed.

Arthropod burrows, in contrast, are larger (3-25 mm in diameter) and serve as dwellings that branch both vertically and horizontally (e.g., *psilonichnus*). The crustacean burrows are typically passively infilled, actively backfilled, or collapsed (Chakrabarti et al. 2006). The three-dimensional burrowing activity of these crustaceans can destroy laminae and bedding, and certainly modify any pre-existing biogenic fabrics (Kendall et al. 2002; Desjardin et al. 2012).

Figure 2.8 is a graphical representation of the changes in burrow fabrics from the upper to lower intertidal zone. In general, there is a proximal to distal change from polychaete worms to crustacean infauna. As crustaceans mix and homogenize the sediment, burrow preservation tends to decrease towards the lower intertidal zone. The depth of burrows potentially correlates to the depth of the rudstone unit, as burrowing activity lessens within the bioclastic accumulations.

Waterbirds, namely the Greater Flamingo (*Phoenicopterus roseus*), and shorebirds, including the Common Sandpiper (*Actitis hypoleucos*) and the Greater Sand Plovers (*Charadrius leschenaulti*), were noted to predate at the margins of tidal channels. Birds scoured the sediment exposed during the falling tide, pecking at surface prey, probing for infauna or stirring sediment to access buried prey items. Peck marks, probe marks, gape marks, foot paddling marks and trackways of waterbird and shorebird foraging (Zonneveld et al. 2023; *in review*) have potential to be preserved following rapid burial of surface sediments. Of note here are fabrics produced by the Greater Flamingo that include large round depressions in the substrates that may extend for several meters as they forage in groups through intertidal sediments.

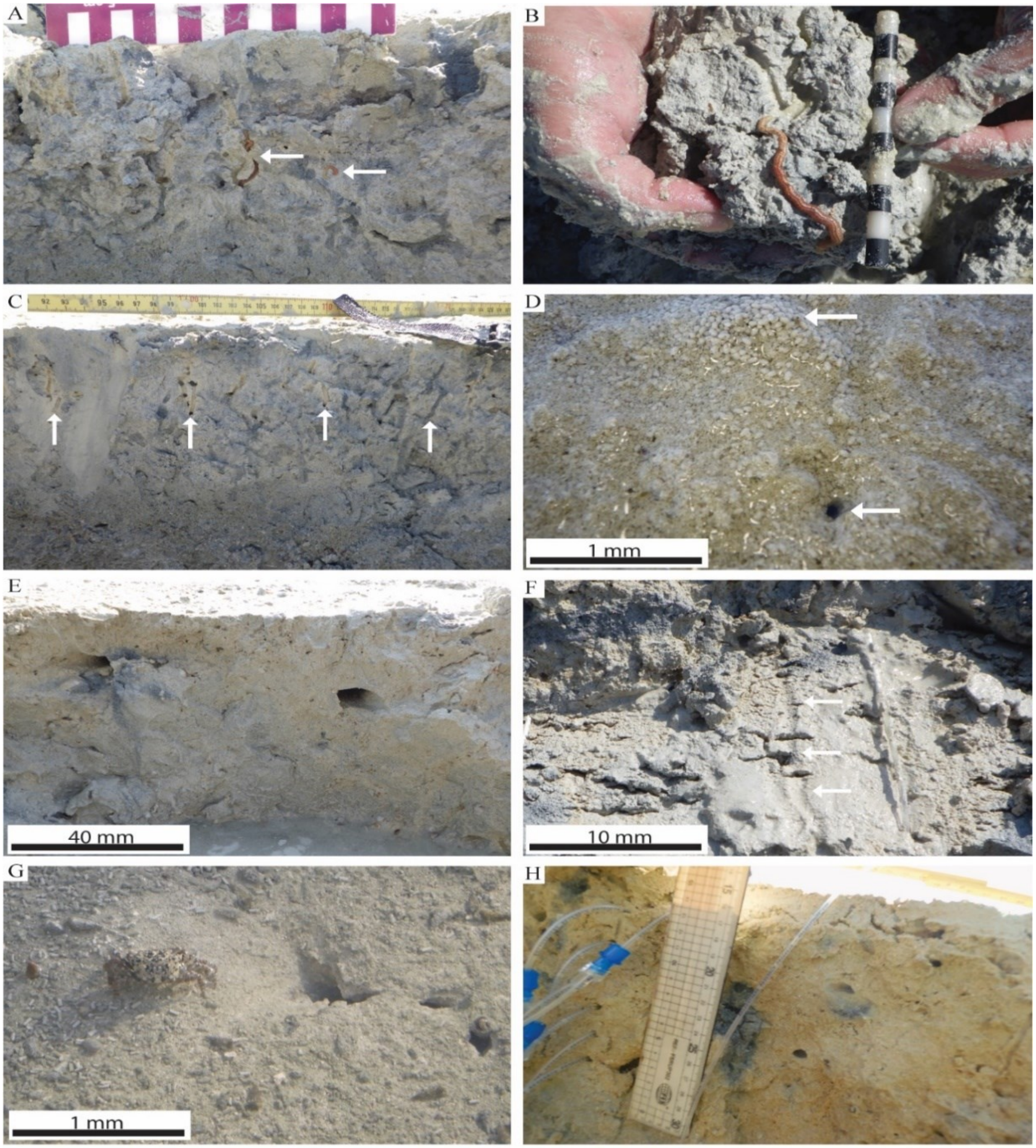


*Figure 2.9:* ***Photos from the lower to middle intertidal zone***. ***A-C****) Polychaete worm* Nereis *sp. (white arrows) and their traces in both field pit and in hand. Note vertical orientation of worm traces and abundance of worm burrows within the field pit at Site 3 (A & C).* ***D****) Open crustacean burrow exposed at low tide at Site 2 and accumulation of pellets outside of burrow opening.* ***E****) Crustacean burrows associated with a crab at Site 2* ***F****) Top view of a shallow angle crustacean burrow extending laterally into the substrate ~ 15 cm below the sediment surface at Site 2. The overlying sediment was removed to reveal this burrow.* ***G****) A crab next to its burrow on the ocean floor during high tide. This photo was taken underwater.* ***H****) Anoxic halos surrounding both burrowing types (worm and crustacean) also showing porewater sampling tubes connected to Rhizons at Site 1.*

## Microphytobenthos

Across the intertidal zone, the upper 3-6 millimeters of the sediment are loosely bound by a microbial matrix of extracellular polymeric substance (EPS) forming a subtle pale-brown coloured microphytobenthos (MPB). Microbial mats or MPB commonly extend over broad areas of the intertidal zone (Hope et al., 2020; Hubas et al., 2018) and comprise a complex assemblage of microorganisms including bacteria, protozoa, fungi, algae, diatoms as well as sporelings of macroalgae (Mandal et al., 2021). We have observed distinctive, black, microbial mats that occur in the upper intertidal zone (Fig. 1.1C), which are morphologically different from the MPB observed in the <1 cm depth of all intertidal substrates. MPB in Al Qantur lagoon creates a "spongy" texture within the shallow sediment surface that is not spatially restricted. The MPB enhances sediment cohesion, stabilizing sediments against resuspension (Paterson et al 2018), but also plays a role in modifying pH and redox chemistry with significant changes over cycles of night-day and tidal inundation (Mandal et al., 2021).

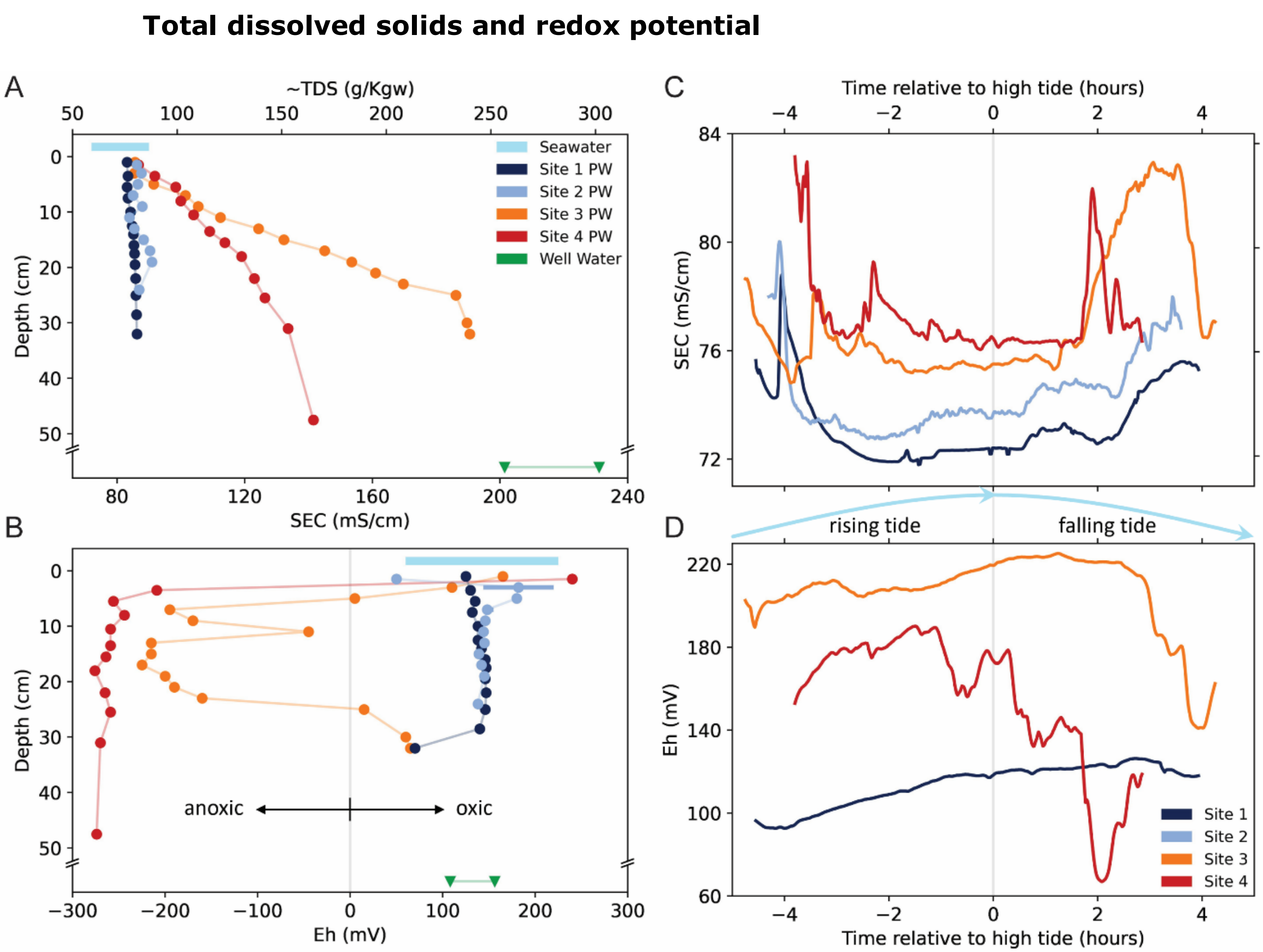


*Figure 2.10:* **Variation in porewater specific electrical conductivity (SEC), total dissolved solids (TDS) and porewater redox potential for each study site *A*)** *Variation in porewater specific electrical conductivity (SEC) and total dissolved solids (TDS) and* ***B****) porewater redox potential for each study site with depth below the sediment surface. Additional data for intertidal zone sea waters shows the range of values measured 0-2 cm above the sediment surface in the study area during the tidal flood and ebb. Wells samples confined continental brines from beneath the hardground underlying the study site.* ***C)*** *Specific electrical conductivity (SEC) and total dissolved solids (TDS) and* ***D)*** *redox potential (Eh) in seawater above the sediment surface. Data for each site spans the period from flood by the rising tide to exposure as the tide recedes. Time is given relative to the high tide, where negative numbers show time before the tidal maximum and represent the period of rising tide, zero is the tidal maximum, and positive numbers are time after this maximum during the falling tide. Samples and data were collected in November 2021 for the larger of the semi-diurnal tides following daytime exposure (tidal minimum ≈ midday) during which porewaters were sampled.*

Figure 2.10 presents specific electrical conductivity/total dissolved solids (TDS) and redox potential measurements of porewaters from the study sites. Porewater TDS ranges from 58 to -218 g/KgW (Fig. 2.10A). Highest TDS is seen in the more proximal sites that show a marked increase with depth to maxima of 133 and 218 g/KgW in Sites 3 and 4 respectively. These values approach those in well water samples from beneath the harground (227 and 278 g/KgW TDS from 3.5 and 6.8 m deep wells). In comparison, TDS at Sites 1 and 2 remains relatively constant at 65.1±1.2 g/KgW and 67.0±2.2 (~69 g/KgW from the sediment surface to the maximum sampled depth. Replicate samples extracted from depths of 1.3, 3.0 and 6.5 cm at Site 2, to understand local scale heterogeneity, showed ranges at individual depths of 1.6-3.3 g/KgW.

The Eh, or redox potential of the porewaters shows significant differences between sites in the degree and patterns of depth-dependent variation between sites (Fig. 2.10B). At Site 4, the shallowest sample (1.5 cm depth) has the highest Eh measured in any porewater (+240 mV). Below this, the redox potential declines markedly and waters are strongly reducing, with values becoming generally more negative with depth (-209 to -276 mV). In Site 3, the upper 25 cm show a similar general trend, but values remain oxic in the upper 5 cm, and Eh values are never less than -225, with a single higher value at 11 cm. In contrast to Site 4, redox potential increases in the lower 10 cm of the profile, with oxic conditions in samples from below 25 cm depth. In Sites 1 and 2, Eh ranges at the surface are less positive than for the more proximal sites, and there is some variability in the upper 10 cm. However all waters remain oxic and most samples have a redox potential of +143±3.5 mV, with a single lower value (+70 mV) for the deepest porewater from Site 1. Oxic porewaters from all but Site 4 accord with redox measured in samples from beneath the hardground samples in the wells (+105 and +155 from 3.5 and 6.8 m deep wells respectively). Positive values of redox potential were also previously reported by Vallack (2021) for continental brines at shallow depth beneath the hardground, and the measurement of anoxia in other well waters during the sampling campaign, confirm these high values are not due to atmospheric contamination.

## Temporal variation in surface water TDS and redox potential

Figure 2.10 presents time series data on specific electrical conductivity/TDS and redox potential for bottom seawater at each of the study sites over the period of one tidal flood event. The TDS of seawater within 2 cm of the sediment interface measured during the 7-9 hour period over which the intertidal zone is inundated ranges from 56 ± 1 to 67 ± 2 TDS (g/KgW) (Fig. 2.10C). All study sites exhibit a similar trend in TDS over time. Values are initially high when the rising tide first floods over a site, and then decline over the succeeding 1-2 hours The least saline waters are recorded during the period spanning two hours before high tide until <2 hours after high tide, after which TDS values then start to increase again. Whilst the values at each site show some variability through time, there are systematic differences between the sites that reflect their position within the intertidal zone.

The duration of inundation decreases from distal to proximal sites, with the notable exception of Site 3 which experiences the most extended period of inundation. In general values of TDS from the flood to the ebb are lower in the more distal sites and increase from the lower to the upper intertidal zone. Only Site 2 shows a simple rapid decrease in TDS after inundation by the rising tide. The other sites show one or more rises in TDS after this initial fall and over the period up to two hours before high tide. After high tide there is a minor increase in TDS (Fig. 2.10 ≈ 1 g/KgW) that starts only half an hour after the tide reverses and is seen only at Sites 1 and 2, but the major rise in TDS occurs 1 ½ to 1 ¾ hours after high tide at sites 3 and 4, and half an hour after that at Sites 1 and 2. The falling tide TDS maximum is also greater relative to the high tide minimum at Site 4 then at Site 2, and smallest at Site 1. The TDS peak during the falling tide at Site 3 is the largest and most extended of those measured at the four sites. Both the two more proximal sites show a marked overall fall in TDS for the final ~1 hour before the sites dry. .

The redox potential (Eh) of the surface waters ranges from +61 to +221 mV, with a clear difference between the sites measured (Sites 1, 2 and 4) and a less systematic pattern of temporal change (Fig. 2.10D). The highest redox potential is seen at Site 3 and the lowest at Site 1. During the rising tide redox potential is systematically ~100 Mv higher at Site 3 than at Site 1, but at both sites increases by ~30 mV from the initial flood to a maximum that occurs ~1.5 hours after high tide at Site 3 and ~3 hours after high tide at Site 1. At Site 3 there is then an overall drop of ~80 mV, with a minor increase before the Site dries, but Site 1 shows only a very minor decrease from the peak redox potential. The Eh values at Site 4 are intermediate between those at Sites 1 and 3 during the rising tide, and also show considerable variability. There is a significant fall in redox potential at Site 4 that appears to start before the tidal maxima, and as at Site 3 values appear to increase in the hour before the site dries.

## INTERPRETATIONS

### High salinity and oxygen impact on animal assemblages

Salinity values, which are interpreted from total dissolved solids, in the intertidal zone fringing the Abu Dhabi sabkha are high. Even the lowest values of ~60 ppt within tide and porewaters approach the upper limits for animal survival (Beadle, 1936; Lyster, 1965; Davenport 1985; Scannell & Jacobs, 2001; Lucrezi, 2010). With this in mind, we may assess how solutes become concentrated within the intertidal zone, and how infauna responds to this heightened stress.

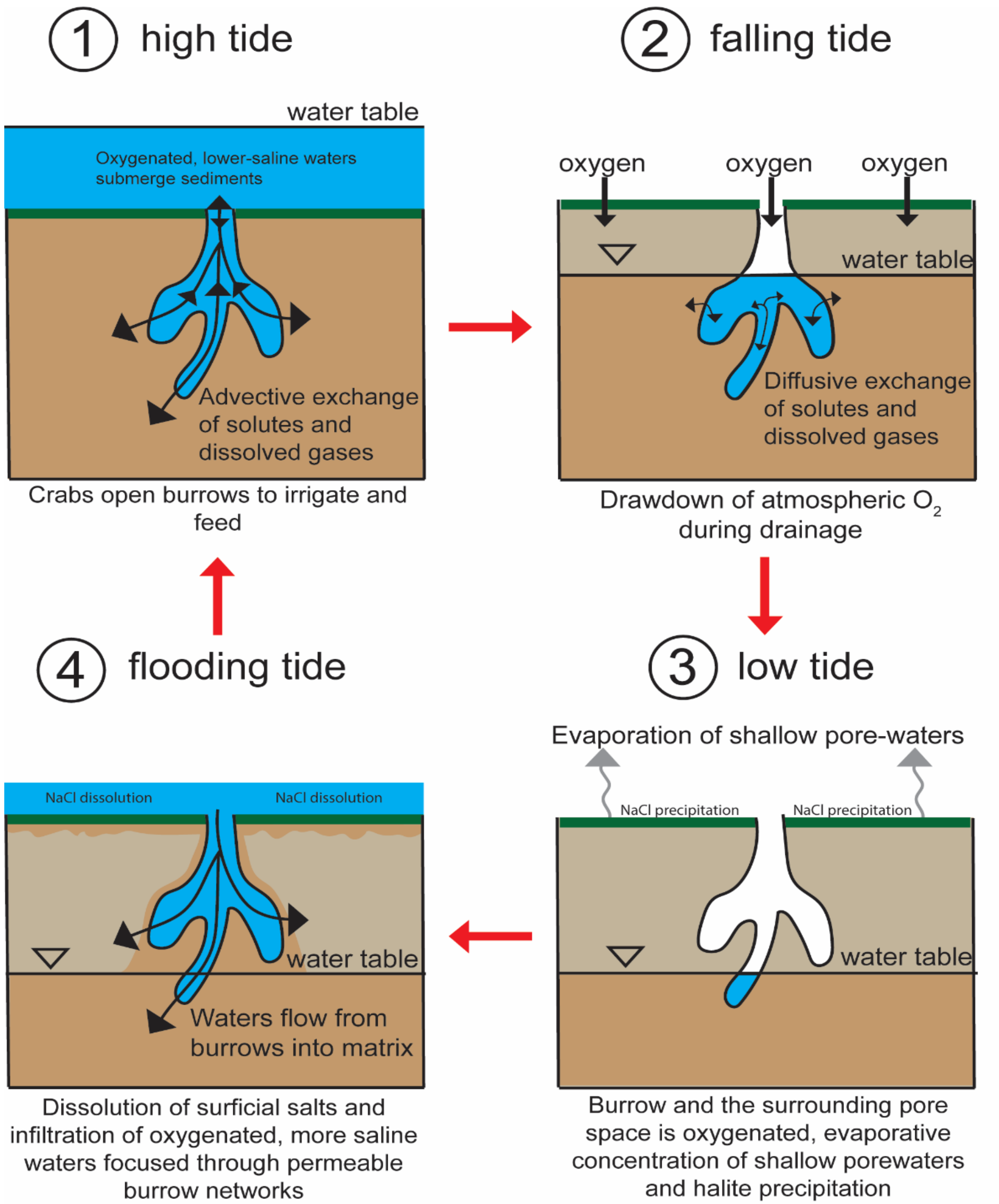


*Figure 2.11: **Schematic illustrating functioning of higher permeable inter-tidal burrow networks** and effect on salinity and oxygen fluxes through the different phases of the tide.*

### ***Salinity Concentration***

Figure 2.10C presents systematic variation in TDS at the sediment surface and with distance up the intertidal zone over a single tidal flood event. As the rising tide floods across the intertidal zone, high TDS are recorded at the sediment surface. This is interpreted as reflecting dissolution of surficial halite that was precipitated due to evaporation of shallow porewaters during the preceding period of low-tide exposure. TDS increases progressively within the tidal front as these waters move landward and continue to dissolve surficial salts. However, TDS subsequently falls at individual sites due to dilution by less saline seawater that continues to flood the intertidal zone. When the tide reverses, the high TDS head-waters move down-ramp with the subsequent low tide (Fig. 2.11). The subtle topography of the intertidal zone gives rise to complex lateral variations in TDS over time. This is exemplified by data at Site 3 which is located within a lower elevation subsidiary channel, which appears to funnel high TDS waters draining from the upper intertidal zone (Fig. 2.10C).

This effect will be most marked when low tide exposure of the intertidal zone corresponds to the period of maximum solar insolation. The data presented here correspond to a period in November when the tidal flood occurred in the afternoon. However, a stronger evaporative concentration and remobilisation of surficial salts would be expected during the summer months. TDS peaks would also be enhanced when spring tides flood areas of the upper intertidal zone that have remained emergent over the preceding neap tides.

Cycling of marine salts contributes to the high TDS tolerated by the intertidal zone communities in Abu Dhabi. However, porewaters below ~5 cm depth at Sites 3 and 4 exhibit significantly elevated TDS relative to the most saline surface waters measured. This is in marked contrast to Sites 1 and 2, where TDS is relatively constant throughout the sediment column. The increase in TDS with depth in proximal areas is attributed to the leakage of continental brines from below the hardground (Wood et al. 2002; Liu et al. 2016;

Vallack, 2021). The upward pressure gradient driven by the continental groundwater head is enhanced during periods of low tide. Spatial variations in the thickness and integrity of the hardground and the sediment thickness and permeability will control the distribution of brine leakage. The TDS of porewaters at depth in Site 3 approach those of the continental brines sampled from below the hardground in the wells (Fig. 2.10A). However those at Site 4 are notably less saline. This may reflect the higher elevation of this site, fewer leakage points within the hardground in this area, and/or the lower permeability of the sediment column that results from the presence of buried mats.

### ***Redox conditions***

Redox potential in porewaters indicates generally reducing conditions in Sites 3 and 4 (Eh < 0 mV), and oxidizing conditions (Eh > 0 mV) in Sites 1 and 2 (Fig. 2.10C). Values close to -300 mV, as occur in Site 4 which includes layers of buried microbial mat, are interpreted to reflect microbial-mediated reduction (Sondergaard, 2009). Notably, porewater redox decreases with depth in Site 3 but then conditions become oxic towards the base of the sediment column. This correlates with the highest porewater salinities (Fig. 2.10B) and provides clear evidence for relatively rapid upward leakage of oxic groundwaters at Site 3.

Within Site 3 and 4, porewaters are initially oxic within the shallow subsurface (< 5 cm), before transitioning to anoxic conditions in the following depths (Fig. 2.10B). Corresponding with this shallow depth oxygenation is the abundance of active worm burrowing (Figs. 2.4, 2.6). Open worm burrows at the sediment-water interface allow oxic seawaters to penetrate into the sediment column, effectively irrigating their domilices. Presumably, bioirrigation is sufficient enough to offset the effect of the processes generating anoxia at depth.

Sites 1 and 2, where porewaters remain oxic and the leakage of continental brines is not apparent, are dominated by the bioturbated peloidal grainstone microfacies that are abundant in burrowing crustaceans (Figs. 2.2 to 2.6). Crustacean burrowers appear to be capable of mixing and homogenizing substrates through more complex, deeper burrow networks. The crustaceans effectively increase permeability in the substrates, creating burrow networks that act as preferential flow pathways (Fig. 2.11), as previously suggested by Gingras et al. (2012). These focus the influx of oxygen-rich air into the sediment when the tide retreats and the water table falls, and subsequently also the recharge of higher TDS waters into the sediment on the tidal flood (Fig. 2.11). Worm burrows may also be capable of enhancing water flow, as in the case of Site 3 where abundant active burrowing occurs, and shallow porewaters are more chemically similar to seawater (Fig. 2.10). However, the variability in redox and salinity within the sediment column suggests that worm burrowing does not modify the substrate's permeability to the extent observed in Sites 1 and 2.

In summary, Sites 1 and 2 more closely resemble seawater values because crustaceans are able to "flush" the sediments with tidal waters through higher-permeable burrows (Figs. 2.10 and 2.12). A major portion of the fluid flux occurs through the higher-permeable animal burrows, while the sediment volume conducts a more minor, but still significant, fluid flow (see "dual-porosity biogenic fabrics," Gingras et al. 2012).

### *Animal Response*

Beadle (1936) describes how polychaete worms are able to withstand drastic changes in salinity using body volume and body fluid concentration control of variably saline waters. Lyster (1965) tested the prolonged exposure to hypersaline waters and found that *Nereis* larvae (and assumed adults) were able to withstand the greatest period of salinity exposure within their study (7 days) at 65 ppt before 50% kill. At 70 ppt, *Nereis* was able to survive one day before 50% kill. Lucrezi (2010) indicates the ghost crab salinity tolerance has a maximum of 40 ppt, but higher ranges have not been documented.

These salinity tolerances suggest that the Abu Dhabi burrowing organisms may only be able to survive within the lower end of the daily tidal water salinity values. This means that the infauna must deploy methods of coping with highly saline waters. Figure 2.10A reveals that salinity measurements in porewaters of all study sites are stabilized at ~70 ppt salinity in the upper 0-10 cm of the subsurface, where we have observed the highest abundance of burrowing worms and crustaceans (Figs. 2.2 to 2.5). This is evidence that where burrowing organisms concentrate, they do so in a high salinity environment. Necessarily, burrowers must be capable of stabilizing salinities in these subsurface waters in order to create ideal habitation conditions.

Methods of salinity management might include irrigation and regular, horizontal, sometimes vertical, substrate movement. Sanders et al. (1965) mentions that burrowing within the subsurface provides protection against strong salinity variations, and horizontal migration minimizes salinity shifts experienced by the organism (Desjardins et al. 2012). However, in areas of such high salinities, active transfer of solutes through irrigation is necessary to withstand the observed daily salinity fluctuations (Fig. 2.10C). Kristensen & Kostka (2005) state that frequent irrigation provides an exchange between reduced burrow waters and oxygenated surface waters, aiding in both solute diffusion and respiration. Presumably, worm and crustacean burrows irrigate the shallow subsurface sediment over periods of inundation using the low salinity water at high tide. Particularly, burrowers may preferentially irrigate following a nocturnal low tide when exposure-related evaporation would be lower. Both during the initial tidal flood and the tidal recession, burrows are either passively filled or actively closed for protection from salinity predation and day-time heat. Burrowing organisms then remain in the subsurface, in lower-salinity, oxygenated waters where survivability is optimal. The reduced environment of a worm burrow can be noted in Fig. 2.9C, where a *Nereis* sp. burrow is seen to have orange coloring within it, indicating anoxic conditions within the burrow before high tide inundated the sediments and irrigation could occur.

## Animal response to subaerial exposure

In an intertidal zone, surface sediments and organisms are subject to periodic exposure as tides ebb and flow. Generally, subaerial exposure is discussed in sequence stratigraphy when referring to extended periods of non-deposition. The associated trace-fossil suites associated with omission surfaces provide evidence for their interpretation (Savrda 1991; Pemberton & MacEachern 2005; MacEachern et al. 2007). However, periodic exposure surfaces, as in the case of a tidal flat, also host ichnological evidence for depositional interpretations (Gingras et al. 2011). For example, in sedimentary strata, the co-occurrence of nereid (*Skolithos*) and crustacean (*Thalassinoides/Psilonichnus*) burrows, alongside avian trackway and surface grazing traces, suggests an intertidal environment (Gingras et al. 1999; Lambias et al. 2003; Zonneveld et al. 2012; Zonneveld et al. 2014).

In the arid conditions of Al Qantur lagoon, subaerial exposure is particularly significant. Low tide presents the highest danger to the burrowing animal. During exposure, temperatures reach extreme highs (up to 50℃), tidal water salinities increase to nearly 160 ppt, and predation from terrestrial animals and shorebirds and other waterbirds increases. It is presumed that organisms will develop tidal cycles of activity, where high tide presents the greatest protection from salinity, temperature and predation while also allowing easiest access of feeding (suspension and predation). As the tide recedes, burrowers likely rebury themselves for protection from these elements. However, some surficial animal activity persists during low tide, as molluscs scour the sediment surface, leaving grazing traces (Fig. 2.7F), and birds forage on the margins of the tidal channels. Indeed, diurnal aerial exposure guides animal movement within Al Qantur lagoon, and the resulting biogenic fabric.

## Substrate cohesiveness, grain size and animal mobility

Substrate consistency, first and foremost, dictates which organisms will inhabit a particular space (MacEachern & Burton 2000; Gingras et al. 2000; Pemberton & MacEachern 2005; Gingras et al. 2011). For example, a softground will host different organisms than a hardground, depending on what is capable of feeding on or within the medium (e.g., a boring clam, or a deposit feeding worm). Furthermore, substrate consistency facilitates preservation, as a soft sediment is more susceptible to collapse, while a firm substrate may remain uncompacted (Goldring 1995; Gingras et al. 2011). Moreover, grain size is a function of depositional energy and availability of food, as well as pore networks and permeability (Gingras et al. 2011). Organisms will inhabit sedimentary layers of the optimal grain size for ease of movement, food processing, and water saturation (Alexander et al. 1993; Zorn 2006; Hauck et al. 2009; Gingras et al. 2011).

Substrate consistency and grain size within Al Qantur lagoon is largely homogenous across the intertidal zone, apart from the base rudstone layer. A firm, partially micrite-coated, peloidal sand characterizes the intertidal sediments, and as such, the endolithic trophic styles are observed to be consistent. Additionally, surficial mats (MPB) are present everywhere in the intertidal zone, and microbial mats occur in the upper intertidal zone (Fig. 2.2 to 2.6). Although subtle differences in the spatial occurrence of MPB are observed, they are not documented in this study. Movement of nereid worms and arthropods is restricted to the grainstone layers and the microbial laminated bindstone, as well as through the surficial MPB (Figs. 2.2A to 2.5A). Rudstone layers, which consist of a bioclastic framework, likely deter macrofauna from feeding or resting in the microfacies due to difficulty of movement, and little accessibility to food. The bioturbated peloidal grainstone microfacies presents the optimal substrate and grain size for burrowing organisms, allowing ease of movement, and the accessibility to food and saturated sediments.

## DISCUSSION

Both siliciclastic and carbonate sabkhas have been well studied and documented as analogues for petroleum reservoir interpretation from ~1960 and onward (eg. Evans et al. 1969; Azer et al. 1995). However, the intertidal margins of these environments have been largely neglected, in particular the identification and distribution of intertidal animal traces is known from only a few studies (John & George, 2004; Knaust et al., 2012; Hamza et al. 2018). Literature describing the successions of sabkha facies and their ancient analogues have characterized a coastal morphology that encompasses the barrier island/lagoonal complex into the intercontinental sabkha (Evans et al. 1969; Alsharhan & Kendall 2003, 2011). What is lacking in these descriptions is an assessment of the lagoonal microenvironment. More recent works by Lokier et al. (2013) and Paul & Lokier (2017) have discussed the sedimentology and subsurface lithology in the intertidal zone, but a discussion of bioturbation and the infaunal community remains lacking. Characteristically, when attempting to classify bioturbation textures of marine environments, the ichnofacies approach is used (Mangano & Buatoi, 2004a,b; MacEachern et al. 2007; Buatois & Mangano 2011; Pemberton et al. 2012). Our observations show a land-to-sea transition of mainly vertical worm burrows through to crustacean-made domiciles. Ostensibly, these would be construed as the *Skolithos* through to *Psilonichnus* ichnofacies. However, in low-diversity assemblages stressed by antagonistic physico-chemical conditions, assigning an ichnofacies can be misleading and unhelpful due to the potential for misrepresentation and misinterpretation of the depositional environment.

## Biofabric preservation potential

Moving water produces primary sedimentary structures and bioturbation causes the formation of biogenic sedimentary structures, characteristically at the expense of physical sedimentary structures (Richter 1936; Brush 1965). The observation of these sedimentary structures provides the basis for sedimentological interpretations of deposition in paleoenvironments (Reineck & Singh 1980). The identification of sedimentary structures is largely controlled by texture and compositional heterogeneity of the sediment. Sedimentary structures are expressions of the sedimentary fabric, and result from variations in lithology, grain size, roundness, and sorting. In Al Qantur lagoon, the observed sediment is predominantly very well sorted, fine grained and monomineralic (calcium carbonate). As such, the sedimentological variability is reduced, and many aspects of the sedimentary fabric are not readily observed. For this reason, both physical and biogenic sedimentary structures should be used to construct a depositional model.

Observing the bioturbate texture is also limited by factors such as grain size, sorting and overall composition, and increased amounts of bioturbation tend to produce sedimentary profiles that are massive in appearance. That said, some traces have greater preservation potential over others. Ekdale et al. (1984) suggest that a crucial factor for preserving bioturbation within carbonates includes the presence of algal mats alongside abundant tube-building organisms (e.g., nereid polychaetes). The tubes may be the most diagnostic element within these mats to survive in the fossil record (Figs. 2.5, 2.10). Knaust et al. (2012) also recognizes the taphonomic importance of microbial mats. The authors note that microbial mats promote a mildly reducing microenvironment that may prevent the oxidation of traces under biofilms. Rapid burial by fine-grained sediment together with early-diagenesis, such as microbial or physico-chemical early marine cementation, further increases the chances of preservation (Knaust et al. 2012).

As reported by Ekdale et al. (1984), Knaust et al. (2012), Kumar (2017), and our own research in the lower-middle intertidal zone, crustacean burrows are more penetrative than other infauna. In these zones dominated by crabs and shrimp, massive-appearing sediment is most common. There is a decrease in the preservation of observable biofabrics and an increase in massive appearance distally, coinciding with the increase of arthropod-associated bioturbation.

Additionally, some burrowing crustaceans backfill their burrows with sediment following their excavation. This behavior is exemplified by the sand bubbler crab *Scopimera* sp. (John & George 2004; Chakrabarti et al. 2006), which is observed in the distal Sites 1 and 2. The infill material in arthropod burrows represents a mixture of the original deposit and surficial sediments (Tedesco & Wanless 1991). Accordingly, the crab's excavation of burrows, followed by subsequent infilling, further alters the biogenic texture, sediment composition and texture. Consequently, infilled material contrasts with the surrounding substrate, opening the door to differential compaction and diagenetic alteration of the burrow infills from syndepositional through burial. Indeed, our observations of surface salinity variations support the role of burrows aiding the infiltration of high salinity waters on a tidal flood. As the burrows facilitate fluid flows which vary from the surrounding sediment, flux dependent reactions (such as dolomitization) may occur surrounding burrows (Gingras et al. 2004; Corlett & Jones, 2012).

Finally, within Al Qantur lagoon, the extensive surficial mat (MPB) encourages ample substrate cohesion to protect the subsurface from low to moderate energy conditions. However, Ekdale et al. (1984), highlight the vulnerability of the intertidal zone's surficial sediment to tidal reworking. Semi-diurnal inundation and recession of tides over the surface sediments reworks most traces of mollusc movement and waterbird trackways.

Based on our observations, we propose that there is a decline in the numbers of preserved burrows as we move from the upper to the lower intertidal zone. Sites 1 and 2 exhibit significant destructive bioturbation caused by crustaceans, Site 3 shows a concentration of vertical worm burrows, both open and closed, whereas Site 4 is distinguished by the presence of microbial mats and minor (primarily vertical) bioturbation by worms.

## Burrow architecture

For a more comprehensive understanding of animal burrow morphology in the intertidal areas of Abu Dhabi, we draw comparisons between ichnologic descriptions provided from the southern Arabian Gulf (Knaust et al. 2012) and neoichnological observations from the Red Sea (Kumar 2017). Knaust et al. (2012) described typical crustacean burrows after the Psilonichnus ichnogenus as "vertical, cylindrical burrows with short horizontal or oblique side branches, often with an upper part that is Y-shaped." Kumar (2017) identified recurring crustacean burrows as unlined domiciles, producing U-, Y-, and J-shaped burrows, which can be attributed to the Psilonichnus ichnogenus in the rock record. Both authors associated crustacean burrowing with the ghost crab (*Ocypode quadrata*), which we also observe at Al Qantur lagoon. Our observations of crustacean burrows are consistent with those descriptions, but there are notable differences in terms of size, horizontality, and branching patterns. In the Red Sea intertidal zone, crustacean burrows have a diameter of 2 cm at the surface, which is, on average, 1 cm larger compared to the crustacean burrows found in Abu Dhabi. In Al Qantur lagoon, crustacean burrows exhibit interconnected networks of unlined domicile burrows that extend laterally with few vertical components. Therefore, the morphology of crustacean burrows in the Abu Dhabi intertidal zone is ~ 1 cm in diameter, horizontal, unlined, cylindrical burrows with significant oblique branches that extend horizontally, and sometimes vertically, also assigned to the Psilonichnus ichnogenus in the rock record.

Additionally, we can compare polychaete worm burrow morphology in Al Qantur lagoon to the aforementioned studies. Kumar (2017) identified a recurring worm burrow made by the Annelid worm (lugworm), characterized by the presence of large accumulations of fecal pellets surrounding the burrows and U- and J-shaped configurations, which correspond to the ichnogenus Arenicolites in the rock record. In contrast, Knaust et al.

(2012) recognized various types of worms (polychaetes, nemerteans, and sipunculids) that burrowed along the channel margins in the intertidal zone of the southern Arabian Gulf but did not taxonomically classify their burrows. Worm burrow morphologies in the Red Sea intertidal area are larger in diameter and length, predominantly exhibiting U- or J-shaped configurations, and displaying a more complex morphology compared to the Abu Dhabi intertidal. Our observations in Al Qantur lagoon revealed only the polychaete worm *Nereis* sp. burrowing in the intertidal sediments, although other polychaetes are likely present in other areas. These burrows consistently exhibited vertical I- and J-shaped configurations, with occasional Y- and helical- shaped configurations. Therefore, the preserved worm burrows in the Abu Dhabi sediments can be characterized as simple, ~1 mm in diameter, shallow (0-15 cm depth), vertical U- and I-shaped burrows, which can be assigned to Arenicolites and Skolithos.

It is also worth noting the role of insects, birds and roots that may be identifiable in the rock record. Mangroves are common in the Abu Dhabi intertidal zone and their root morphologies are observable in the upper-intertidal zones. Root traces are a common characteristic of backshore, sabkha and supratidal sediments (Knaust et al. 2012; Desjardins et al. 2012). Arthropod insects are also common in these settings within and above the upper intertidal zone but were not seen in abundance during our study.

## Comparing carbonate and clastic intertidal environments

Intertidal zones with different tidal energies are compared in Table 2.2 using sedimentological and neoichnological characteristics. Distributions of bioturbation within a tidal flat is largely based on the primary stressing agents (i.e., salinity, turbidity, sedimentation rate, etc.) and the local sedimentology. As infaunal populations choose survivable areas with easy access to food and safety, their habitation is largely shaped by the energy regime of the tidal flat (Gingras et al. 1999).

| Depositional environment | Common infauna | Common ichnogenera | Degree of bioturbation | Primary stressors | Sedimentological attributes | Other key observations |
|---|---|---|---|---|---|---|
| Clastic, microtidal, intertidal flats and lagoons<br><br>(Garrison et al. 2007; Hauck et al. 2009) | • polychaetes,<br>• enteropnuests;<br>• ghost & fiddler crabs<br>• gastropods & bivalves. | • *Skolithos*<br>• *Arenicolites*<br>• *Thalassinoides*<br>• *Psilonichnus*<br>• *Siphonichnus*<br>• *Lockeia*<br>• crypto-bioturbation | • moderate to high (BI 4 to 6) | • high or low salinity<br>• low dissolved oxygen content<br>• substrate consistency and grain size<br>• subaerial exposure | • comparably fine grained sediments<br>• abundant bioturbation<br>• abundant fecal pellets<br>• shell accumulations<br>• some horizontal to weakly inclined planar beds and/or wave ripples | • hydrodynamic conditions largely influence animal distributions<br>• sediment texture, food resources, oxygenation and periodic exposure is dictated by tidal regime |
| Clastic, mesotidal, intertidal flats<br><br>(Gingras et al. 1999; Dashtgard 2011; Hodgson 2013) | • polychaetes and enteropnuests<br>• *Upogebia i.e.* mud shrimp; *Callianassa i.e.* sand shrimp<br>• *Corophium,*<br>• crabs<br>• diverse bivalves | •*Skolithos*<br>•*Arenicolites*<br>•*Gyrolithes*<br>•*Thalassinoides*<br>•*Paleophycus*<br>•*Planolites*<br>•*Siphonichnus* | • variable, low (1-2) to very high (4 to 6).<br>• Low BI in proximity to brackish water input or where sedimentation rates are elevated.<br>• Higher in more distal positions and / or where sedimentation rates are low | • salinity<br>• turbidity<br>• sedimentation rate<br>• substrate consistency and grain size | • fine to medium grained sediments<br>• common to abundant bioturbation<br>• some shell debris<br>•common ripple lamination<br>• horizontal to low angle cross bedding | • mappable, ichnological suites to the outer and inner flats<br>• outer flats experience increased hydraulic energy<br>• inner flats may have lowered salinities and prolonged exposure |
| Clastic, macrotidal, foreshore, tidal flats and creeks (Yang & Chang 2018; Dashtgard et al. 2006) | • polychaetes<br>• soldier & bubbler crabs<br>• thalassinid shrimp<br>• bivalves | •*Skolithos*<br>•*Arenicolites*<br>•*Planolites*<br>•*Thalassinoides*<br>•*Paleophycus*<br>•*Psilonichnus*<br>•*Ophiomorpha*<br>•*Siphonichnus*<br>•*Lockeia* | • low (0 to 1) or moderate to high (3 to 5)<br>• highest degrees (3 to 5) observed in energy sheltered zones<br>• other exposed zones have a low BI (0 to 3) | • wave action<br>• sedimentation rate<br>• subaerial exposure<br>• substrate consistency and grain size | • fine to medium grained sand with mud and gravel<br>• trough cross bedding; storm deposits<br>• exhumed firmgrounds | • these settings are better classified as "tidally modulated shorefaces," as wave action has significant effect on the tide and sediment distribution |
| Carbonate, microtidal, intertidal flats and lagoons (this study; Kumar 2017) | • polychaetes<br>• sand and bubbler crabs<br>• insects<br>• gastropods & bivalves | • *Skolithos*<br>• *Arenicolites*<br>• *Psilonichnus*<br>• crypto-bioturbation | • moderate to high (BI 2 to 6)<br>• bioturbation quickly diminshes in the presence of algal mats in the upper intertidal zone, and goes to 0 further landward | • hypersalinity<br>• subaerial exposure<br>• substrate consistency | • fine grained sediments<br>• abundant bioturbation<br>• abundant fecal pellets<br>• shell accumulations<br>• algal mats<br>• some ripple lamination | • fully marine, restricted tidal flat signatures are similar to a clastic envrionment with far less diversity of traces and tracemakers due to salinity stressors |
| Carbonate meso- and macro- tidal intertidal zones | • not established | • not established | • not established | • not established | • not established | • not established |

*Table 2.2:* ***A comparison of siliciclastic micro- meso- and macro- intertidal zones*** *(defined by tidal ranges of <2 m, 2-4 m and >4 m respectively) to a microtidal carbonate environment.*

From high energy to low energy, stressors transition from physical (turbidity, sedimentation rate) to primarily chemical (salinity, oxygenation). Sedimentological characteristics transition from more firm, coarser sediments with major, higher energy sedimentary structures, to soft, fine sediments with minor sedimentary structures. In high tidal energy environments, animal populations depend more on protection from processes like wave action, exposure, or elevated sedimentation rates, and so their distributions are often concentrated to the energy-sheltered zones. As tidal energy decreases, the threat from physical processes (e.g. wave action) is reduced, whereas the challenges posed by chemical variations may be elevated. Freshwater/brine input, evaporation, and redox potential play significant roles in changing salinity and oxygenation in many low energy environments. Shifts in these parameters make survivability more difficult, thus infaunal distributions are often concentrated in areas with less chemical variability (MacEachern et al. 2007; Gingras et al. 2011).

Save for Knaust (2007), our study of a carbonate microtidal environment is one of few neoichnological studies of low-latitude carbonate environments to date. Conversely, the sedimentology of temperate-zone associated mixed siliciclastic/carbonate and clastic settings is more prevalent in the literature (Button & Vos 1977; Nombela et al. 1995; Hilton & Ming 1999; Rollet et al. 2006; Arribas et al. 2010). The neoichnological discussion of carbonates demands more attention, as subsurface carbonate successions can be difficult to interpret. The continuous addition of neoichnological information to the rock record not only contributes to interpretation of carbonate strata, but also provides valuable ethological data for ichnology in general.

## SUMMARY

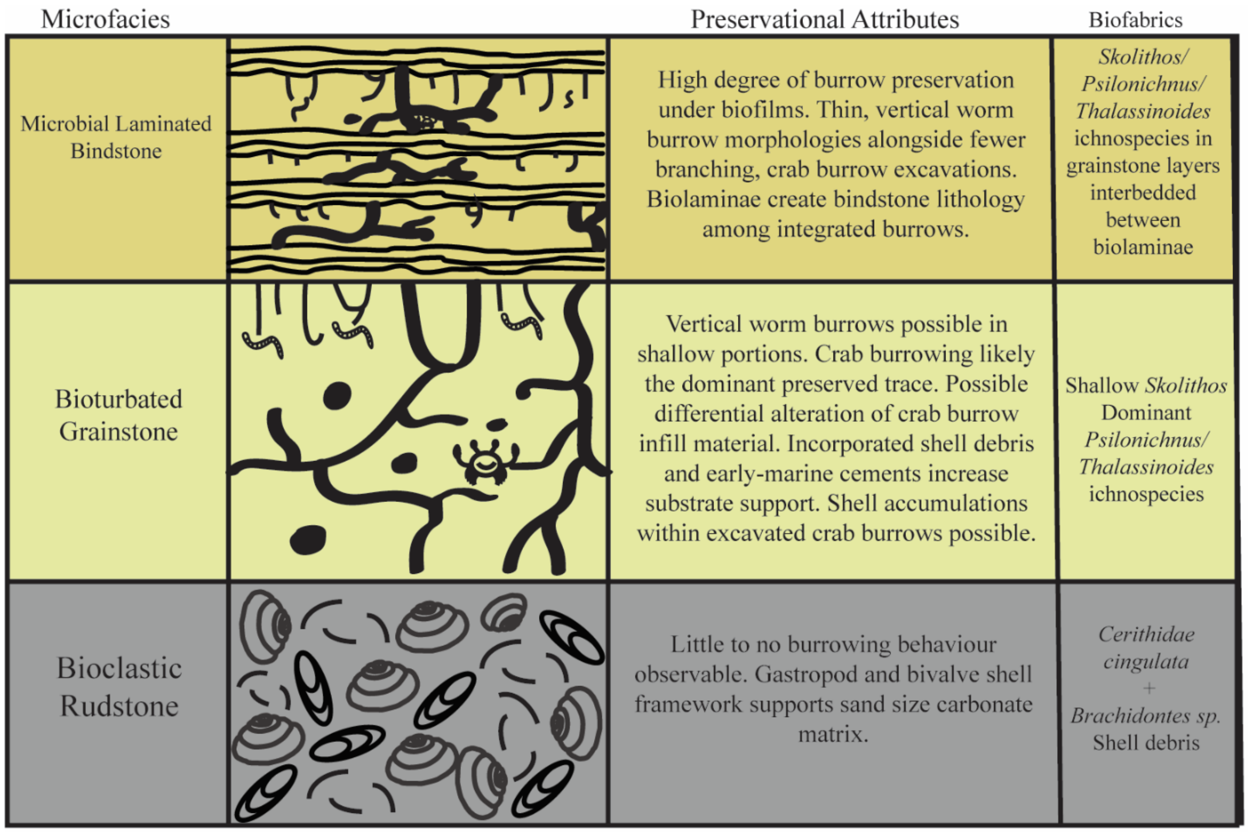


*Figure 2.12:* ***Summary of morphologies of each microfacies*** *and expected preservational attributes for rock record identification, including details of biofabrics and associated trace fossils.*

The Abu Dhabi coast has been a point of geological significance for the past five decades with particular interest in the supratidal "sabkha" (Shearman 1963, 1978, 1980; Evans et al. 1964). Recently, the associated intertidal zone has received more attention (Lokier et al. 2013, 2015; Paul & Lokier 2017), but neoichnology has been relatively understudied. Our study aims to fill this void by combining modern sedimentological, hydochemical and biogenic observations to produce a framework that aids the interpretation of ancient carbonate depositional systems. To do this, we have described the Abu Dhabi intertidal zone using a microfacies approach (Fig. 2.12). Three microfacies occur utilizing the Dunham classification scheme:

1. Bioturbated peloidal grainstone: The archetypal Abu Dhabi intertidal sediment

accumulation consisting of fine-grained sized carbonate sand. The carbonate sand is composed almost entirely of peloidal (fecal-pellet) grains, foraminifera, and shell debris. All allochems are partially to fully coated in isopachous cements. The grainstone is heavily burrowed by both worms and crustaceans. Preservation of the burrowing fabric is largely dependent on the burrowing type, as crustaceans homogenize sediments in the distal sites.

2. Microbial laminated bindstone: This microfacies occurs in the lower-upper intertidal zone. It consists of an alternating, 1 mm thick, fine-grained carbonate sand interbedded between 1 mm thick microbial mats. Microbial mats in the intertidal zone have been attributed to communities of Cyanobacteria, proteobacteria and other specialist bacterias, which change morphologically based on geographic location.

3. Bioclastic rudstone: This microfacies occurs in the intertidal zone above all basal hardgrounds as a bioclastic accumulation, and is interpreted as a transgressive lag deposit. The rudstone consists almost entirely of a shell debris framework supported by a fine-grained sized carbonate sand matrix.

Additionally, a thin surficial mat (MPB) extends throughout the entire intertidal zone within the upper 1 cm of the sediment column. This mat is pale-brown in color and morphologically distinct from the black microbial mats within the upper intertidal zone.

Two burrowing types were observed. One type is formed by the polychaete worm, *Nereis* sp. is responsible for one type, and is found to be concentrated in the lower-upper intertidal zone. Worm burrows display a prior connection to the sediment water interface and are simple. Two crustaceans, the ghost crab (*Ocypoda rtundata*) and the sand bubbler crab (*Scopimera crabricauda*) were responsible for the other burrow type, and are condensed in the upper-lower intertidal zone. Crustaceans excavate burrows for dwelling structures utilizing a backfilling strategy which mixes and homogenizes sediments alongside passive infilling from tidal deposition, making their biofabric difficult to recognize in the substrates. However, infilled material may be more susceptible to secondary processes.

Burrowing morphologies from the Abu Dhabi intertidal zone are simpler, less diverse, and smaller in comparison to other modern environments. The reduction in burrow complexity in Abu Dhabi is attributed to heightened environmental stressors, namely salinity, heat, subaerial exposure, and saline groundwater leakage. Porewaters point to the stabilization of TDS in burrows indicating that infauna irrigate their burrows to cope with increasing salinity. Crustacean burrows are also noted to influence the flow of solutes in the lower intertidal zone by effectively increasing substrate permeability, allowing lower saline waters to penetrate to greater depths.

Given the role of climatic aridity and discharge of continental brines in sites such as the southern Arabian Gulf, we encourage more neoichnological studies of a wider range of carbonate environments. The neoinchnological observations described herein differ substantially from those, for example, in the Bahamas, Australia and cool-water carbonate environments widely used as modern analogues for carbonate successions in the rock record. The addition of modern infaunal studies greatly facilitates the interpretations of complex carbonate strata.

## References

Al Suwaidi, A.S., Hami, M.E., Hagiwara, H., Aziz, S.K., and Al Habshi, A.R. (2010) Carbonates and evaporites of the Upper Jurassic Arab Formation, Abu Dhabi: a petroleum exploration challenge, *Quaternary carbonate and evaporite sedimentary facies and their ancient analogues: a tribute to Douglas James Shearman: John Wiley & Sons, Hoboken, NJ*, 421–429.

Alexander, R.R., Stanton, R.J., and Dodd, J.R. (1993) Influence of Sediment Grain Size on the Burrowing of Bivalves: Correlation with Distribution and Stratigraphic Persistence of Selected Neogene Clams: *PALAIOS*, 8, 289–303.

Alsharhan, A.S., and Kendall, C.G.St.C. (2003) Holocene coastal carbonates and evaporites of the southern Arabian Gulf and their ancient analogues: *Earth-Science Reviews*, 61, 191–243.

Arribas, J., Alonso, Á., Pagés, J.L., and González-Acebrón, L. (2010) Holocene transgression recorded by sand composition in the mesotidal Galician coastline (NW Spain): *The Holocene*, 20, 375–393.

Azer, S.R., Peebles, R. G. 1995) Sequence Stratigraphy of the Hith I Upper Arab Formations Offshore Abu Dhabi, U.A.E. *SPE Middle East Oil and Gas Show and Conference, Bahrain*, SPE-29799-MS.

Beadle, L.C. (1937) Adaptation to Changes of Salinity in the Polychaetes: *Journal of Experimental Biology*, 14, 56–70.

Brush, L.M., Jr. (1965) Sediment Sorting in Alluvial Channels: *SEPM Special Publication*, 12, 25-33.

Buatois, L.A., and Mángano, M.G. (2011) Ichnology: Organism-Substrate Interactions in Space and Time: *Cambridge University Press*, 371.

Butler, G.P. (1969) Modern Evaporite Deposition and Geochemistry of Coexisting Brines, the Sabkha, Trucial Coast, Arabian Gulf: *Journal of Sedimentary Research*, 39, 70-89.

Button, A., and Vos, R.G. (1977) Subtidal and intertidal clastic and carbonate sedimentation in a macrotidal environment: an example from the lower proterozoic of South Africa: *Sedimentary Geology*, 18, 175–200.

Chakrabarti, A., Chakrabarti, R., and Hertweck, G. (2006) Surface traces and bioturbate textures from bubbler crabs: an indicator of subtropical to tropical tidal flat environments*: Senckenbergiana maritima*, 36, 19–27.

Corlett, H.J., and Jones, B. (2012) Petrographic and Geochemical Contrasts Between Calcite- and Dolomite-Filled Burrows In the Middle Devonian Lonely Bay Formation, Northwest Territories, Canada: Implications for Dolomite Formation In Paleozoic Burrows: *Journal of Sedimentary Research*, 82, 648–663.

Dashtgard, S.E., and Gingras, M.K. (2012) Marine Invertebrate Neoichnology: *Developments in Sedimentology: Elsevier*, 273–295.

Davenport, J. (1985) Osmotic control in marine animals: *Symposia of the Society for Experimental Biology*, 39, 207–244.

Desjardins, P.R., Buatois, L.A., and Mángano, M.G. (2012) Tidal Flats and Subtidal Sand Bodies: *Developments in Sedimentology: Elsevier*, 529–561.

El-Sayed M.I. (1999) Sedimentological characteristics and morphology of the aeolian sand dunes in the eastern part of the UAE, a case study from Ar Rub'Al Khali: *Sedimentary Geology*, 123(3-4), 219-238.

Ekdale, A.A., Bromley, R.G., and Pemberton, S.G. (1984) *SEPM Short Course: Ichnology: The Use of Trace Fossils in Sedimentology and Stratigraphy: SEPM (Society for Sedimentary Geology).*

Evans, G. (2005) Douglas James Shearman, 1918–2003: *Proceedings of the Geologists' Association*, 116, 191–205.

Evans, G. (1966) The Recent Sedimentary Facies of the Persian Gulf Region: *Philosophical Transactions of the Royal Society of London. Series A, Mathematical and Physical Sciences*, 259(1099), 291-298.

Evans, G., Kendall, C.G.St.C., and Skipwith, P. (1964) Origin of the Coastal Flats, the Sabkha, of the Trucial Coast, Persian Gulf: *Nature*, 202, 759–761.

Evans, G., Schmidt, V., Bush, P., and Nelson, H. (1969) Stratigraphy and Geologic History of the Sabkha, Abu Dhabi, Persian Gulf: *Sedimentology*,12, 145–159.

Garrison, J., Henk, B., and Creel, R. (2007) Neoichnology of the Micro-Tidal Gulf Coast of Texas: Implications for Paleoecological and Paleoenvironmental Interpretations of Ancient Micro-Tidal Clastic Shoreline Systems: *Gulf Coast Association of Geological Societies Transactions*, 57, 319-330.

Ge, Y., Lokier, S.W., Hoffmann, R., Pederson, C.L., Neuser, R.D., and Immenhauser, A. (2020a) Composite micrite envelopes in the lagoon of Abu Dhabi and their application for the recognition of ancient firm- to hardgrounds: *Marine Geology*, 423, 106141.

Ge, Y., Pederson, C.L., Lokier, S.W., Traas, J.P., Nehrke, G., Neuser, R.D., Goetschl, K.E., and Immenhauser, A. (2020b) Late Holocene to Recent aragonite-cemented transgressive lag deposits in the Abu Dhabi lagoon and intertidal sabkha: *Sedimentology*, 67, 2426–2454.

Gingras, M.K., Baniak, Greg., Gordon, John., Hovikoski, Jussi., Konhauser, K.O., La Croix, Andrew., Lemiski, Ryan., Mendoza, Carl., Pemberton, S.G., Polo, Camilo., and Zonneveld, J.P. (2012) Porosity and Permeability in Bioturbated Sediments, *Developments in Sedimentology: Elsevier*, 837–868.

Gingras, M.K., and MacEachern, J.A. (2012) Tidal Ichnology of Shallow-Water Clastic Settings, *Principles of Tidal Sedimentology: Springer Netherlands, Dordrecht*, 57–77.

Gingras, M.K., MacEachern, J.A., and Dashtgard, S.E. (2011) Process ichnology and the elucidation of physico-chemical stress: *Sedimentary Geology*, 237, 115–134.

Gingras, M.K., Pemberton, S.G., and Saunders, T. (2000) Firmness Profiles Associated with Tidal-Creek Deposits: The Temporal Significance of Glossifungites Assemblages: *Journal of Sedimentary Research*, 70, 1017–1025.

Gingras, M.K., Pemberton, S.G., Saunders, T., and Clifton, H.E. (1999) The Ichnology of Modern and Pleistocene Brackish-Water Deposits at Willapa Bay, Washington: Variability in Estuarine Settings: *PALAIOS*, 14, 352.

Gingras, M.K., Pemberton, S.G., Muelenbachs, K., and Machel, H. (2004) Conceptual models for burrow-related, selective dolomitization with textural and isotopic evidence from the Tyndall Stone, Canada: *Geobiology*, 2, 21–30.

Gingras, M.K., and Zonneveld, J.P. (2015) Tubular Tidalites: A Biogenic Sedimentary Structure Indicative of Tidally Influenced Sedimentation: *Journal of Sedimentary Research*, 85, 845–854.

Goldring, R. (1995) Organisms and the substrate: response and effect: *Geological Society, London, Special Publications*, 83, 151–180.

Grizzle, R.E., Bricelj, V.M., AlShihi, R.M., Ward, K.M., and Anderson, D.M. (2018) Marine Molluscs in Nearshore Habitats of the United Arab Emirates: Decadal Changes and Species of Public Health Significance: *Journal of Coastal Research*, 345, 1157–1175.

Hamza, W., Al Hameli, S., Ramadan, G., and Hameli, M.A. (2018) Coastal Alterations and Its Impact on Diversity of Macrobenthic Fauna in the Intertidal Zone of Abu Dhabi Western Coast (UAE): *Journal of Marine Biology & Oceanography*, 7, 2-11.

Hauck, T.E., Dashtgard, S.E., Pemberton, S.G., and Gingras, M.K. (2009) Brackish-Water Ichnological Trends in a Microtidal Barrier Island Embayment System, Kouchibouguac National Park, New Brunswick, Canada: *PALAIOS*, 24, 478–496.

Hazzouri, K.M., Sudalaimuthuasari, N., Saeed, E.E., Kundu, B., Al-Maskari, R.S., Nelson, D., AlShehhi, A.A., Aldhuhoori, M.A., Almutawa, D.S., Alshehhi, F.R., Balan, J., Mundra, S., Alam, M., Salehi-Ashtiani, K., et al. (2022) Salt flat microbial diversity and dynamics across salinity gradient: *Scientific Reports*, 12, 11293.

Hilton, M.J., and Loke Ming, C. (1999) Sediment Facies of a Low-Energy, Meso-Tidal, Fringing Reef, Singapore: *Singapore Journal of Tropical Geography*, 20, 111–130.

Hodgson, C.A. (2013) Sedimentology and Neoichnology of a Wave-Dominated, Tidally-Influenced, Fully Marine Bay, Oregon, USA, unpublished M.S. thesis, University of Alberta, Edmonton, 312

Hope, J.A., Paterson, D.M., and Thrush, S.F. (2020) The role of microphytobenthos in soft-sediment ecological networks and their contribution to the delivery of multiple ecosystem services: *Journal of Ecology*, 108, 815–830.

Hubas, C., Passarelli, C., and Paterson, D.M. (2018) Microphytobenthic Biofilms: Composition and Interactions, Mudflat Ecology: *Aquatic Ecology Series, Springer International Publishing, Cham*, 63–90.

John, D., and George, J. (2004) Intertidal and subtidal benthic communities in Abu Dhabi: *Marine Atlas of Abu Dhabi*, 94–123.

Kendall, C.S.C., Alsharhan, A. S., Cohen, A. (2002) The Holocene tidal flat complex of the Arabian Gulf coast of Abu Dhabi: *Sabkha Ecosystems*: *The Arabian Peninsula and Adjacent Countries*, 1, 21.

Kendall, C., and Alsharhan, A. (2010) Quaternary carbonate and evaporite sedimentary facies and their ancient analogues: *A Tribute to Douglas James Shearman: John Wiley & Sons, Hoboken, NJ*, 496.

Kendall, C., and Skipwith, P. (1968) Recent Algal Mats of a Persian Gulf Lagoon: *SEPM Journal of Sedimentary Research*, 38, 1040-1058.

Kidwell, S.M., Fursich, F.T., and Aigner, T. (1986) Conceptual Framework for the Analysis and Classification of Fossil Concentrations: *PALAIOS*, 1, 228.

Kinsman, D.J.J., (1969) Modes of Formation, Sedimentary Associations, and Diagnostic Features of Shallow-Water and Supratidal Evaporites1: *AAPG Bulletin*, 53, 830–840.

Kirkham, A., (1998) A Quaternary proximal foreland ramp and its continental fringe, Arabian Gulf, UAE: *Geological Society, London, Special Publications*, 149, 15–41.

Knaust, D. (2007) Meiobenthic Trace Fossils as Keys to the Taphonomic History of Shallow-Marine Epicontinental Carbonates, *Trace Fossils: Elsevier, Amsterdam*, 502–517.

Knaust, D., and Costamagna, L.G. (2012) Ichnology and sedimentology of the Triassic carbonates of North-west Sardinia, Italy: *Sedimentology*, 59, 1190–1207.

Kopcznski, K., Buynevich, I., Curran, H.A., Caris, J., and Nyquist, J. (2017) Imaging Bioturbation in Supratidal Carbonates: Non-Invasive Field Techniques Enhance Neoichnological and Zoogeomorphological Research, San Salvador, The Bahamas: Bollettino della Società *Paleontologica Italiana*, 56, 289–297.

Kristensen, E., and Kostka, J.E. (2005) Macrofaunal Burrows and Irrigation in Marine Sediment: Microbiological and Biogeochemical Interactions, in Interactions Between Macro- and Microorganisms in Marine Sediments: *American Geophysical Union*, 60, 125–157.

Kulkarni, K.G., and Panchang, R. (2015) New Insights into Polychaete Traces and Fecal Pellets: Another Complex Ichnotaxon? *PLOS ONE*, 10, e0139933.

Kumar, A. (2017) Recent biogenic traces from the coastal environments of the southern Red Sea coast of Saudi Arabia: *Arabian Journal of Geosciences*, 10, 500.

Lambeck, K. (1996) Shoreline reconstructions for the Persian Gulf since the last glacial maximum: *Earth and Planetary Science Letters*, 142, 43–57.

Lambiase, J.J., Damit, A.R., Simmons, M.D., Abdoerrias, R., and Hussin, A. (2003) A Depositional Model and the Stratigraphic Development of Modern and Ancient Tide-Dominated Deltas in NW Borneo: *Sedimentology, Stratigraphy, and Petroleum Geology, Special Publication–Society for Sedimentary Geology*, 76, 109–123.

Liu, Y., Jiao, J.J., and Luo, X. (2016) Effects of inland water level oscillation on groundwater dynamics and land-sourced solute transport in a coastal aquifer: *Coastal Engineering*, 114, 347–360.

Lokier, S.W., Knaf, A., and Kimiagar, S. (2013) A quantitative analysis of Recent arid coastal sedimentary facies from the Arabian Gulf Coastline of Abu Dhabi, United Arab Emirates: *Marine Geology*, 346, 141–152.

Lokier, S., and Steuber, T. (2009) Large-scale intertidal polygonal features of the Abu Dhabi coastline: *Sedimentology*, 56, 609–621.

Lucrezi, S. (2010) Ghost crabs as ecological indicators of human stressors on sandy beaches: Ph.D dissertation, University of the Sunshine Coast, Queensland, 360.

Lyster, I.H.J. (1965) The Salinity Tolerance of Polychaete Larvae: *Journal of Animal Ecology*, 34, 517–527.

MacEachern, J.A., Bann, K.L., Gingras, M.K., Zonneveld, J.-Paul., Dashtgard, S.E., and Pemberton, S.G. (2012) The Ichnofacies Paradigm, Developments in Sedimentology: *Trace Fossils as Indicators of Sedimentary Environments, Elsevier*, 103–138.

MacEachern, J.A., Bann, K.L., Pemberton, S.G., and Gingras, M.K. (2007a) The Ichnofacies Paradigm: High-Resolution Paleoenvironmental Interpretation of the Rock Record, Applied Ichnology: *SEPM Society for Sedimentary Geology*, 0

MacEachern, J.A., and Burton, J.A. (2000) Firmground Zoophycos in the Lower Cretaceous Viking Formation, Alberta: A Distal Expression of the Glossifungites Ichnofacies: *PALAIOS*, 15, 387–398.

MacEachern, J.A., Gingras, M.K., Bann, K., Dafoe, L.T., and Pemberton, S.G. (2007b) Applications of Ichnology to High-Resolution Genetic Stratigraphic Paradigms, Applied Ichnology: *SEPM Society for Sedimentary Geology*, 0

Mandal, A., Dutta, A., Das, R., and Mukherjee, J. (2021) Role of intertidal microbial communities in carbon dioxide sequestration and pollutant removal: A review: *Marine Pollution Bulletin*, 170, 112626.

Mángano, M.G., and Buatois, L.A. (2004a) Ichnology of Carboniferous tide-influenced environments and tidal flat variability in the North American Midcontinent: *Geological Society, London, Special Publications*, 228, 157–178.

Mángano, M.G., and Buatois, L.A. (2004b) Reconstructing Early Phanerozoic intertidal ecosystems: ichnology of the Cambrian Campanario Formation in northwest Argentina, Trace Fossils in Evolutionary Palaeoecology: *Fossils and Strata*, Taylor & Francis, 17–38.

Nombela, M.A., Vilas, F., and Evans, G. (1995) Sedimentation in the Mesotidal Rías Bajas of Galicia (North-Western Spain): *Ensenada De San Simón, Inner Ría De Vigo, Tidal Signatures in Modern and Ancient Sediments: John Wiley & Sons, Ltd*, 133–149.

Paterson, D.M., Hope, J.A., Kenworthy, J., Biles, C.L., and Gerbersdorf, S.U. (2018) Form, function and physics: the ecology of biogenic stabilisation: *Journal of Soils and Sediments*, 18, 3044–3054.

Paul, A., and Lokier, S.W. (2017) Holocene marine hardground formation in the Arabian Gulf: Shoreline stabilisation, sea level and early diagenesis in the coastal sabkha of Abu Dhabi: *Sedimentary Geology*, 352, 1–13.

Pederson, C.L., Ge, Y., Lokier, S.W., Swart, P.K., Vonhof, H., Strauss, H., Schurr, S., Fiorini, F., Riechelmann, S., Licha, T., and Immenhauser, A. (2021) Seawater chemistry of a modern subtropical 'epeiric' sea: Spatial variability and effects of organic decomposition: *Geochimica et Cosmochimica Acta*, 314, 159–177.

Pemberton, S.G., and Maceachern, J.A. (2005) Significance of Ichnofossils to Applied Stratigraphy, in Koutsoukos, E.A.M., Applied Stratigraphy: *Topics in Geobiology, Springer, Netherlands*, 279–300.

Pemberton, S.G., MacEachern, J.A., Dashtgard, S.E., Bann, K.L., Gingras, M.K., and Zonneveld, J.P. (2012) Shorefaces, Developments in Sedimentology: *Trace Fossils as Indicators of Sedimentary Environments, Elsevier*, 563–603.

Pemberton, S.G., and Wightman (1992) Applications of ichnology to petroleum exploration—A core workshop: *Society of Economic Paleontologists and Mineralogists, Core Workshop*, 17, 141–67.

Reineck, H., and IB, S. (1980) Depositional Sedimentary Environments with Reference to Terrigenous Clastics, 2, 430–456.

Richter, R. (1936) Marken und Spruren im Hunsriick-Schiefer. II: *Schichtung und Grund-Leben. Senckenbergiana*, 18, 215-244.

Rodríguez-Tovar, F.J., Seike, K., and Allen Curran, H. (2014) Characteristics, Distribution Patterns, and Implications for Ichnology of Modern Burrows of Uca (Leptuca) Speciosa, San Salvador Island, Bahamas: *Journal of Crustacean Biology*, 34, 565–572.

Rollet, N., Logan, G.A., Kennard, J.M., O'Brien, P.E., Jones, A.T., and Sexton, M. (2006) Characterisation and correlation of active hydrocarbon seepage using geophysical data sets: An example from the tropical, carbonate Yampi Shelf, Northwest Australia: *Marine and Petroleum Geology*, 23, 145–164.

Sanders, H. L., Mangelsdorf Jr, P. C., & Hampson, G. R., (1965) Salinity and faunal distribution in the Pocasset River, Massachusetts: *Limnology and Oceanography*, 10, 216-229.

Savrda, C.E. (1991) Ichnology in Sequence Stratigraphic Studies: An Example from the Lower Paleocene of Alabama: *PALAIOS*, 6, 39–53.

Scannell P.W.,, Jacobs, L.L. (2001) Effects of total dissolved solids on aquatic organisms*: Alaska Department of Fish and Game: Division of habitat and restoration*, 01-06

Serk, H. (2008) Community Structures of Microbial Mats in the Sabkha Environment of Abu Dhabi, UAE: unpublished Ph.D dissertation, Newcastle University, Newcastle, 82

Shearman, D.J. (1963) Recent anhydrite, gypsum, dolomite and halite from the coastal flats of the Arabian shore of the Persian Gulf: *Proc. Geol. Soc. London*, 1607(63), 5.

Shearman, D.J.(1978) Evaporites of Coastal Sabkhas: *Evaporites of Coastal Sabkhas*

Shearman, D.J. (1980) Sabkha facies evaporites: *Evaporite Deposits.-Editions Technip*, 19, 96-109.

Shinn, E.A. (1969) Submarine Lithification of Holocene Carbonate Sediments in the Persian Gulf: *Sedimentology*, 12, 109–144.

Smith, C.R., A. Levin, L., Hoover, D.J., McMurtry, G., and Gage, J.D. (2000) Variations in bioturbation across the oxygen minimum zone in the northwest Arabian Sea: Deep Sea Research Part II: *Topical Studies in Oceanography*, 47, 227–257

Smythe, K. R. (1979) The marine Mollusca of the United Arab Emirates, Arabian Gulf*: Journal of Conchology*, 30, 57.

Søndergaard, M. (2009) Redox Potential: Likens, G.E., *Encyclopedia of Inland Waters: Academic Press, Oxford*, 852–859.

Tedesco, L.P., and Wanless, H.R. (1991) Generation of Sedimentary Fabrics and Facies by Repetitive Excavation and Storm Infilling of Burrow Networks, Holocene of South Florida and Caicos Platform, B.W.I.: *PALAIOS*, 6, 326–343

Vallack, H.L. (2021) Physical and biogeochemical drivers of Modern carbonate diagenesis in intertidal sediments of Abu Dhabi: Ph.D. dissertation, University of Bristol, Bristol, 309

Wood, W.W., Sanford, W.E., and Habshi, A.R.S.A. (2002) Source of solutes to the coastal sabkha of Abu Dhabi: *GSA Bulletin*, 114, 259–268.

Yang, B.C., and Chang, T.S. (2018) Integrated sedimentological and ichnological characteristics of a wave-dominated, macrotidal coast: a case study from the intertidal shoreface of the Dongho coast, southwest Korea: *Geo-Marine Letters*, 38, 139–151.

Zonneveld, J.P., Gingras, M.K., Hodgson, C.A., McHugh, L.P., Myers, R.A., Schoengut, J.A., and Wetthuhn, B. (2014) Biotic Segregation in an Upper Mesotidal Dissipative Ridge and Runnel Succession, West Salish Sea, Vancouver Island, British Columbia, Experimental Approaches to Understanding Fossil Organisms: *Lessons from the Living: Topics in Geobiology, Springer Netherlands, Dordrecht*, 169–194.

Zonneveld, J.P., Zaim, Y., Rizal, Y., Ciochon, R.L., Bettis, E.A., Aswan, and Gunnell, G.F. (2012) Ichnological constraints on the depositional environment of the Sawahlunto Formation, Kandi, northwest Ombilin Basin, west Sumatra, Indonesia: *Journal of Asian Earth Sciences*, 45, 106–113.

Zorn, M.E., Lalonde, S.V., Gingras, M.K., Pemberton, S.G., and Konhauser, K.O. (2006) Microscale oxygen distribution in various invertebrate burrow walls: *Geobiology*, 4, 137–145.

# Chapter 3: Modern marine hardground formation in the Abu Dhabi coastal sabkha: Investigating the interaction between sediments and porewaters

## INTRODUCTION

Hardgrounds are traditionally interpreted as lithified seafloor (Christ et al., 2015), and when observed in the ancient rock record, are often interpreted as a depositional hiatus. Hardgrounds form through marine cementation of carbonate sediments and are frequently documented in warm, tropical waters that are saturated with respect to $CaCO_3$ (Garrison et al., 1969; Shinn, 1969; Dravis, 1979; Paul & Lokier, 2017; Ge et al., 2020a,b; Pedersen et al., 2021; Ge et al., 2023). Conventional interpretation of early marine precipitation events are attributed to ideal marine seawater chemistry that favor $CaCO_3$ precipitation at the sediment surface (Shinn, 1969; Kennedy & Garrison, 1975), with more recent studies highlighting the biologic involvement in carbonate precipitation (Dupraz & Visscher, 2005; Dupraz et al., 2009; Paul & Lokier, 2017; Pedersen et al., 2021; Ge et al., 2020b; Diaz & Eberli, 2022; Diaz et al., 2022). Yet, the processes controlling early marine diagenesis are complex and require ongoing research, particularly in shallow marine environments where influence from surface and groundwaters also influence post-depositional processes. Insights into several facets of the early marine, rapid cementation events that take place in contemporary carbonate depositional systems can be gained from the current firmgrounds and hardgrounds that occur in the Abu Dhabi coastal sabkha.

The stratigraphic and sedimentological descriptions of the Abu Dhabi coastal sabkha complex are numerous (Curtis et al., 1963; Evans et al. 1964; Evans 1966; Evans et al. 1969; Azer & Peebles. 1995; Al Suwaidi et al. 2011; Lokier et al. 2013; Paul & Lokier, 2017). In particular, the lagoonal setting and intertidal zone has received attention in recent years (Chapter 2; Lokier & Steuber, 2009; Paul & Lokier, 2017; Ge et al., 2020a,b; Pedersen et al., 2021; Ge et al., 2023), with additional focus on the microbial mats which occur in the upper intertidal zone (Kendall & Skipwith 1968, Dupraz & Visscher, 2005; Lokier & Steuber, 2009; Dupraz et al., 2009; Bontognali et al., 2010; Bontognali et al., 2012). Only recently discussed is the modern bioturbation fabrics that vary along a seaward to landward transect within the intertidal substrates (Chapter 2). Biogenic structures in carbonate sediment, namely burrows, are responsible for variable permeability, sediment mixing, and in some locations, preferential diagenetic alteration (Gingras et al., 2004; Meysman et al., 2006; Zorn, 2010; Corlett & Jones, 2012; Gingras et al., 2012; Baniak et al., 2022). In Abu Dhabi, the Al Qantur lagoonal substrate, which is variably affected by bioturbation, also interacts with twice-daily tides, advecting brines, and rarer meteoric input (Wood et al., 2002; Hippler et al., 2009; Lokier & Steuber, 2009; Pedersen et al., 2021). Despite the role of bioturbation in affecting geochemical processes, the utilization of ichnology within carbonate sedimentological studies is comparatively infrequent. Therefore, recognition of the infaunal influence on carbonate precipitation and diagenesis provides new insights into carbonate depositional systems. In this study, we provide one example of how bioturbation distributions affect the formation and diagenesis of firmgrounds and hardgrounds.

Modern studies of the Abu Dhabi coastal lagoons and intertidal zones document aragonitic firmgrounds and hardgrounds within the shallow subsurface (Chapter 2; Ge et al., 2020a; Pedersen et al., 2021; Vallack, 2021). These observations question the conventional understanding of hardgrounds, and calls for a review of their development outside of exposed seafloor lithification. For any carbonate system, hydrodynamics, chemical, physical, and biological processes are all essential drivers. In many studies, delineating the primary influence is both a goal, and a challenge. To fully understand the system, we must take into consideration all key drivers, as carbonate depositional systems are vulnerable to change by a variety of mechanisms. In particular, it is essential to consider the role of porewater in these systems, which in many studies, is typically inferred rather than measured directly and compared to sediment geochemistry. This study is therefore undertaken with the goal of assessing the interplay of the sediment-water system by assessing both the hydrological and sedimentological characteristics of the Abu Dhabi coastal intertidal zone.

## METHODS

Four sampling sites from the south-western margin of Al Qantur Lagoon were selected based on distinct differences in biogenic and physical sedimentary structures and macrofauna present at the surface. These four sites each represent a distinct component of the Al Qantur intertidal succession. Coring was performed at each study site using two different core barrels. Cores consisted of a 60 cm WaterMark Polycarbonate core barrel (7 cm internal diameter), and a 25 cm long PVC core barrel (10 cm internal diameter). Cores were pressed into the substrate by hand and hammer until reaching the hardground base, or until flush with the sediment surface. Please see Chapter 2 for more detailed descriptions of field methods. Here, we discuss laboratory methods and data collection methods.

Computed Tomography (CT) analyses were performed using a Nikon XTH 225 ST Industrial CT Scanner (Nikon Corporation, Tokyo, Japan) at the Permafrost Archives Sciences (PACS) Lab at the University of Alberta. Results were enhanced using Adobe® Photoshop®. Using the curves and levels tools, CT images were contrasted so that the changes in sediment density were easily distinguishable. No other alterations to the photographs were made.

Microscopic analysis of sediments was executed using the Zeiss Sigma 300 VP-FESEM scanning electron microscope (ZEISS Microscopy, Jena, Germany) at the University of Alberta SEM laboratory. Sediments were placed on low profile SEM pin mounts using an adhesive sticker, blasted with compressed air to remove excess debris and carbon coated.

Thin section analysis was performed using a Nikon Eclipse 50i POL Polarizing Microscope (Nikon Corp., Tokyo, Japan) and photographed using a Nikon DS-Ri2 microscope camera at the University of Alberta.

Raman spectrometry analysis was conducted using Horiba (Horiba, Kyoto, Japan) Xplora Plus Raman Spectrometer-Confocal Raman Microscope at MacEwan University. Parameters for all point and map analysis included 532nm laser, 1800 lines/mm diffraction grating, 100x objective or 50x objective, 300 mm focal length, and 100μm entrance slit width providing a spectral coverage of up to 1912 cm - 1. The 532 nm laser has 100mW of power at the source and its power outage can be modified by using custom laser filters from 0.1% (lowest laser power) to 100% (highest laser power). Laser power could only be estimated as a custom filter of 10% was used to reduce the laser power to ~ 10mW. Point spectra were obtained with 6 accumulations over 2s of acquisition time and Raman maps were created with SWIFT mode (1s acquisition time and 1 accumulation). Spectral peak positions were calibrated using a silicon wafer and peak fitting was conducted in Labspec 6 spectroscopy-suite software. Observed Raman peaks were compared to literature and the RRUFF database (https://rruff.info/) to determine mineral phases.

Inductively coupled plasma mass spectrometry (ICP-MS) was performed using an Agilent 8800 ICP-MS/MS (Agilent Technologies, Santa Clara, California, USA) at the University of Alberta. During analysis, the RF power was set to 1550 W and the reflected power was 18 W. Samples were aspirated with a micromist nebulizer and nickel/copper cones were used. MS/MS mode was used for sample analysis to acquire greater mass resolution, and the gas collision/reaction cell was utilized with either He, $O_2$ or $H_2$ gas depending on the element. To account for instrument drift, a standard solution of 0.5 ppm indium (In) was added to each sample utilizing an inline addition system.

Samples were extracted from core in centimeter increments and removed of all shell debris. Samples were then placed onto 50 micron filter paper and rinsed with DI water. The samples were then dried in a fumehood until no moisture remained. Samples were prepared for ICP-MS by adding 100 mg of sediment to 50 mL falcon tubes. Three mL of HCL (37 %) and 1 mL HNO3 (70 %) were added to each tube and swirled (not shaken). Samples were re-capped loosely, not completely sealed, and left in a fume hood overnight. The following day, samples were topped with DI water to 50 mL, swirled, and left in the fume hood again overnight. Samples were then centrifuged at 3000 rpm for 10 minutes, and 5 g of supernatant were syringed out and combined with 5 g of acid (2 % HNO3 and 0.5 % HCL) for a total of 10 g liquid used in ICP-MS analysis.

Water chemistry was measured in the field using a Hach Portable Multi-Parameter Meter (Hach Company, Loveland, Colorado, USA) with Intellical probes recording oxidation redox potential (ORP/Redox; MTC101, accuracy ± 5 mV), specific electrical conductivity (SEC; CDC401, accuracy ± 0.5%) and temperature (accuracy ± 0.3 °C). These instruments were also used to measure groundwaters that are confined by the shallow (40-50 cm) hardground from seven previously drilled groundwater wells. Depth of ITZ wells are 3.5 and 6.8 m below sediment surface, CR wells are 1.04 and 2.98 m deep, and PW wells are 2.73 m in the subsurface (Fig. 1.1). These instruments were also used to measure porewater samples in the field laboratory. Porewaters were extracted through Rhizon CCS porewater samplers (Rhizosphere Research Products, Wageninge, Netherlands) which consist of a hydrophilic porous tip (length 5 or 10 cm) with a pore size of 0.12–0.18 μm and into 60 ml syringes. At each study site Rhizons were inserted horizontally into the substrate at intervals of typically 2 cm in a vertical line from the shallow subsurface until insertion was impeded by either the upper surface of the hardground or a layer containing significant shell debris. Porewater samples were capped and stored in the syringes they were collected in to avoid atmospheric exchange. Surface water samples were collected in HDPE bottles and filtered through Millex-GP PES Millipore Express membrane hydrophilic syringe filters with a pore size of 0.22 μm. All samples were collected during daylight hours (7:00 to 17:00) during spring tides (November, 2021). All water samples were refrigerated and returned to the field laboratory where porewater SEC and ORP were measured from an aliquot expressed from each syringe (allowing up to 1 hour for ORP measurements to stabilize) in isolation from atmospheric exchange. The total dissolved solids (TDS) was calculated from Specific Electrical Conductivity using a site specific non-linear relationship based on analysis of 101 water samples from the study area (TDS (g/KgW) = 0.00296 x SEC + 0.518 x SEC (mS/cm)).

X-Ray diffraction analyses were performed using two different instruments due to availability. The sample labeled "THGT" was measured using a Bruker D8 Advance (Bruker, Billerica, Massachusetts, USA) instrument using a cobalt tube anode at 35 kV and 40 mA for the radiation source. Wavelength's (Å) are: $K\alpha_1$ (100): 1.78897; $K\alpha_2$ (50): 1.79285; and $K\beta_1$: 1.62079. Bragg Brentano was used as the focusing geometry method with a 250 mm goniometer. A LYNXEYE_XE_T (1D), K-beta digitally filtered detector was used with a detector opening of 3.305° (lower discriminator: 0.674 V; upper discriminator: 0.724 V). The primary and secondary Soller slits were placed at 2.5°. The divergence slit is adjusted for 0.340°, and the antiscatter slit is 18.000 mm with an automatic airscatter screen. The scan mode was continuous and ranged from 3 to 80° on a scan axis of 2Θ/Θ. Sampling width (step size) was 0.0200° with a scan speed of 1.00 s/step with no spin. Samples were back loaded.

All other samples were measured using the Rigaku Ultima IV (Rigaku, Tokyo, Japan) using a cobalt tube anode at 38 kV and 38 mA for the radiation source. Wavelength's (Å) are: $K\alpha_1$ (100): 1.78900; $K\alpha_2$ (50): 1.79283; and $K\beta_1$: 1.62083. Bragg Brentano was used as the focusing geometry method with a D/Tex Ultra detector using an Fe filter (K-beta filter). The divergence slit is 2/3°, and the divergence height limiting slit is 10 mm. The scattering and receiving slits were open. The scan mode was continuous and ranged from 5 to 90° on a scan axis of 2Θ/Θ. The steep size was 0.0200° with a scan speed of 2.00 °/min and no spin. Samples were front loaded into well mounts. Data was converted using JADE MDI 9.6 software. Phase identification was performed using DIFFRAC.EVA V5 software using the 2022/2023 ICDD PDF 4+and PDF +/Organics databases.

Total DNA was extracted from the samples using a DNEasy PowerSoil Pro Kit (Qiagen, Hilden, Germany), following the kit protocol. Following extraction, DNA concentrations were determined using the QuBit dsDNA HS Assay Kit™ on a Qubit 3.0. Bacterial community composition was analyzed using 16S rRNA gene sequencing. The V3V4 hypervariable region of the 16S rRNA gene was targeted, with primers containing a six-base index sequence for sample multiplexing 1,2. Sequencing was conducted at the High Content Analysis Core facility (University of Alberta), where a 4.5 pM library containing 50% PhiX Control v3 was sequenced on a MiSeq instrument (Illumina Inc., CA, USA) using a 2 × 300 cycle MiSeq Reagent Kit v3 (Illumina Canada Inc). The MiSeq reads were demultiplexed using the MiSeq Local Run Manager (Windows 10). Outputs from sequencing were analyzed using QIIME2 v.2021.4 3 Cutadapt was used to trim adapters and primers from the raw forward and reverse reads, which were then truncated, denoised, merged through their overlaps, and filtered for chimeras using and DADA2 denoise-paired commands 4. Amplicon sequence variants were generated by clustering sequences using the q2-feature-classifier and classified using the SILVA (v.138, 2019) reference database 2,5. Data analysis and figure generation for the ASV dataset was conducted in R (4.1.2) 6 . For general data-manipulation and visualization, the following packages were used: plyr, tidyverse, ggplot2, ape, dplyr, vegan, and magrittr 7-15. Composition of the microbial communities was assessed through comparison of average relative abundance.

## RESULTS

The physical bioturbation fabric from cores removed from the study area and a variety of geochemical analyses are used to evaluate fluid flow and diagenetic drivers in the shallow subsurface of the intertidal zone. We present the findings of porewater and groundwater compositions alongside sediment, firmground, and hardground geochemistry to understand the post-depositional exchange between these phases. Carbonate microfacies described from the cored sediment are described using Dunham's classification scheme (1962), with additions from Embry and Klovan's modification (1971). Dunham classifications provided in this study are for unlithified, loose sediments taken from study sites in the intertidal zone on the basis of the inferred texture they would resemble when lithified.

# Geochemical and Physical Characteristics of Sediments and Hardgrounds

## *Bioturbation fabrics*

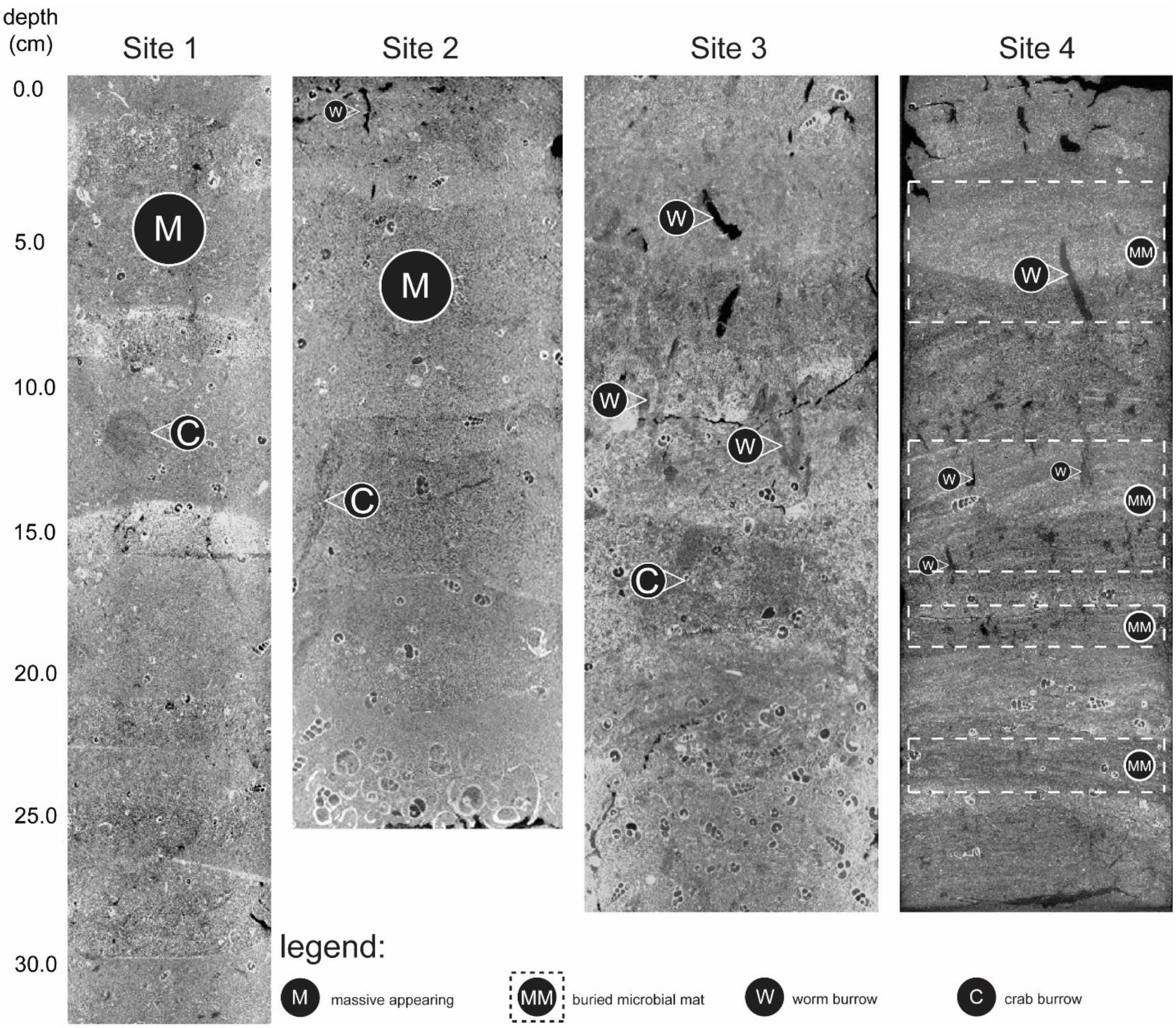


*Figure 3.1:* ***CT images of the four study sites are presented side-by-side with labeled burrow types and biogenic fabrics.*** *Sites 1 & 2 generally lack distinct sedimentary structures, and are regarded as "massive appearing," apart from isolated crab burrows. Site 3 is primarily worm burrowed, and although only three worm burrows are labeled, all vertical, linear, darker-colored features surrounding the labels are also worm burrows. Only one observed crab burrow is labeled in Site 3. Site 4 is characterized by horizons of buried microbial mat material, which have been outlined by white boxes. CT imaging is performed at different intervals, and so slices of the same core are stitched together. The stitching process may result in image amalgamation, potentially misrepresenting the true fabric. Therefore, the precise outlining of buried mat horizons is based on their original observation from the exposed core.*

CT scans (Fig. 3.1) reveal distinct burrow types, microbial mat horizons, shells, and sedimentary features. In Sites 1 and 2, we observe one worm burrow in the shallow subsurface and two crab burrows at 10-15 cm depth. Crustaceans, particularly in Sites 1 and 2, are the primary burrowers, and produce a massive texture. Site 3 exhibits abundant worm burrows throughout the section, with a larger crab burrow at approximately 17 cm depth. Site 4 is characterized by buried microbial mat horizons at various depths (3-7 cm, 12-16 cm, 18-20 cm, and 23-25 cm). Diminutive worm burrows were observed within these microbial mat horizons. For a more comprehensive analysis of burrow morphologies and infaunal trophic strategies in the Al Qantur lagoon, please see Chapter 2.

The burrows are found in the bioturbated peloidal grainstone microfacies and the microbial laminated bindstone represents horizons of buried microbial mats. Bioclastic rudstones, composed of mollusc shells, occur at the base of all the sediment cores, except Site 1, where the core was not long enough to penetrate to the deeper bioclastic layer at ~ 50 cm depth. All bioclastic rudstones overlie the basal hardground. More detailed descriptions of each sediment core and the location of microfacies are reported in Chapter 2.

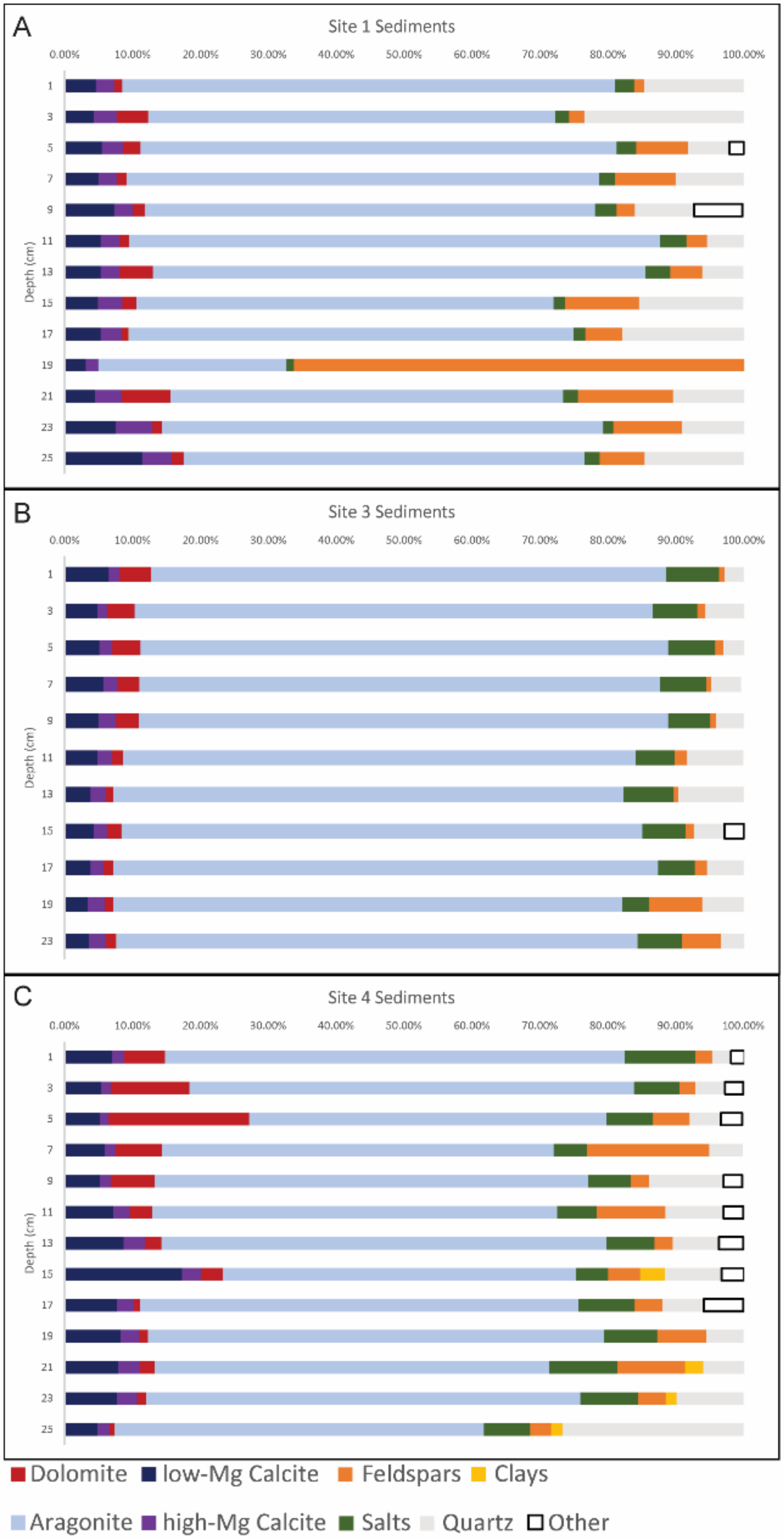


*Figure 3.2:* ***X-Ray diffraction of sediments from Sites 1 (A), 3 (B) & 4 (C).*** *Site 2 was not analyzed due to the previously noted chemical similarity to Site 1. Salts encompass halite, gypsum, anhydrite and sylvite, however halite is the dominant salt, and the others were only found in minor amounts. Feldspars include albite, anorthite and microcline, with albite being the most common feldspar. Clays include illite, kaolinite, palygorskite, clinochlore, and pyrophyllite but were only noted in minor amounts. Other minerals were minor and attributed to detrital processes.*

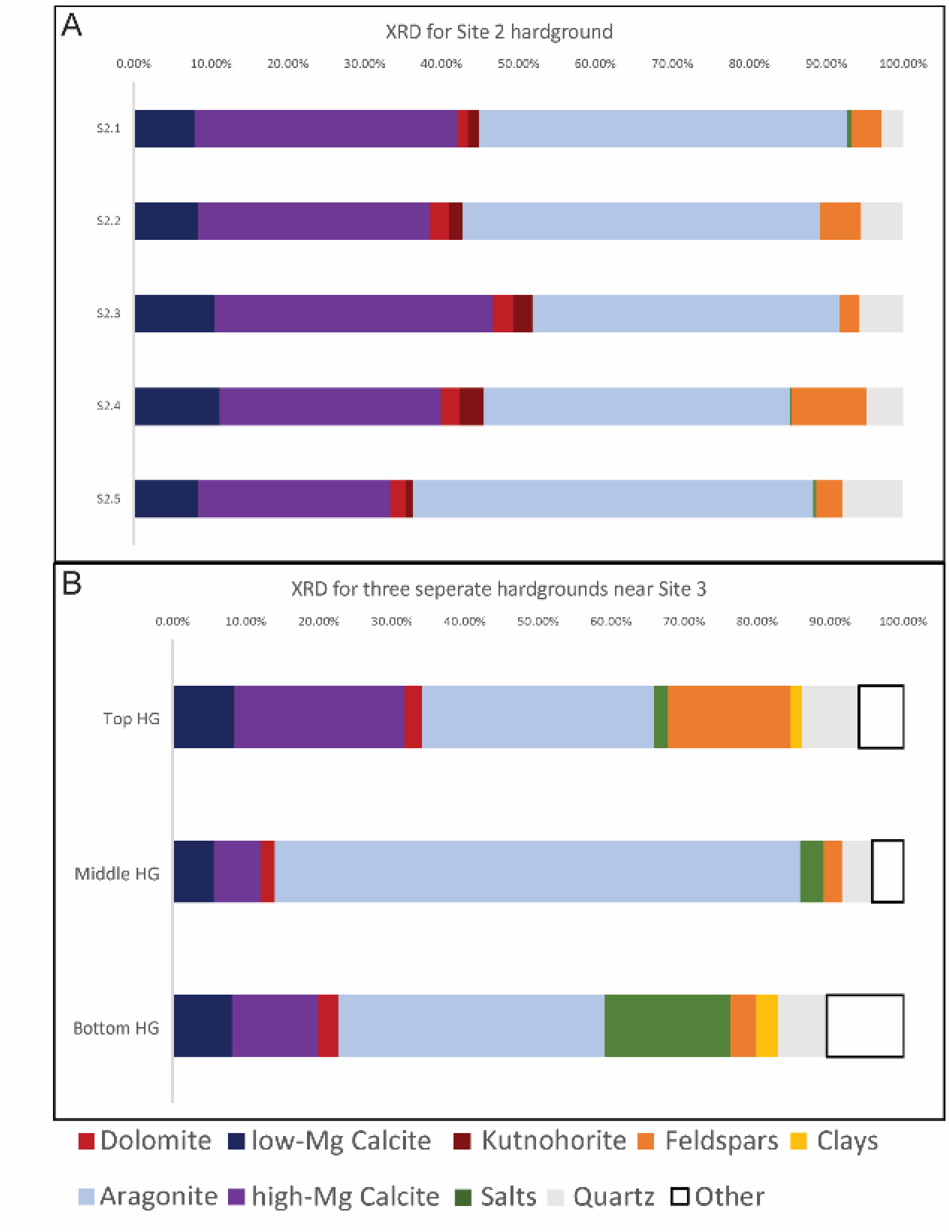


*Figure 3.3:* ***X-Ray diffraction of hardgrounds****.* ***A)*** *Hardground sampled from near Site 2 (Fig. 1D). This hardground was sampled vertically, where S2.1 represents the top of the hardground, and S2.5 is the bottom of the hardground, with sampling intervals in cm's.* ***B)*** *Three separate hardgrounds samples from near Site 3 (Fig. 1D). Three vertically stacked hardgrounds were discovered beneath intertidal sediments near a tidal channel. These are referred to as 'Top HG' (THGT), 'Middle HG' (THGM), and 'Bottom HG' (THGB). Mineral descriptions align with those provided in Figure 3.1.*

## *Sediment and hardground mineralogy*

X-Ray diffraction measurements from the study sites 1, 3 & 4 (Fig. 3.2), and four different hardgrounds (Fig. 3.3) are presented. Additional XRD plots of solely carbonate minerals are provided in Figure 3.9. Primary a) andte cements are the most readily observed precipitates within our study (Fig. 3.4) and occur as the major carbonate mineral in our samples, while Mg-calcites and dolomites are the minor carbonate minerals (Figs. 3.2, 3.3).

In the Site 1 sediments (Fig. 3.2A), aragonite weight % is more or less constant throughout the sediment column at 63.52 +/- 14.68 %. At 19 cm depth, Site 1 aragonite is anomalously 27.7 %, which is probably a misrepresentation due this particular sample submission containing comparatively heightened feldspar concentrations. Low Mg-Calcite increases from 1 to 9 cm, ranging from 4.6 % to 7.3 %, then decreases to 3.1 % at 19 cm before enriching to 11. 4% at 25 cm. High Mg-Calcite decreases from 1 to 19 cm from 2.7 +/- 0.9 % to 1.9 %, followed by an increase to 5.4 % at 23 cm and a slight decrease to 4.4 % at 25 cm. Dolomite exhibits minor variations, peaking at 3, 13, and 21 cm depths with concentrations of 4.6 %, 4.9 %, and 7.2 %, respectively. In other depths, Dolomite ranges from 1 to 2.6 %. Salts are generally higher in concentration from 1 to 13 cm depth (2 to 3. 6%), whereas beyond 13 cm, they average 1.7 +/- 0.4 %. Feldspars, Quartz, and other detrital minerals do not show specific trends.

In the Site 3 sediments (Fig. 3.2B), Aragonite is constant at 76.7 +/- 4.5 %. Low Mg-Calcite and Dolomite decreases down section from 6.5 to 3.6 %, and 4.6 to 1.5 %, respectively. High Mg-calcite increases down section from 1.6 to 2.5 %. Salts are generally more concentrated in the upper 1 to 13 cm, however they do not show a significant variation, and are measured at 5.7 +/- 1.2 %. Feldspars increase down section from 0.8 to 7.8 %, with the largest concentrations at 19 & 23 cm depth. Quartz and other detrital minerals do not show any significant trends.

Site 4 sediments (Fig. 3.2C) are again dominated by Aragonite (61 +/- 8.9 %), with a significant dolomite presence in the shallow subsurface. Dolomite becomes increasingly enriched from 1 to 5 cm from 6.0 to 20.7 %, the highest amount of dolomite recognized in the sediment samples. From 7 to 25 cm, dolomite decreases from 6.9 to 0.8 %. Low Mg-calcite increases from 1 to 13 cm from 7 to 17.3 %, followed by a decrease to 4.8 % at 25 cm depth. High Mg-calcite generally increases down section from 1.4 to 3.2 +/-0.4 %.

Salts, Feldspars, clays, Quartz and other detrimental minerals do not display any notable trends.

In the Site 2 hardground (Fig. 3.3A), no significant vertical trends are observed. Low Mg-Calcite measures 10.5 +/- 2.6%, high Mg-Calcite accounts for 30.2 +/- 6%, Dolomite is minimal at 2.5 +/- 1.2%, and Kutnohorite (Mn-dolomite) is even less prominent at 1.8 +/- 1.3%. Salts, Feldspars, and other detrital minerals do not exhibit any specific patterns.

Distinct trends are not observed in the comparison of three different hardgrounds (Fig. 3.3B) near Site 3 (Fig. 1.1D). High-Mg calcite is most abundant in the top hardground at 23.3%, while the middle is most depleted at 6.5%, and the bottom slightly increases to 11.8%. Aragonite is most abundant in the middle hardground at 71.9%, while the top and bottom hardgrounds are more similar at 31.8% and 36.6%, respectively. Low Mg-calcite is most concentrated in the top hardground at 8.4%, while the middle and bottom are similar at 5.6% and 8.1%, respectively. In addition to a specific enrichment of feldspars in the top (THGT) hardground and relatively higher salts in the bottom (THGB) hardground, the other minerals show no significant variations.

## *Carbonate cements and hardground textures*

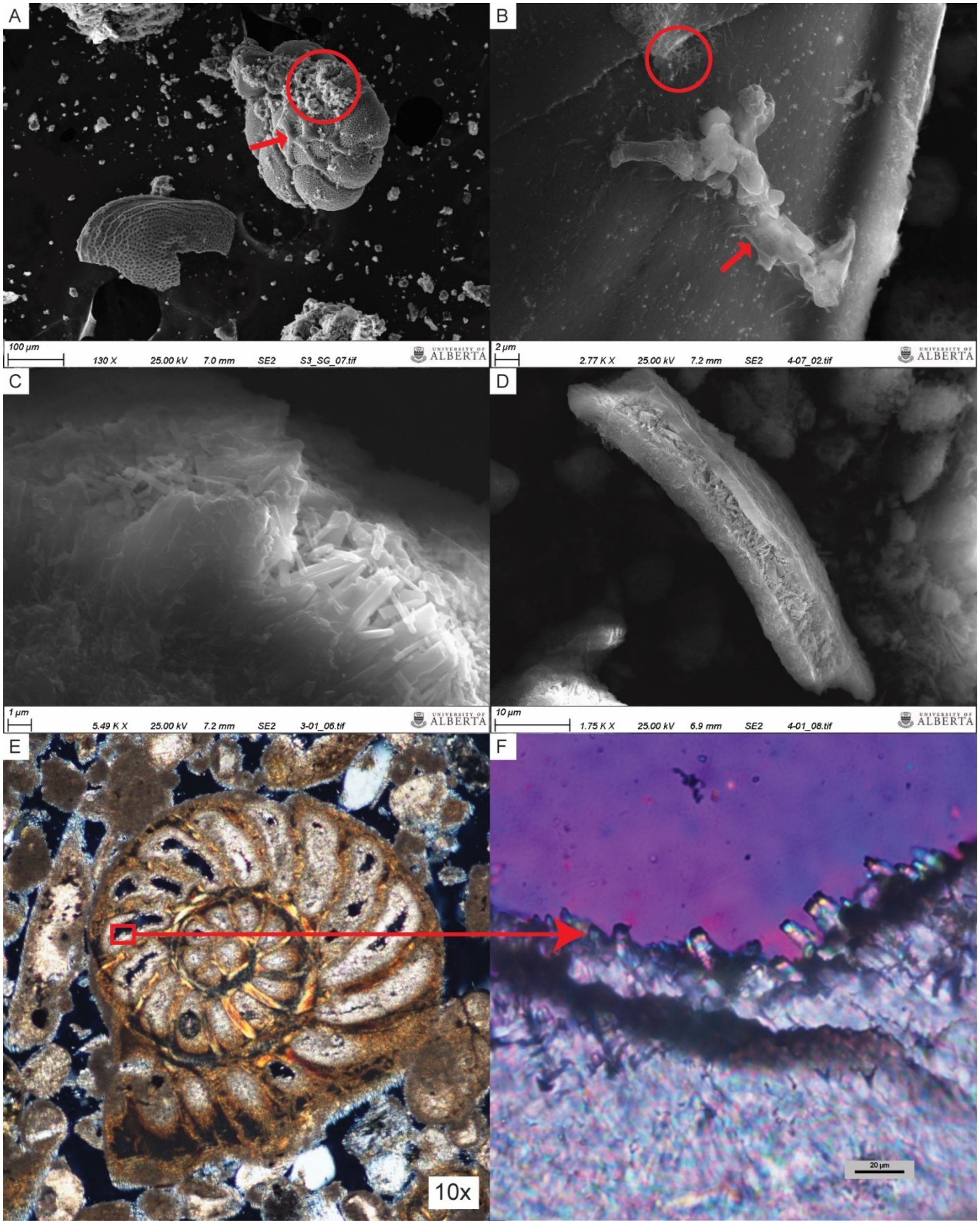

*Figure 3.4:* ***Six images illustrate key features of intertidal sediments under the Scanning Electron Microscope (A to D) and thin sections of a hardground (sample THGT) (E to F).*** *Red circles highlight areas where acicular aragonite is observed, and red arrows indicate EPS veneers.* ***A)*** *Depicts foraminifera with EPS and aragonite growth occurring on the surface, accompanied by broken foraminifera and clumps of carbonate in the background.* ***B)*** *EPS and aragonite growth on the exterior of a bioclast.* ***C)*** *Acicular aragonite on a peloid, featuring variable crystal orientation and platy edges.* ***D)*** *Displays a cross-section of a bivalve shell with acicular aragonite between shell walls, again revealing sporadic crystal orientation.* ***E)*** *Reveals foraminifera exhibiting two cement types: micritic calcite enveloping the foram and some surrounding peloids, alongside acicular aragonite within foram chamber walls, highlighted in a red box.* ***F)*** *Offers a closer view of the red box in E, showcasing the aragonite growth within foraminifera chambers.*

Figure 3.4 is a compilation of SEM photos from Site 3 and 4 sediments (A to D), and thin section photos (E to F) taken of hardgrounds near Site 2 (Fig. 1.1D). Figure 3.5 illustrates the same hardground using Raman spectroscopy. Generally, our observations indicate the majority of crystalline carbonate material is acicular aragonite, with calcite and high-Mg calcite occurring as "halos'' surrounding bioclasts or as micrite. Acicular aragonite crystals commonly line the interior and exterior chamber walls of bioclasts (Fig. 3.4B), foraminifera (Fig. 3.4A), and surrounding extracellular polymeric substances (EPS) (Figs. 3.4A,B). Calcite is more commonly located on the exteriors of foraminifera and bioclasts, within lime-mud, or as carbonate grain coatings (Figs. 3.4E; 3.5B).

EPS is observed coating foraminifera and accumulating on the exterior of gastropod shells and other carbonate grains (red arrows, Figs. 3.4A,B). Acicular aragonites are commonly seen in proximity to EPS growth (red circles, Figs. 3.4A, B). Acicular aragonite crystals are also observed on peloids (Fig. 3.4B) and lining bivalve shells (Fig. 3.4D). One foraminifera observed in thin section displays two different cement phases. Micritic calcite is found on the brown, exterior edges of the shell (Fig. 3.4E), while acicular aragonite needles are lining the interior chambers (red box Figs. 3.4E,F).

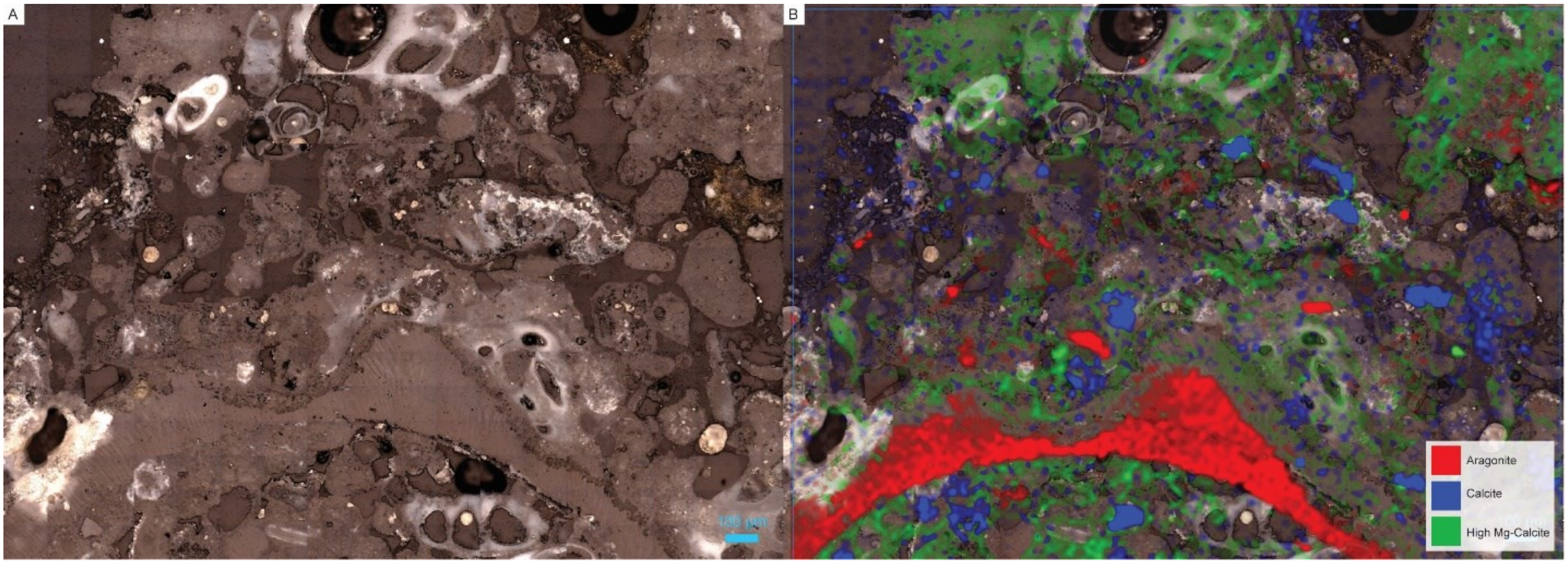


*Figure 3.5:* ***Raman spectroscopy of the hardground "Triple Hardground Top (THGT)." A)*** *The original hardground image with no overlay, features epoxy at the top left corner, denoted by a dark-brown color, which extends across the image, emphasizing sample porosity. Lighter-browns, whites, and yellows represent hardground grains, while black circles indicate air bubbles.* ***B)*** *The same image is superimposed with Raman-identified carbonate phases. A significant feature is the large red aragonitic grain, representing a bivalve shell's edge. White halos, commonly encircling foraminiferal grains, consist primarily of high-Mg calcite, while other calcites are found in the matrix cements.*

Raman spectroscopy differentiates carbonate mineral phases within one section of the Site 2 hardground (Fig. 3.5). One bivalve shell observed in the section is composed of aragonite, and the other aragonite grains are assumed to be peloids. High-Mg calcite is observed surrounding bioclastic debris, as well as in areas of lime-mud accumulation. Low-Mg Calcite also occurs within the matrix of the hardground.

Hardground samples "THG" were taken in proximity to Site 3, and "S2" was removed from near Site 2 (Figs. 1D & 3.6). The dominant grain types found in each hardground sample in order of decreasing abundance are peloids, foraminifera, and molluscs. Additionally, clastic detrital grains are observed near the edges of the thin section THGB, marked by a red box (Fig. 3.6). Hardgrounds observed in thin section are notably porous with intra- and intergranular pore types.

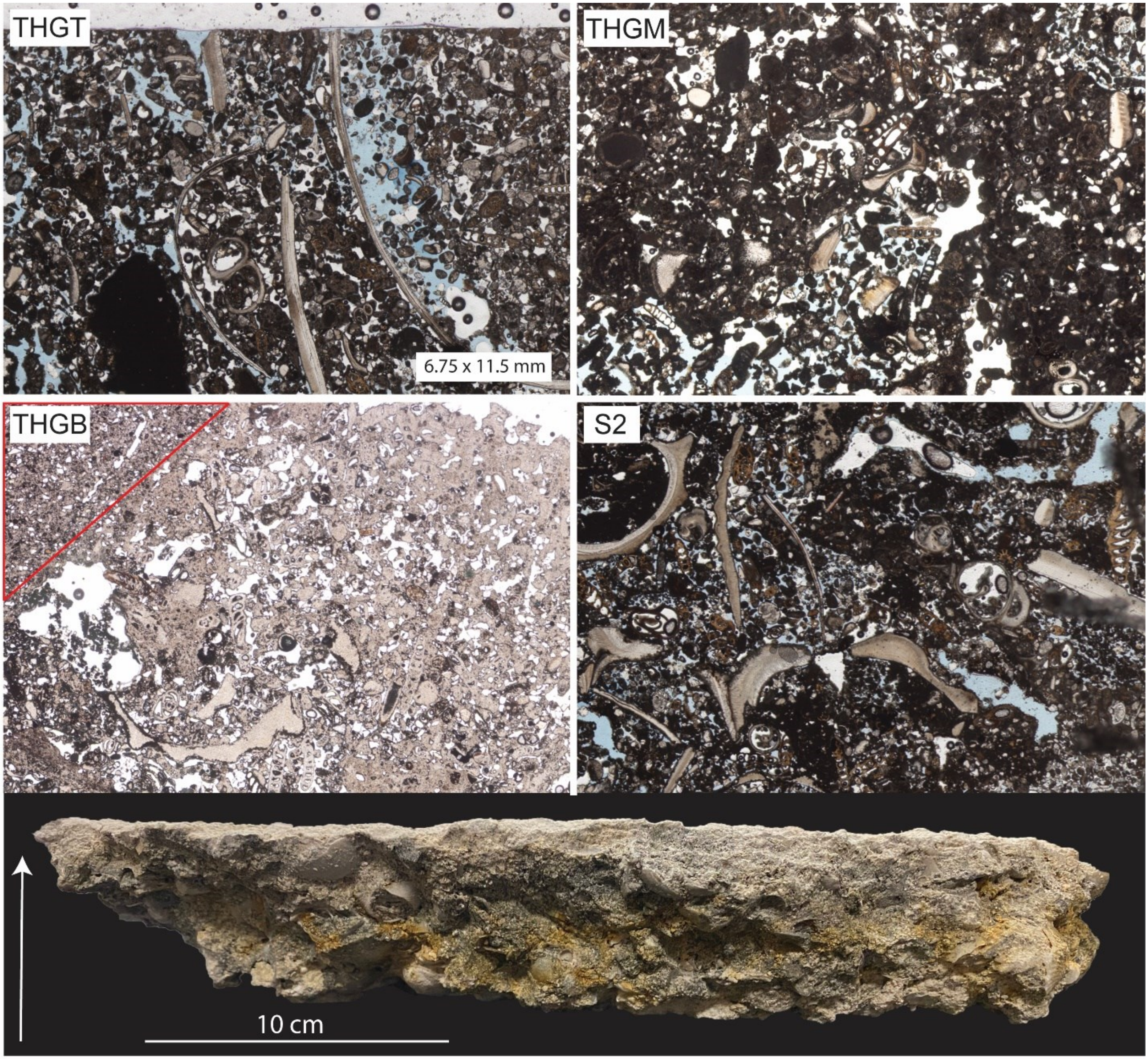


*Figure 3.6:* ***Thin section scans of the four sampled hardgrounds and hand sample*** *(Fig. 1D). All scans are presented top-up and are 6.75 x 11.5 mm. Note the substantial porosity and bioclastic composition. Bioclasts are mainly mollusc shells and foraminifera with more minor peloids. The red triangle indicates detrital grain accumulations. Below the thin section scans is a cross section of the "THGT" hardground. Note the planar upper surface and discontinuous bottom surface.*

### *Sediment manganese and iron fluxes*

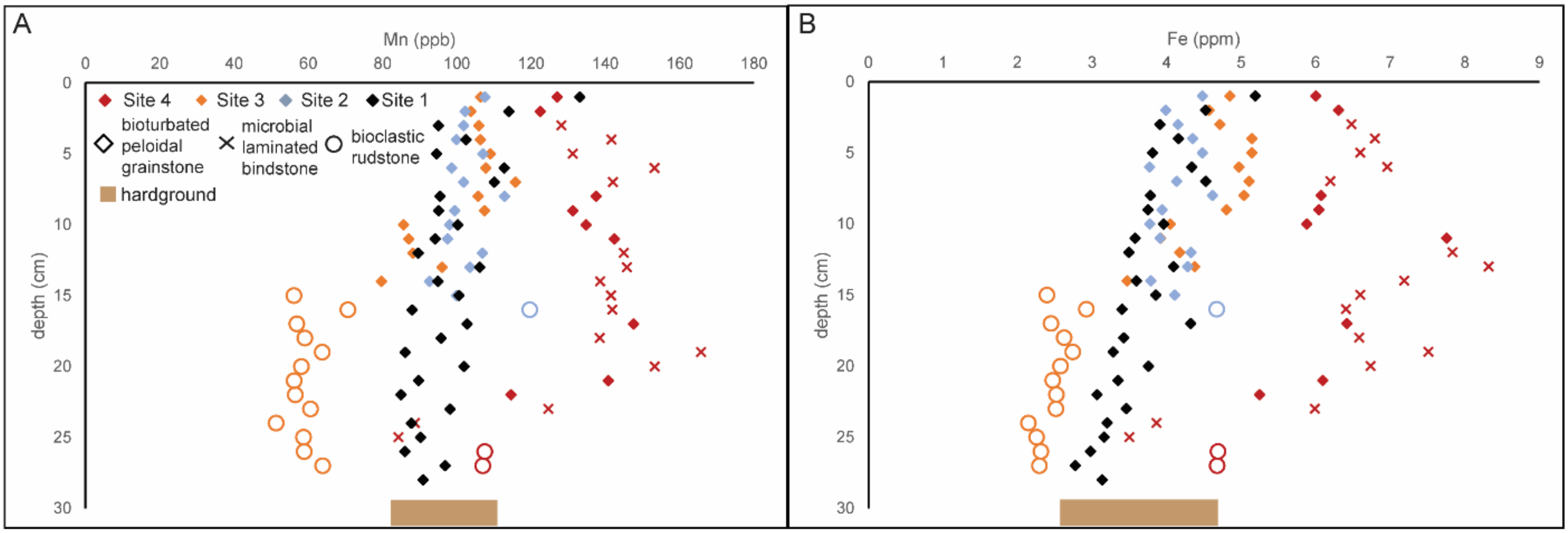


*Figure 3.7:* ***Systematic changes in the concentration of Mn and Fe in the intertidal sediments with depth****. Note how the Site 4 fluxes correspond to buried microbial mat horizons, and how major reductions of both elements occur in Site 3 past 15 cm depth within the bioclastic rudstone microfacies. Error bars are smaller than the data points.*

Manganese (Mn) and iron (Fe) concentrations from the sediments are presented in Figure 3.7. Generally, in Sites 3 and 4, Mn and Fe are enriched in the shallow subsurface and then decrease with depth. In Sites 1 and 2, there is little variation between the elements.

Overall, Mn varies in the sediment column from 51.30 ppb to 165.77 ppb (Fig. 3.7A). In Site 4, Mn concentrations range from 84.29 to 165.77 ppb. Mn fluctuations at this site include a minor reduction at 1 to 2 cm (from 127.04 to 122.47 ppb), followed by an enrichment to 153.25 ppb at 6 cm. A subsequent depletion occurs until 9 cm, followed by an overall enrichment of Mn to 165.77 ppb at 19 cm. A major depletion is then measured to 84.29 ppb at 25 cm, followed by an enrichment to the maximum depth of 27 cm at 106.97 ppb. In Site 3, Mn varies from 51.30 to 115.77 ppb. A minor enrichment of Mn begins at 1 to 7 cm (from 106.42 to 115.77 ppb), followed by a minor depletion until 10 cm depth at 85.67 ppb, and a subsequent increase to 13 cm at 96.06 ppb. This is concluded by a major depletion of Mn to the maximum depth of 27 cm, reduced to 58.13 ppb +/- 5.7 ppb. In Sites 1 and 2, Mn concentrations are fairly consistent within the sediment column, ranging from 100 +/- 20 ppb, with a shallow outlier in Site 2 at 1 cm depth, measured at 133.10 ppb.

Fe follows similar trends to Mn in the study sites (Fig. 3.7B). In Site 4, Fe concentrations range from 3.50 to 8.32 ppm. Initially, Fe becomes enriched from 6.00 to 6.96 ppm at 1 to 6 cm depth, followed by a reduction to 5.88 ppm at 10 cm depth. A major enrichment occurs in the following 3 cm, reaching 8.32 ppm. From 13 to 17 cm, another reduction occurs, reaching 6.42 ppm, followed by a minor enrichment to 7.51 ppm at 19 cm. There's an Fe reduction to 5.25 ppm from 19 to 22 cm, followed by a quick increase to 5.99 ppm at 23 cm and a final reduction to 3.50 ppm at 25 cm. Fe is enriched to the maximum depth of 27 cm at 4.68 ppm in Site 4. In Site 3, Fe concentrations range from 2.15 to 5.14 ppm. Fe decreases rapidly from 1 to 2 cm to 4.52 ppm, followed by an enrichment to 5.04 +/- 0.24 ppm at 8 cm. From 8 to 10 cm, there's a reduction to 3.96 ppm, followed by an increase to 4.28 ppm at 13 cm depth. The final variance in Fe concentrations in the sediment column at Site 3, down to the maximum depth of 27 cm, is measured at 2.58 +/- 0.43 ppm. Sites 1 and 2 again show little fluctuation in their Fe concentrations throughout the sediment column, generally measuring at 4.40 +/- 0.79 ppm in the distal sites.

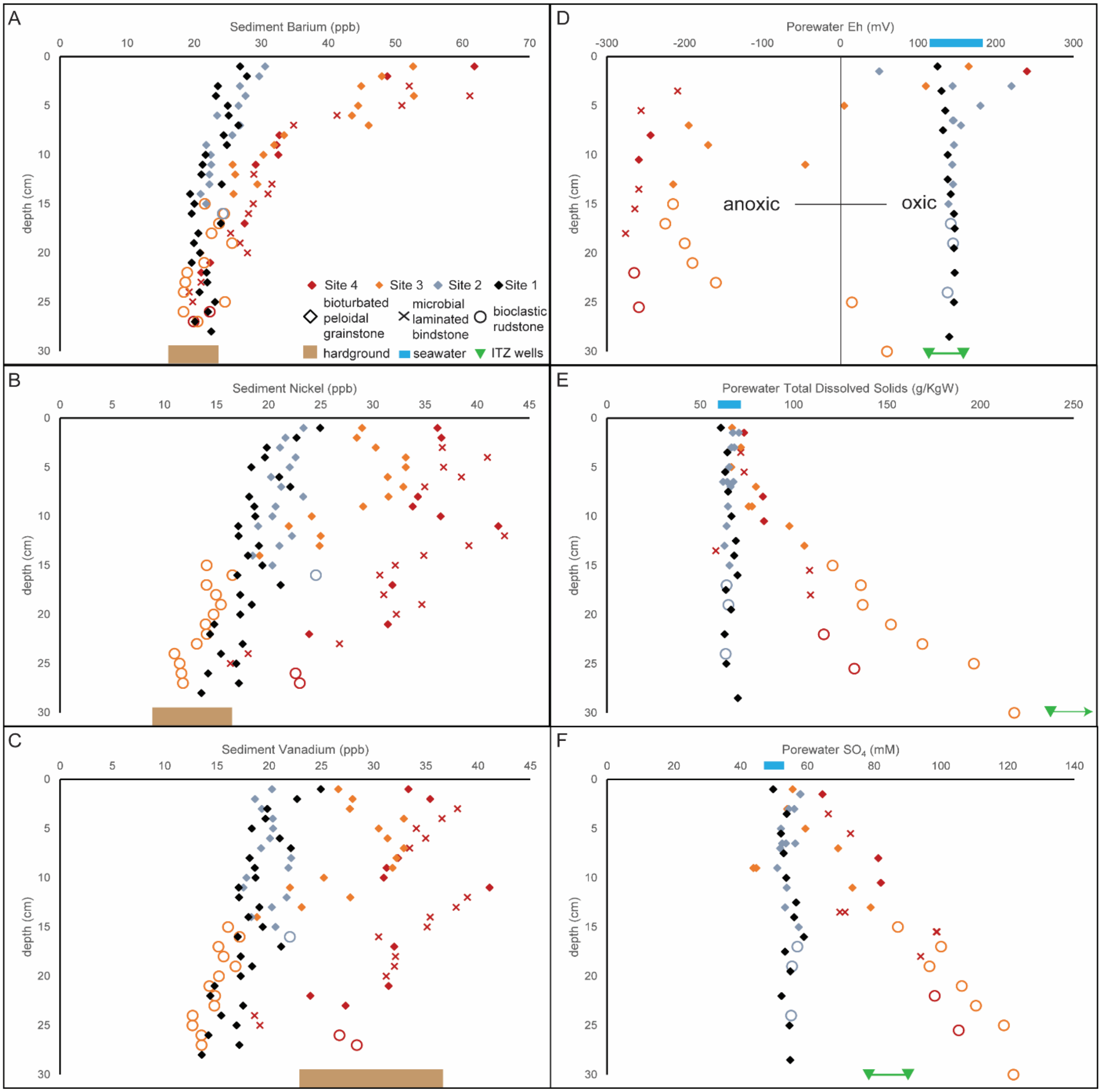


*Figure 3.8:* ***Systematic changes in sediment geochemistry (Fig. 9.1A-C) and porewater chemistry (Fig. 9.1D-F) of the four study sites are compared with depth****. Warm colors (red & orange) depict the middle to upper intertidal Sites 3 & 4, and cool colors (black and blue) display the lower intertidal Sites 1 & 2. Hardground, seawater and groundwater measured ranges are depicted by the length of the respective symbol. Error bars are smaller than the data points.*

## Sediment and porewater geochemistry

### *Changes in transition metal, redox, salinity and sulfate concentrations*

Sediment geochemistry and porewater chemistry analysis was conducted at all of the four study sites (Fig. 3.8). Sites 1 and 2 display relatively homogenous chemical versus depth profiles, while Sites 3 and 4 are heterogenous and differ from each other and the other two sites.

Concentrations of three transition-metal elements, barium (Ba), nickel (Ni), and vanadium (V) were examined in the intertidal sediments to evaluate changes in primary productivity and redox. Ba, Ni and V have been used in previous studies as proxies for productivity, as these particular elements are often biogenically produced and biosynthesised in microbial mat production (Pfeifer et al., 2001; Wong et al., 2015; Steiner et al., 2017; Lagrange et al., 2020). Additionally, V has been used in studies identifying paleoredox conditions (Wanty & Goldhaber, 1992; Calvert & Pedersen, 1993; Tribovillard et al., 2006; Lagrange et al., 2020). In Sites 3 and 4, Ba (Fig. 3.8A) ranges from 0.04 to 0.06 ppm in the upper 7 cm of sediment, gradually decreasing to ~0.02 ppm with depth. Ni (Fig. 3.8B) exhibits alternating enrichment-depletion patterns in Sites 3 and 4. In Site 4, Ni concentrations peak at 5 cm (max. 0.041 ppm), 12 cm (max. 0.043 ppm), and 20 cm (max. 0.035 ppm), followed by corresponding depletion to 0.034, 0.031, and 0.016 ppm. Site 3 shows enrichment zones at 5-7 cm (max. 0.033 ppm) and 12-13 cm (max. 0.025 ppm), with depletion phases at 8-11 cm (min. 0.022 ppm) and 14-27 cm (min. 0.011 ppm). V (Fig. 3.8C) displayed similar patterns to Ni. In Site 4, V exhibits enrichment in the 0-3 cm (max. 0.038 ppm), 11 cm (max. 0.041 ppm), and 26-27 cm (max. 0.028 ppm) intervals, with depletion in 4-10 cm (min. 0.031 ppm) and 12-25 cm (min. 0.019 ppm). Site 3 shows a parallel trend, with V enrichment from 0-4 cm (max. 0.033 ppm), followed by a minor depletion from 4-5 cm (min. 0.030 ppm), and another enrichment from 5-7 cm (max. 0.033 ppm). Subsequently, V is generally depleted from 9-27 cm (min. 0.013 ppm). In contrast, Sites 1 and 2 maintain relatively constant concentrations of Ba (~0.025 ppm), Ni (~0.017 ppm), and V (~0.02 ppm) throughout the sediment column.

Porewater redox potential (Eh) data are presented for the four sites (Fig. 3.8D), covering a range from -276 to 240 mV. At Site 4, Eh is 240 mV at a depth of 1.5 cm, with values becoming progressively more negative as depth increases (-276 to -209 mV). Site 3 exhibits Eh values >0 mV from 0-5 cm, transitioning to -225 to -45 mV between 7-23 cm, and back to >0 mV from 25 to 32 cm. In Sites 1 and 2, Eh ranges from 50-180 mV, with most measurements around 140 mV. For Site 2, multiple measurements were taken at depths of 1.5, 3, and 6.5 cm, resulting in Eh values of 50 mV, 144-220 mV, and 139-145 mV, respectively.

Porewater sulfate concentrations (Fig. 3.8F) at Site 4 show enrichment from 0.065 to 0.082 M in the 1.5-10.5 cm depth range, followed by a reduction to ~0.07 M at 13.5 cm. A second enrichment occurs at 15.5 cm, reaching 0.1 M, with a slight reduction to 0.09 M at 18 cm. From 18-31 cm, sulfate is enriched from 0.09 to 0.11 M. At Site 3, sulfate is enriched from 0.05 to 0.07 M in the 1-7 cm depth range, followed by a reduction to 0.04 M at 9 cm, and a gradual increase to 0.07-0.12 M from 11-30 cm. In Sites 1 & 2, sulfate remains relatively constant at 0.05-0.06 M across all depths.

Porewater salinities (Fig. 3.8E) vary from 58.40 to 218.18 Total Dissolved Solids (TDS) in g/L. In Sites 3 and 4, salinities generally increase with depth. Site 4 ranges from 84.17 to 132.53 TDS (g/L) at depths of 10.5-25.5 cm, while Site 3 ranges from 97.75 to 218.18 TDS (g/L) at depths of 11-30 cm. Conversely, Sites 1 and 2 maintain relatively constant salinities at approximately 69 TDS (g/L) throughout the subsurface. Specifically, at Site 2, salinity at 1.5 cm depth varies from 67.45 to 70.72 TDS (g/L), at 3 cm depth from 66.74 to 68.26 TDS (g/L), and at 6.5 cm depth from 64.50 to 67.78 TDS (g/L).

### Changes in strontium and magnesium

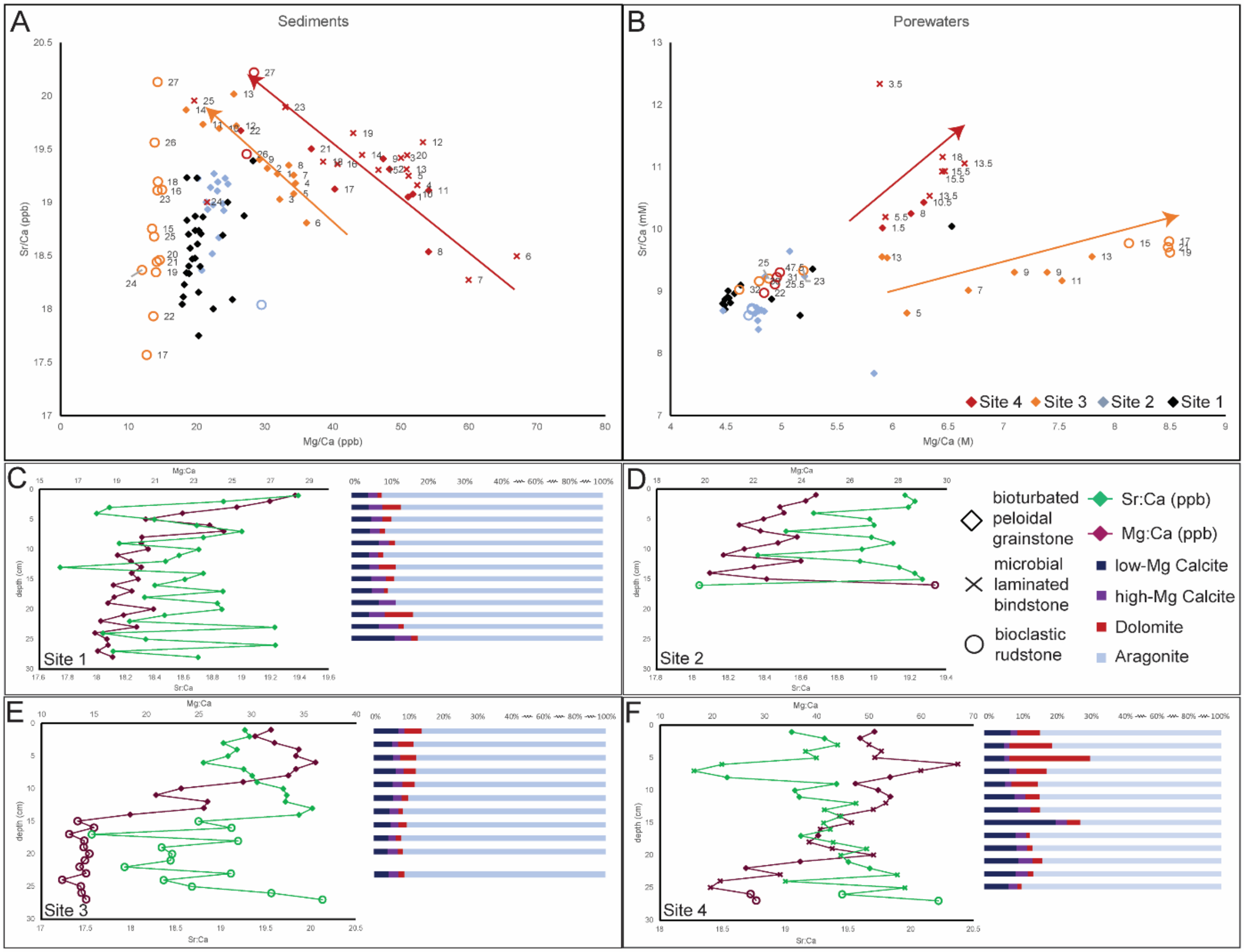


*Figure 3.9:* ***Systematic variations in Sr:Ca, Mg:Ca, and carbonate minerals are presented***. ***A***) *Cross plot of sediment Sr:Ca and Mg:Ca ratios. Arrows point towards increasing depth in Site 3 & 4. Note the large reduction in strontium in Site 3 past 14 cm depth.* ***B***) *Cross plot of porewater Sr:Ca and Mg:Ca ratios. Note that trends in both measurements exist only from 1 to 21 cm in Sites 3 & 4, and the remaining porewaters plot similarly.* ***C***) *Site 1 sediment Sr:Ca and Mg:Ca plotted with depth and compared to the corresponding carbonate mineral concentrations. Note the lack of distinct trends in ratio and mineral concentrations.* ***D***) *Site 2 sediment Sr:Ca and Mg:Ca plotted with depth. XRD analysis not conducted for Site 2, but a similar absence of ratio trends is noted.* ***E***) *Site 3 sediment Sr:Ca and Mg:Ca plotted with depth, compared to corresponding carbonate mineral concentrations. Significant reductions in both ratios are observed beyond 15 cm depth in the bioclastic rudstone layer.* ***F***) *Site 4 sediment Sr:Ca and Mg:Ca plotted with depth, along with corresponding carbonate mineral concentrations. Dolomite concentration corresponds to a significant spike in Mg:Ca and a decrease in Sr:Ca. Error bars are smaller than the data points.*

Sr and Mg fluxes in both the sediments and porewaters are compared in Figure 3.9. In the sediments (Fig. 3.9A), two linear trends are observed in Sites 3 and 4, while three vertical trends are evident in Sites 1, 2, and 3. In Site 4, a linear relationship exists from shallow samples to the deepest sample (27 cm) with Sr:Ca increasing from 18.27 to 20.22 ppb and Mg:Ca decreasing from 67.03 to 19.65 ppb. Site 3 shows another linear relationship from 6 to 14 cm depth, with Sr:Ca increasing from 18.81 to 19.87 ppb and Mg:Ca decreasing from 36.11 to 18.45 ppb. Following the Sr:Ca increase in Site 3, a vertical trend occurs from 15 to 27 cm depth, where Sr:Ca increases from 17.57 to 20.13 ppb, while Mg:Ca remains relatively consistent at 13.7 +/- 0.6 ppb. Site 2's ratio is also vertically plotted, with Sr:Ca increasing from 18.04 to 19.37 ppb throughout the sediment column, and Mg:Ca remaining relatively constant at 23.02 +/- 2.82 ppb, except for one outlier at the greatest depth of 16 cm (29.52 ppb). In Site 1, a vertical relationship is observed, where Sr:Ca increases from 17.75 to 19.23 ppb, and Mg:Ca exhibits variability with an average of 18.7 +/- 8 ppb.

In the porewaters (Fig. 3.9B) there exists two linear relationships in Site 3 & 4, while Sites 1 & 2 are generally not represented along any particular trend. In Site 4, Sr:Ca increases from 8.97 to 11.16 ppb throughout the sediment column, while one outlier exists at 3.5 cm depth (12.33 ppb). Mg/Ca varies from 4.84 to 6.65 ppb. The lowest Sr:Ca & Mg:Ca ratios are found in the deep porewaters (22 to 47.5 cm depth), while the high Sr:Ca & Mg:Ca ratios occur in the mid-depth to shallow sections (1.5 to 18 cm depth). Site 3 is also linear, but with lower concentrations of Sr:Ca. Sr:Ca ratios range from 9.03 to 9.80 ppb, and Mg:Ca ranges from 6.13 to 8.50 ppb throughout the sediment column. Again, the lowest ratios of Sr:Ca & Mg:Ca occur in the deep porewaters of Site 3 (23 to 32 cm depth), while the highest ratios exist in the mid-depth to shallow porewaters (1 to 21 cm depth). Generally, Sites 1 & 2 are low in Sr:Ca & Mg:Ca ratios with little variability. Sr:Ca varies from 8.39 to 9.64 ppb, and Mg:Ca ranges from 4.47 to 5.28 ppb. Two outliers exist within the distal sites. In Site 1, 22 cm depth, Sr:Ca is 10.04 ppb and Mg:Ca is 6.53 ppb. In Site 2, at 5 cm depth, Sr:Ca is 7.68 ppb and Mg:Ca is 5.83 ppb.

In Figure 3.9C-F, the changes in Sr:Ca and Mg:Ca ratios are plotted against depth alongside the associated XRD carbonate mineral phases. Site 1 and 2 do not exhibit significant trends in ratio variability or mineral phase identity. Sr:Ca and Mg:Ca ratios repeatedly shift between enriched and depleted measurements with successive centimeter increments throughout the sediment column.Site 3 (Fig. 3.9E) shows more distinct variability in Sr:Ca and Mg:Ca. In the middle to shallow subsurface (0 to 15 cm), both ratios are comparatively enriched, followed by a reduction in both measurements past 15 cm depth, occurring within the bioclastic rudstone layers. However, Sr:Ca becomes enriched once more past 25 cm depth, extending to the final measured depth of 27 cm. Carbonate mineral phases remain relatively constant, with a noticeable decrease in dolomite downsection. Site 4 (Fig. 3.9F) exhibits systematic changes in the ratios with depth. Initially, a large reduction in Sr:Ca corresponds to a significant enrichment in Mg:Ca from 5-7 cm depth, which coincides with the first buried microbial mat (microbial laminated bindstone). This change is also accompanied by the largest enrichment in dolomite. Dolomite concentrations decrease downsection, and the ratios return to near-surface values until 25 cm depth. Beyond 25 cm depth, in the bioclastic rudstone layer, both Mg:Ca and Sr:Ca become enriched.

## Water analyses

### *Groundwater composition*

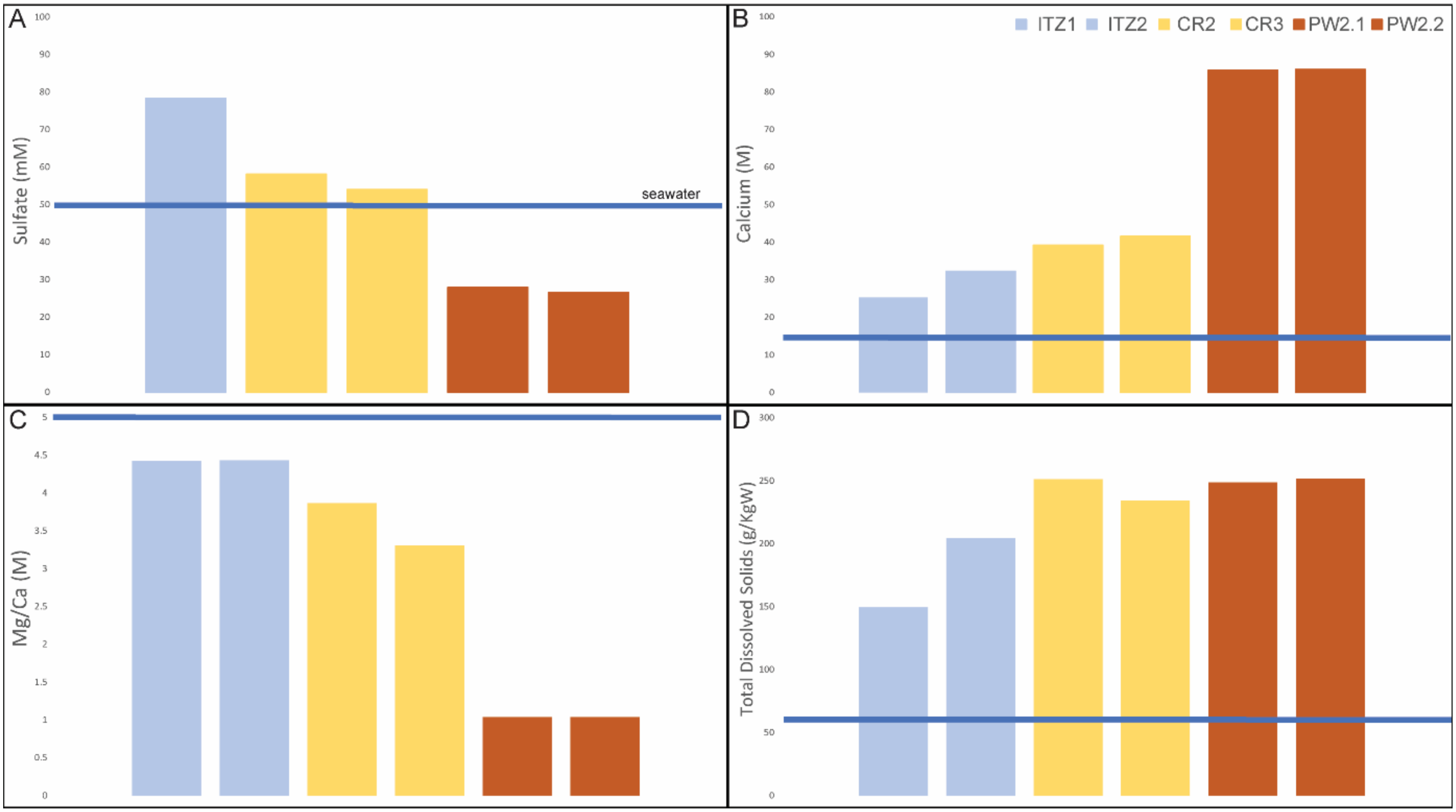


*Figure 3.10:* ***Groundwater chemical characteristics from the three well locations*** *(Fig. 1E). Measured seawater compositions are provided for each graph, and are marked by the horizontal blue line.* ***A)*** *Sulfate (mM). ITZ1 was not recorded in this graph due to measured error.* ***B)*** *Calcium (M).* ***C)*** *Mg:Ca (M).* ***D)*** *Salinity, interpreted from total dissolved solids (G/KgW).*

Groundwater measurements were obtained from three locations spanning from the middle intertidal zone (ITZ) to the supratidal (CR) and the more proximal supratidal sabkha (PW) (Figs. 1, 3.10). This report presents sulfate, Ca, Mg/Ca, and conductivity measurements from these three well sites.

Sulfate concentrations (Fig. 3.10A) are highest in the most seaward wells, ITZ2, measuring 78.32 mM. Concentrations decrease landward into the sabkha. In the lower supratidal (CR2 and CR3), sulfate measures 58.03 mM and 60.39 mM, respectively. In the upper supratidal sabkha (PW2.1 and PW2.2), sulfate concentrations are lowest at 27.89 mM and 26.52 mM, respectively. Seawater sulfate averages around 50 mM.

Ca measurements (Fig. 3.10B) show the lowest values in the most distal wells, ITZ1 and ITZ2, at 25.31 M and 32.16 M, respectively. Values increase landward into the sabkha. In the lower supratidal (CR and CR3), Ca is measured at 39.17 M and 41.55 M, respectively. In the upper supratidal sabkha (PW2.1 and PW2.2), Ca measurements reach their highest levels at 85.80 M and 85.97 M, respectively. Seawater Ca averages around 15 M.

Mg:Ca ratios (Fig. 3.10C) are highest in the most seaward wells, ITZ1 and ITZ2, at 4.42 and 4.44 M, respectively. Ratios decrease landward into the sabkha. In the lower supratidal, CR2 and CR3 have a Mg:Ca ratio of 3.86 and 3.31 M, respectively. In the upper supratidal sabkha (PW2.1 and PW2.2), Mg/Ca ratios are at their lowest, measuring 1.04 M. Seawater Mg/Ca ratios are approximately 5 M.

Total Dissolved Solids (TDS) measurements (Fig. 3.10B) are lowest in the most distal wells, ITZ1 and ITZ2, measuring 149.48 g/KgW and 204.22 g/KgW, respectively. TDS values increase landward into the sabkha. In the lower supratidal (CR2 and CR3), TDS is measured at 251.22 g/KgW and 234.26 g/KgW, respectively. In the upper supratidal sabkha (PW2.1 and PW2.2), TDS concentrations are at their highest, measuring 248.68 g/KgW and 251.77 g/KgW, respectively. Seawater TDS averages around 65 g/KgW.

### *Seawater and brine mixing*

Figure 3.11 compares water compositions to assess the impact of groundwater-seawater mixing. A "mixing line" is represented in red, which represents expected concentrations if mixing of seawater and groundwaters were to occur. Sites 1 and 2 consistently exhibit values near marine conditions across all presented data. In Figure 3.11A, the Sr:Na variability is shown. Seawater values range from 0.00158 to 0.0019 M for Sr:Ca and approximately 0.7 M for Na. Site 3 displays measurements below the mixing line, with relatively low Na concentrations and Sr:Na ratios from 1 to 21 cm depth. In contrast, the deeper depths (23 to 32 cm) exhibit higher Na concentrations (~ 2.4 to 3.3 M) and relatively constant Sr:Na ratios (0.0018 +/- 0.001 M). For Site 4, porewaters from 1.5 to 10.5 cm plot near seawater values. Porewaters from 13.5 to 18 cm

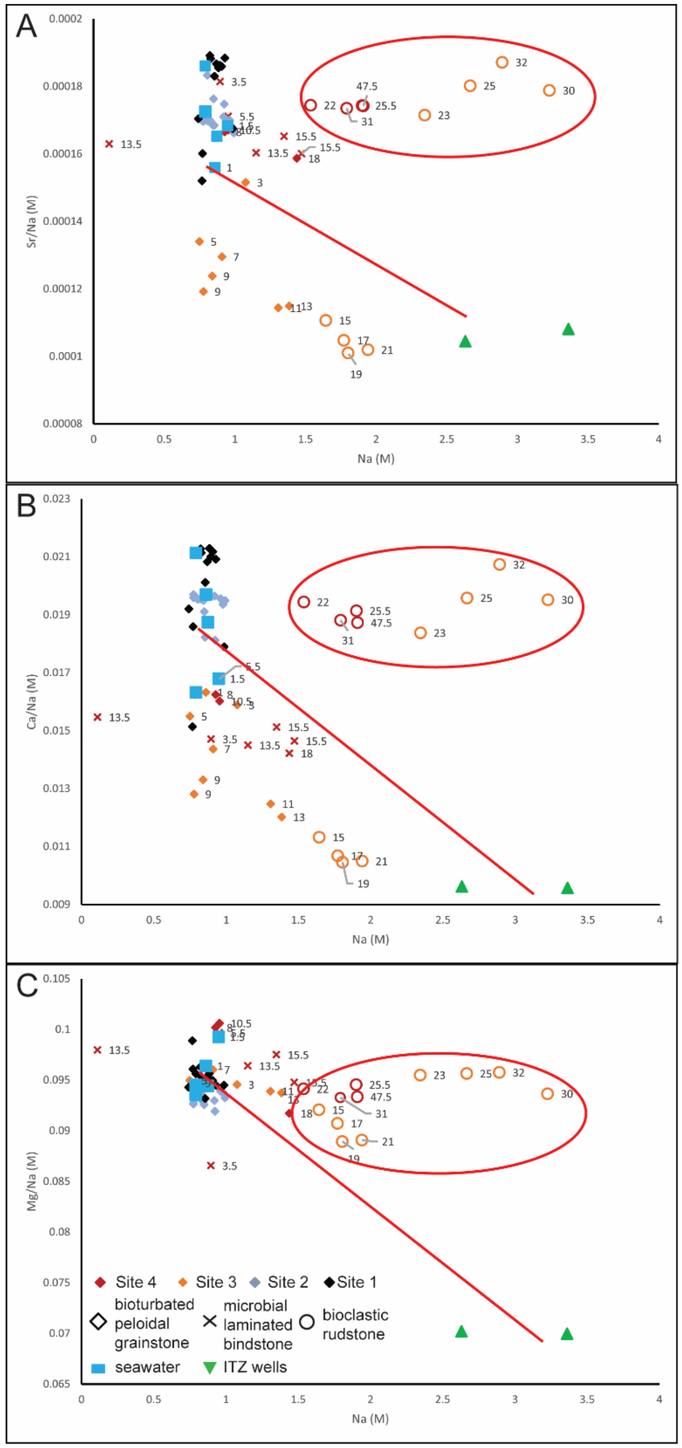

*Figure 5.11:* ***Graphical analysis reveals systematic in the concentrations of Sr, Ca and Mg normalized to Na and plotted against Na.*** *Seawater (blue squares), intertidal groundwaters (green triangles), and porewaters (remaining data) are presented. Depths of Site 3 & 4 porewaters are included, while those of Sites 1 & 2 are omitted as they closely resemble seawater with minimal variations.* ***A)*** *Strontium normalized to sodium and plotted against sodium.* ***B)*** *Calcium normalized to sodium and plotted against sodium.* ***C)*** *Magnesium normalized to sodium and plotted against sodium. Red lines represent the mixing line, denoting the desired range for mixed seawater and groundwater. Red circles indicate porewaters that deviate from seawater, groundwater, or the mixing line, suggesting the influence of diagenetic processes.*

generally plot above the mixing line but have lower Na concentrations (1 to 1.3 M), while the deeper depths (22 to 47.5 cm) are enriched in Na (~ 1.5 to 2 M).

Figure 3.11B illustrates the Ca:Na variability. Seawater values range from 0.016 to 0.021 M Ca:Na, with approximately 1 M for Na. Site 3 generally falls below the mixing line in the 1 to 21 cm depth range, exhibiting the lowest Ca:Na ratios (0.010 to 0.016 M). In contrast, the deeper depths (23 to 32 cm) show higher Na concentrations (around 2.4 to 3.3 M) with Ca:Na ratios averaging around 0.019 +/- 0.002 M. Site 4 porewaters from 1.5 to 18 cm fall below the mixing line but have slightly higher Ca:Na ratios compared to Site 3 (0.014 to 0.016 M). Porewaters from 22 to 47.5 cm plot above the mixing line with Ca:Na ratios averaging 0.019 +/- 0.001 M but are relatively depleted in Na compared to Site 3 (1.5 to 2 M).

Figure 3.11C represents the Mg:Na/Na variability. Seawater plots from 0.093 to 0.099 M Mg:Na, at ~0.07 Na M. Site 3 & 4 plot above the mixing line, apart from one porewater at 3.5 cm in Site 4 that is anomalously low. Porewaters above the mixing line are measured ranging from 0.089 to 0.01 M Mg:Na, and span from 0.9 to 3.3 M Na.

**DNA of surficial microbial mats**

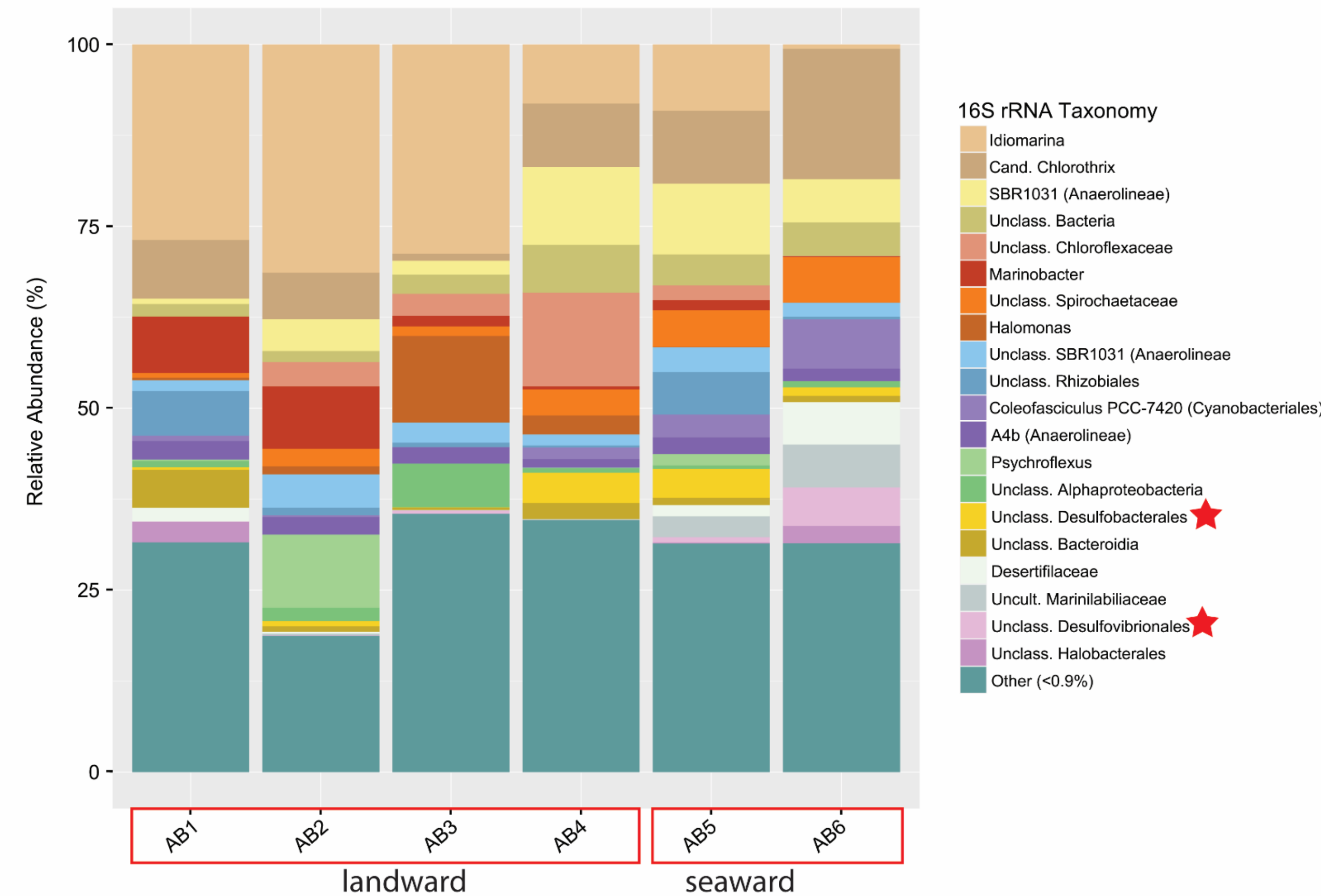


*Figure 3.12****: DNA analysis of six microbial mat samples from the upper intertidal zone*** *to determine microorganism abundance. Approximate locations of mat samples are highlighted and labeled in red boxes, and precise locations are presented in Figure 1E. Two microorganisms of importance are sulfate reducing bacteria marked by red stars.*

Figure 3.12 is a graphical representation of variations in microbial mat microorganism abundance, determined from DNA sequencing. Samples are labeled from AB1 to AB6. AB1 to AB4 are taken from more landward portions of the upper intertidal zone, and AB5 and AB6 are the most distal samples, but still taken from within the upper intertidal zone (Fig. 1.1E). From AB1 to AB6, *Idiomarina* and *Marinobacter* decrease in relative abundance. Conversely, *Cand. Chlorothrix*, *Anaerolineae*, Unclassified *Spirochaetacae* and Unclassified

*Desulfobacterales* increase in occurrence. All other microorganisms do not show any outstanding variations in abundance. However, two bacteria, *Desulfobacterales* and *Desulfovibrionales*, are of particular importance, and are observed to increase from AB3 to AB6.

## INTERPRETATIONS

### Impacts of bioturbation on geochemical variation in the intertidal zone

Firmgrounds within Al Qantur lagoon are restricted to the middle-upper intertidal zone, and absent within the lower intertidal zone (Fig. 1.1; Vallack, 2021). The seaward decrease of firmgrounds is accompanied by an increase in bioturbation. Burrows in Site 3 and 4 are largely restricted to the shallow portions of the sediment column, thereby restricting the depth of seawater penetration, whereas in Site 1 and 2, burrows extend deeper, and tidal waters permeate further (Figs. 2.2 to 2.5). With this in mind, unique chemical changes related to bioturbation intensity and depth are observed in the sediment column, with firmgrounds occurring only at shallow-depths (5-15 cm) where bioturbation intensity is reduced.

Geochemically, the porewaters in sites 1 and 2 are most similar to seawater (Figs. 3.8, 3.11) with no distinguishable trends in Sr:Ca or Mg:Ca ratios, nor in their carbonate mineral phases (Fig. 3.9). Sites 1 and 2 are heavily bioturbated, resulting in infaunal mixing of the sediment, which reduces variation in sediment and porewater chemistry in the upper-lower intertidal zone. Bioturbation by crustaceans in the upper-lower intertidal zone creates a massive-appearing texture that is responsible for increased permeability throughout the sediment column. These large burrows (5-20 mm) act as preferential pathways for water to move through the substrate, allowing tidal water to advect through the burrow fabrics twice daily, resulting in porewater chemistry that closely resembles seawater (Figs. 3.8, 3.11).

Effectively, bioturbation is homogenizing the chemical signature by “flushing” the sediment with seawater through higher-permeable burrow networks. Additionally, crustaceans excavate the substrate, creating burrows that become subsequently infilled, or left open when inhabited, effectively transporting sediments up and down in the subsurface (Fig. 2.11). The movement of deeper sediments to shallower areas, and vice versa, is probably represented by cm-scale variability of Sr:Ca/Mg:Ca, as well as the lack of any trends in carbonate mineral phases with depth (Fig. 3.9C, D).

Barium (Ba), nickel (Ni) and vanadium (V) (Fig. 3.8A-C) are transition metals that serve as proxies for primary productivity (Pfeifer et al., 2001; Steiner, 2017; LaGrange et al., 2020). Metal fluxes suggest that organic matter and productivity are restricted to the near-surface environment. Ba concentrations are highest within the shallow Site 3 and 4 sediments, indicating primary productivity is highest from 0-10 cm depth in the sedimentary column. The variability in Ni in Site 4 coincides with horizons of buried mat material (Fig. 3.1). Ni is a high-affinity element for use in hypersaline microbial mat cell regulation (Campbell et al., 2020), suggesting that Ni enrichment in the Site 4 sediments is likely attributed to microbes that include Ni in their metabolic processes. Additionally, V (Fig. 3.8C) is known to be preferentially used in the surface metabolic processes of hypersaline mat growth (Wong et al., 2015). Both Ni and V in Site 4 fluctuates on either side of buried microbial mat horizons, again suggesting microbial mats are including V in their synthesis. Of the three sediment geochemical proxies discussed, Site’s 1 & 2 remain constant, reflecting comparably reduced primary productivity in the middle-lower intertidal zone.

V also serves as a redox potential proxy, where enrichment of V represents reducing conditions (Wanty & Goldhaber, 1992; Calvert & Pedersen, 1993; Tribovillard et al., 2006; LaGrange et al., 2020). As V’s concentrations in Site 4 likely reflect two systems (redox and primary productivity), we use direct measurements of porewater redox potential (Fig. 3.8D) to interpret oxygen levels. Values > 0 mV are considered oxic, and values < 0 mV are considered reduced. Values close to -300 mV are interpreted as microbial-mediated reduction (Sondergaard, 2009). Evidently, sites 3 and 4 are reducing past 5 cm depth, and the Site 4 sediment column is affected by microbial related reduction, whereas sites 1 and 2 remain oxic throughout the sediment column.

Ongoing sediment mixing from infauna and advection of marine waters through burrow fabrics result in a lack of early marine cementation. Presumably, solutes are unable to concentrate or deplete in any manner that promotes carbonate precipitation or diagenesis. The greater advection of seawater in the distal substrates reduces Ba, Ni and V (Fig. 3.8A-C), enhances sulfate (Fig. 3.8F), and creates oxic conditions (Fig. 3.8D). Reduction in primary productivity (Fig. 3.8A-C) implies that microbial mediated precipitation would not take place in sites 1 and 2 (Yallop et al., 2000; Dupraz & Visscher, 2005; Dupraz et al., 2009; Gerbersdorf & Wieprecht, 2015; Diaz et al., 2022). Additionally, enriched sulfate and oxygenated porewaters (Fig. 3.8F) produces unfavorable conditions for carbonate precipitation (Muci et al., 1989; Machal, 2001; Sumner & Grotzinger, 2004; Morse et al., 2007; Dupraz et al., 2009; Ge et al., 2023). No evidence for diagenesis exists, as the Sr:Ca and Mg:Ca ratios in sites 1 and 2 are inconsistent (Fig. 3.9C,D). Overall, the effects of bioturbation on the site 1 and 2 geochemistry imply that, in contrast to the proximal sites, carbonate formation and diagenesis are not evident. Indeed, primary precipitation (aragonite, high-Mg calcite) and diagenesis likely occurs within the distal sites, but with far less distinction when compared to proximal sites, and not to the extent as to promote cementation and early lithification. Discussion of early marine cementation and diagenetic processes will be discussed in the following sections.

### Brine advection from the sabkha

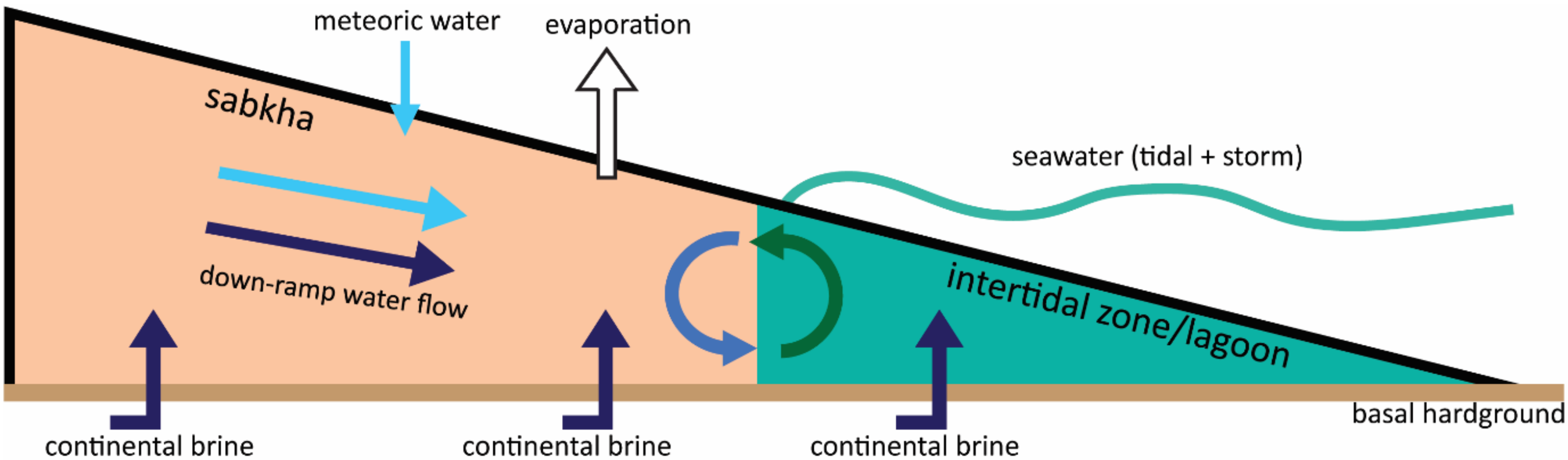


*Figure 3.13:* ***Brine advection model modified after Wood et al. (2002)'s "ascending-brine model."*** *This model is adapted to further emphasize that groundwater leakage occurs across the coastal sabkha complex, and is not limited to the sabkha. Additionally, we recognize how brine waters and seawaters mix within the intertidal zone.*

Advection of hypersaline, continental brines down-ramp is responsible for mixing with deep porewaters and altering their geochemical signature in Al Qantur lagoon (Wood et al., 2002; Liu et al. 2016; Vallack, 2021). Wood et al. (2002) performed a study on a Tertiary-aged brine in the subsurface aquifer of the Abu Dhabi coastal sabkha. The brine has a greater average equivalent of calcium than carbonate and sulfate, which is attributed to the precipitation of anhydrite and carbonate in the aquifer (Wood et al., 2002). The authors then propose an "ascending-brine" model, in which the sabkha-covered aquifer provides the majority of solutes (>95%) to the coastal sabkha system. The authors infer that there is little to no horizontal mixing of the brine water with seawater, but rather attribute the observed seawater solutes to interstitial trapping by prograding sediments. While we have also observed the "ascending-brine" chemical signature from well water samples located in the supratidal sabkha (Fig. 3.10), we also recognize marine water and brine water signatures within our study sites in the intertidal zone (Fig. 3.8). We propose that ascending brines mix with seawater in the upper-intertidal zone as groundwaters advect from below the laterally extensive basal hardground, and possibly less frequently flow down-ramp atop the hardground base (Figs. 3.11; 3.13). Figure 3.10 highlights the "original" brine signature that is mentioned by Wood et al. (2002), as the most proximal groundwater sample is enriched in calcium and depleted in sulfate. Additionally, the most supratidal signature of the brine has a lower Mg/Ca ratio and is hypersaline with respect to seawater. However, as the groundwaters move towards the intertidal zone, their measurements shift towards seawater values. This suggests that the initial ascending brine in the sabkha is both ascending and flowing down-ramp where mixing with marine waters occurs. This mixing signature is highlighted by the increase in salinity and sulfate measurements in porewaters below 15 cm at sites 3 and 4 (Fig. 3.8EF). Notably, Site 3 salinity and $SO_4$ values are higher than Site 4 at depth. This is probably because of locally enhanced groundwater leakage at Site 3. Notably, porewater redox decreases with depth in Site 3 and conditions become oxic towards the base of the sediment column. This correlates with the highest porewater salinities and provides clear evidence for relatively rapid upward leakage of oxic and more saline groundwaters at Site 3 (Figs. 3.8E,F; 3.10D).

Further agreement of a mixing process is recognized in Figure 3.11. Seawater is depicted by blue squares, and intertidal groundwaters are presented by green triangles. A "mixing line" is presented (red line, Fig. 3.11) that represents expected concentrations if mixing of seawater and groundwaters were to occur. Noticeably, sites 3 and 4 porewater values generally plot in proximity to this line, again supporting groundwater leakage and mixing in the proximal sites. Sites 1 and 2 plot near seawater because of enhanced seawater infiltration via burrows, and most of the Site 3 and 4 samples that do not plot near the mixing line are from within the bioclastic rudstone. This is probably indicative of diagenesis and will be discussed in the section "Water mixing and the evidence of brine-induced diagenesis at depth".

At low tide, in which marine waters have completely receded from upper-intertidal sediments, a large enough pressure gradient exists above the basal hardground to promote a leakage of groundwaters through the hardground, and into the sediment column (Vallack 2021). The distribution of brine leakage will be influenced by irregularities in the hardground's thickness and continuity as well as the sediment permeability (Fig. 3.6).

As identified by Wood et al. (2002), the continental brine is responsible for adding significant solutes to the coastal water system. Chemical exchange and solute fluxes play an important role in where carbonate precipitation and dissolution may occur in the intertidal zone (Milliman, 1993; Morse et al., 2007; Swart, 2015; Declet et al., 2016). In this instance, the advecting brine enhances magnesium, sulfate, and salinity concentrations (Figs. 3.8EF; 3.10). Fluxes in transition metal concentrations are also probably linked to advection of the continental brine (Figs. 3.7; 3.8A-C), however it is important to note that shifts in redox conditions also impact transition metal distributions (Tribovillard et al., 2006). Brine advection is observed at depths > 15 cm in Site 3, and > 20 cm in Site 4 (Figs. 3.8EF; 3.9EF). The bioclastic rudstone microfacies occurs at or near these depths, correlating with changes in Sr:Ca, Mg:Ca, Sr:Na, Ca:Na, and Mg:Na that suggest dissolution of certain mineral phases and precipitation of others (Figs. 3.9EF; 3.11). Therefore, we propose that the continental brine may be one major driver in producing diagenetic conditions in the deeper subsurface.

## Early cementation and diagenesis in the upper intertidal shallow subsurface

Firmgrounds and hardgrounds in Abu Dhabi form by means of early marine precipitation of phreatic carbonate cements (Paul & Lokier, 2017; Ge et al., 2020a,b; Ge et al., 2023). Additionally, microbial mat communities (Fig. 3.12) and microphytobenthos (MPB) are abundant across the intertidal zone (Kendall & Skipwith; 1968; Lokiet et al., 2013; Hubas et al., 2018; DiLoreto et al., 2019). These microorganisms enhance sediment cohesion, and contribute to sediment stabilization (Paterson, 1994; Yallop et al., 2000; Folk & Lynch, 2001; Lundkvist et al., 2007; Gerbersdorf & Wieprecht, 2015). Generally, along the Abu Dhabi intertidal zone, firmgrounds form when subsurface sediments, namely peloids, become partially lithified (Fig. 3.4; Ge et al., 2020a), and hardgrounds are characterized by aragonite and calcite cemented foraminifera, bioclasts, and peloids (Fig. 3.6; Paul & Lokier, 2017).

Aragonite and high-Mg calcite is documented as the primary carbonate early marine precipitating phases for the Abu Dhabi coast (Shinn, 1969; Evamy, 1973; Paul & Lokier, 2017; Ge et al., 2020a,b; Ge et al., 2023). In our study, the dominant carbonate phase observed in the sediments in Al Qantur lagoon is acicular aragonite, which precipitates on peloids, bioclasts and surrounding EPS (Figs. 3.2; 3.4). To a lesser degree, micritic Mg-calcite envelopes surround bioclasts within hardground samples (Fig. 3.4E), and Mg-calcite is observed as a "halo" around foraminifera and in cement (Fig. 3.5).

In addition to petrographic and Raman mapping of cementation, our study uses the shifts in sediment and porewater geochemistry to decipher horizons of precipitation and diagenesis in the shallow subsurface. For the purpose of determining early marine precipitation that may locally create firmgrounds, we analyze sulfate, redox, Mn and Fe sediment fluxes. In our study, the geochemical variability at Site 4 provides a locality to assess certain chemical drivers in diagenetic alteration. Site 4 porewaters are microbially reduced (Fig. 3.8E; Sondergaard, 2009), and sulfate is initially reduced in the mid-depth subsurface, corresponding to a buried microbial mat horizon (12 to 16 cm depth; Fig. 3.8F). Microbial sulfate reduction is commonly cited as contributing to diagenesis (Machel, 2001; Baldermann et al., 2015), where microbial-mediated sulfate reduction increases porewater alkalinity and carbonate saturation state, while reducing sulfate (Dupraz et al., 2009; Ge et al., 2020a). Low sulfate accompanied by increased Mn and Fe, and reducing conditions promote Mg-calcite precipitation (Muci et al., 1989; Sumner & Grotzinger, 2004; Morse et al., 2007; Ge et al., 2023). Focusing where sulfate reduction occurs, we evaluate Mn and Fe concentrations in the sediments (Figs. 3.7; 3.8A-E). Elemental decreases in porewaters correspond to elemental increases in sediments, and vice versa. With this in mind, we observe that the sediment hosts less Mn in the depths near the initial sulfate reduction, indicating that the porewaters in these depths are more enriched in Mn (Fig. 3.7A). Similarly, Fe is greatly reduced within the same sediment horizon, again suggesting Fe enrichment in porewaters (Fig. 3.7B). These observations imply that within the mid-depths (> 10 cm) in Site 4, there exists porewater conditions that favor the precipitation of Mg-calcite. This is supported by XRD of Site 4 sediments, where Mg-calcite cements are at their greatest weight percent (20.1%) at 13-15 cm depth (Figs. 3.4; 3.9).

At Site 3, we see sulfate reduction in the porewater (Fig. 3.8F), reduced conditions (Fig. 3.8D), and Fe and Mn reduction in the sediments (Fig. 3.7) from 7-9 cm depth. While the prior fluxes could support Mg-calcite precipitation, we do not see this reflected in the sediment mineralogy (Fig. 3.2) The absence of Mg-calcite at Site 3 relative to Site 4 may be related to the lack of microbial mat communities and further highlights the chemical complexities that can occur over small geographic distances.

The mid-sediment column depths (7-15 cm) of sites 3 and 4 are interpreted as areas where early marine cements (i.e. acicular aragonites, micritic Mg-calcite) are precipitated, enhancing partial lithification of carbonate sediments. Of the four sites sampled, intervals of higher Mg-calcite cementation occur at Site 4 in the middle of the sediment column. Sites 1 and 2 are affected by crustacean burrowing, and so solutes do not vary at any particular horizon. Notably, the transition metals (Figs. 3.7; 3.8A-E), undergo significant fluxes within the bioclastic rudstone layer of 15 - 25 cm depth in Site's 3 & 4. These changes can most likely be attributed to continental brine dissolution. Additionally, sulfate is enhanced in the middle-upper intertidal zone (sites 3 & 4) at depths > 15 cm (Fig. 3.8F), and so conditions are not favorable for Mg-calcite precipitation at these depths. Sulfate enrichment likely occurs via brine advection (Fig. 3.10A), and perhaps additionally due to reduced SRB abundance at depth, as SRB are typically restricted to the near-surface environment (Dupraz & Visscher, 2005).

To further assess shallow subsurface cement precipitation, dissolution and paragenesis, we examine the Sr:Ca and Mg:Ca ratios of porewaters and sediments. Generally, carbonate diagenesis can be interpreted from changes in Sr:Ca and Mg:Ca ratios (Schroeder, 1969; Swart, 2015; Ahm et al., 2018). Strontium preferentially substitutes within aragonite than in other carbonate polymorphs due to its orthogonal crystal structure (Morse et al., 2007; Sunagawa et al., 2007), and high Mg:Ca ratios are understood to restrict calcite growth (Folk, 1974). Accordingly, when aragonite transitions into high Mg-calcites, and high Mg-calcites transition into low-Mg calcites, Sr and Mg should be expelled from the crystal structure, respectively (Berner, 1966; Stehli & Hower, 1961; Schroeder, 1969; Katz et al., 1972; Folk, 1974; Baker et al., 1982; Schlanger, 1988; Swart, 2015). In light of this, when assessing diagenesis, we would ideally observe depleting Sr or Mg from the sediment and increasing Sr or Mg in the porewaters if primary aragonite or Mg-calcite carbonate phases were undergoing alteration.

In the sediment cores of sites 3 and 4, Sr and Mg undergo important variations that indicate precipitation and diagenetic events (Fig. 3.9). Strontium enrichment in the sediments and porewaters suggests that there is consistent direct precipitation of aragonite throughout the sediment column, which agrees with the observed cements (Fig. 3.4). These aragonite cements are partially responsible for lithifying unconsolidated sediments (namely peloids) within the intertidal zone. Subsequently, if these early marine aragonite cements dissolve or are replaced, Sr would become reduced. Particularly in Site 3, there occurs a major reduction of Sr:Ca and Mg:Ca within the bioclastic rudstone layer, indicating dissolution past 15 cm depth (Fig. 3.9A,E). This evidence implies dissolution is responsible for producing the observed hardground textures, which are notably bioclastic rich, and porous (Fig. 3.6).

However, Mg depletion in the sediments, despite the complimentary increase in the porewaters poses an interesting shift. Mg is enriched in the observed porewaters, presumably due to calcium being precipitated out of solution, which drives the Mg:Ca ratio up (Azer & Peebles, 1998; Moore, 2001). Conversely, Mg is depleted in the sediments downward through the sediment column. This implies that Mg cannot be included in the carbonate lattice despite Mg-saturated porewaters. Probably, the increasing Mg:Ca pore fluid ratios with depth inhibits high-Mg-calcites to grow (Morse et al., 1997). This process would occur if Mg saturation is able to poison the calcite surface enough to prevent further Mg-calcite growth, thus allowing aragonite to precipitate on the calcite substrate, and allowing Mg to concentrate further in porewaters, which would agree with the dominance of aragonite cements (Figs. 3.2; 3.4; Morse et al., 1997; Morse et al., 2007). Additionally, the stark decrease in Mg in Site 3 sediments past 15 cm is representative of dissolution (Fig. 3.9E), while the increase in Mg and dolomite at 7 cm in Site 4 sediments is attributed to microbial processes (Fig. 3.9F).

Together, Sr:Ca and Mg:Ca ratios imply that precipitation and early diagenesis is mediated by porewater conditions in the subsurface, as also concluded by Ge et al. (2023). Aragonite and high-Mg calcite occur as primary precipitates, as discussed in the previous section, (Figs. 3.4, 3.5; Shinn, 1969; Paul & Lokier, 2017; Ge et al., 2023), and alteration of the cements occurs via changing porewater conditions at depth (Figs. 3.7; 3.8; 3.9). Variations in Sr/Mg:Ca ratios in sites 1 and 2 are again lacking distinct variation (Fig. 3.9C,D). Additionally, porewater values are more or less homogenous at near-marine concentrations (Fig. 3.9B). These observations further support the bioturbators role in mixing sediments (Figs. 3.9C, D) and in increasing seawater advection within the sediment column (Fig. 3.9B).

## Water mixing and the evidence of brine-induced diagenesis at depth

Analysis of brine advection provides evidence for the mixing of seawater and groundwater within intertidal sediments, particularly in Site 3, and to a lesser degree in Site 4 (Figs. 3.8E,F; 3.11). Additionally, enhanced groundwater leakage at Site 3 is recognized, and significant chemical fluxes are reflected in the Site 3 bioclastic rudstone layer described here (Chapter 2; Figs. 3.7; 3.8; 3.9; 3.11).

Based on our observations of Sr:Ca and Mg:Ca changes, we recognize that dissolution occurs within intervals of bioclastic rudstone (Fig. 3.9E) where permeability is likely highest in the sediment column, and enhanced brine advection occurs. Additionally, the bioclastic rudstone is characterized by mollusk shells, which, owing to their aragonitic mineralogy, are susceptible to dissolution (Morse et al., 2007; Swart, 2015). Therefore, we propose that the continental brines drive diagenesis at depth, as groundwaters leak through the basal hardground. Modern marine carbonates have a high chloride content, and so the dissolution of carbonate sediments would release significant Na in the porewaters (Land & Hoops, 1973). Deep (> 22 cm) bioclastic rudstone samples in sites 3 and 4 plot away from the three mixing lines (Sr/Na, Ca/Na, Mg/Na) and in each, are in excess of sodium (Fig. 3.11, red circles).

Notably, where groundwaters begin to mix with seawater, diagenesis is reduced. This is supported by the observation that the shallower rudstone samples in Site 3 (15 to 21 cm) plot along the mixing line, and do not behave like the deeper rudstone samples that directly overly the hardground (23 to 32 cm), implying seawater inhibit dissolution, and groundwaters enhance it (Fig. 3.11).

## Microbial-mediated dolomite

Dolomite precipitation in a coastal sabkha system is traditionally interpreted to occur following the "reflux model" where Mg is concentrated in interstitial waters following evaporation and precipitation of carbonate, effectively removing Ca and driving the Mg:Ca ratio up (Azer & Peebles, 1998; Saller & Henderson, 1998; Warren, 2000; Moore, 2001; Melim & Scholle, 2002). Additionally, in Abu Dhabi and other similar environments, dolomitization is attributed to microbial processes (Vasconcelos & McKenie, 1997; Bontognali et al., 2010, 2012; Sandooni & El-Saiy, 2010; Strohmenger et al., 2010; Geske et al., 2015). Vasconcelos et al. (1995) first summarized how the direct mediation of sulfate reducing bacteria (SRB) provides ideal conditions for dolomite precipitation in modern, natural environments, as SRB increase alkalinity and pH through their metabolic processes (Bontognali et al., 2010).

The highest weight percent of dolomite in the subsurface of Al Qantur lagoon is at Site 4, where we observed buried microbial mats, and where Mg:Ca saturation is the highest (Figs. 3.1; 3.2; 3.9F). The surficial mats that occur landward of our study sites also host sulfate reducing bacteria (*Desulfobacterales* and *Desulfovibrionales*) that are presumably a constituent of the buried mats in Site 4 (Fig. 3.12). Undoubtedly, the co-occurrence of the most concentrated dolomite in proximity to buried microbial mat communities (and some abundance of SRB) imply that modern, biologically mediated dolomite precipitation is occurring in the upper intertidal zone of Al Qantur lagoon.

Dolomite decreases in concentration down section in Site 4, despite deeper horizons of buried microbial mat material (Fig. 3.9F). Notably, Mg:Ca is significantly enriched surrounding the most recently buried mat alongside a major depletion in Sr:Ca, which produces conditions promoting dolomite precipitation. It's possible that older, buried mats have stopped photosynthesizing, subsequently decreasing primary productivity. Therefore, the lack of microbial mediation of the microenvironment could prevent enrichment of Mg:Ca and the ensuing dolomite. This is partially observed in Ba concentrations, which progressively decrease down section in Site 4 (Fig. 3.8A), however V and Ni suggest there is still some degree of primary productivity at depth (Fig. 3.8B,C). Alternatively, dedolomitization could be occurring. Dolomite transitioning back into calcite would release Mg out of the crystal structure, and back into porewaters. Indeed, the sediment Mg concentration is reducing past ~ 7 cm, and increasingly enriched in porewaters (Fig. 3.9B, F).

In addition to microbial mediated dolomite in Site 4, dolomite is also recognized within the more distal sediments and within the hardgrounds of Al Qantur lagoon (Figs. 3.2; 3.3). Dolomite in the sediment samples of sites 1 and 3 are attributed to detrital wind-blown sediment, as previously studied dolomite grains from Al Qantur lagoon were rounded and weathered (pers. comm.; Vallack, 2021). The dolomite that is observed in the hardgrounds is not as clear. Mg:Ca decreases with depth in the sediments in sites 3 and 4, and decreases past 21 cm in the porewaters (Fig. 3.9A,B), which contradicts reflux-driven dolomite precipitation, a process that is traditionally explained in sabkha settings (Saller & Henderson, 1998; Warren, 2000; Melim & Scholle, 2002). Detrital incorporation could explain the comparatively minor weight % of dolomite (~5%), and would agree with the observations of wind-blown grains in the sediments. Alternatively, we have outlined how continental brines and seawater mix within the intertidal zone of Al Qantur lagoon. The freshwater-seawater mixing-zone model (Petrash et al., 2021) describes how brine and seawater mixing produces a suite of redox-sensitive reactions alongside a complex subsurface biosphere to produce dolomite. There are multiple possible explanations for the dolomite found within our hardground samples, however, a definitive determination of the dolomite source in Al Qantur lagoon is limited by the analyses conducted in this study.

Additionally, across the intertidal zone, the upper 3-6 millimeters of the sediment are loosely bound by a microbial matrix of extracellular polymeric substance (EPS) named microphytobenthos (MPB). MPB commonly extend over broad areas of the intertidal zone (Hope et al., 2020; Hubas et al., 2018) and comprise a complex assemblage of microorganisms (Mandal et al., 2021). The MPB helps buffer the effects of pollution, enhance sediment cohesion, and support biofilm and microbial mat survival. In doing so, MPB plays a role in modifying pH and redox chemistry with significant changes over cycles of night-day and tidal inundation (Mandal et al., 2021). Presumably, the concentration of MPB across the entire intertidal zone would promote carbonate precipitation, as they occur in association with significant EPS, and EPS is pertinent to early marine carbonate precipitation (Dittrich & Sibler, 2010; Diaz et al., 2022; Diaz & Eberli, 2022). However their role in dolomite formation is less pronounced. If MPB were to sufficiently mediate the shallow (< 1 cm) substrates geochemistry as to allow dolomite precipitation, then we should expect more widespread dolomite at the surface in our analyses. However, it is rather only the dense accumulation of dolomite in Site 4 that is ostensibly attributable to organic processes.

## DISCUSSION

### Firmgrounds versus hardgrounds: subsurface precipitation and diagenesis

In this study we have recognized two subsurface, early marine features that occur within the intertidal zone. Firmgrounds, which generally are observed from 5 to 15 cm depth in the lower-upper intertidal zone (Sites 3 & 4), and basal hardgrounds that occur under the sediments of Al Qantur lagoon across the entire intertidal zone. Firmgrounds are characterized by partially lithified peloids, and hardgrounds are completely cemented intervals of mostly foraminifera, and some peloids and bioclasts.

We have described how early marine cements, produced by ideal seawater and interstitial water chemistry, partially lithify sediments. Additionally, microbial processes promote sediment cohesion and mediate porewater chemistry supporting primary precipitation (Folk & Lynch, 2001; Diaz et al., 2022; Diaz & Eberli, 2022). Largely, the sediments that become partially lithified as firmgrounds in the shallow subsurface are peloids with minor bioclastic components. The hardgrounds, which are primarily foraminifera, molluscs, and peloids, are also features that were lithified by primary precipitation, but have experienced some dissolution. Continental brine advection leads to dissolution, creating a porous bioclastic texture (Fig. 3.6). The hardground's upper surface is flat, while the underside's unevenness may indicate further evidence of dissolution (Fig. 3.6). Likely, hardgrounds represent the lithification of the bioclastic rudstone accumulation that has been interpreted as a cemented transgressive lag (Paul & Lokier, 2017). The fact that firmgrounds and hardgrounds are early marine cementation features has been well documented (Christ et al., 2015; Paul & Lokier, 2017; Ge et al., 2020a), but we see here that they may be distinguished by the type of carbonate sediment lithified, and the degree of resultant diagenesis.

## Bioturbation as a diagenetic inhibitor

Diagenetic processes are explored by multidisciplinary scientists who each deploy a unique combination of methods to unraveling diagenetic histories, as original carbonate environments are seldom preserved without significant chemical overprinting. Accordingly, the observation of modern, early marine diagenetic environments are crucial in understanding carbonate strata. Furthermore, the study of bioturbation in carbonates is extremely difficult, as trace fossils are rarely preserved in comparison to siliciclastic systems (Ekdale, 1984; Knaust, 2007; Kumar, 2017).

As described here and in Chapter 2, crustaceans in the distal intertidal zone are responsible for creating massive appearing sedimentary textures that subsequently produce higher permeability biogenic structures within the sediment column. Tidal waters flow through burrow networks, directly providing solutes into the sediment column via burrows, as opposed to solely downward or upward movement of water through sediment pore space (Meysman et al., 2006; Gingras et al., 2012; Baniak et al., 2022). With this in mind, we have observed that the distal crustacean-related burrow networks facilitate solute movement that differs from the fluid flow in the proximal intertidal zone.

Decisively, crustacean burrowing in the upper-lower to middle intertidal zone, and the resultant impact on fluid flow, is responsible for homogenizing the chemical compositions of the distal sediments (Figs. 3.8; 3.9; 3.11). Recalling that firmground occurrence within Al Qantur lagoon is restricted to the middle-upper intertidal zone, and absent within the lower intertidal zone (Fig. 1.1; Vallack, 2021), we conclude that the bioturbated mixing of distal sediments is responsible for the lack of early marine processes that are observed in the upper intertidal zone. Bioturbation prevents early marine cement lithification of intertidal sediments through continuous mixing, and reduces the likelihood of diagenetic alteration by chemical stabilization. Supportingly, sites 1 & 2 plot chemically similar to seawater in nearly all analyses (Figs. 3.8; 3.9; 3.11), there is no evidence of dissolution (Figs. 3.9C,D; 3.11) and there are no observed firmgrounds in sites 1 & 2.

The implication that bioturbation is capable of preventing early diagenetic processes is not well discussed in the literature. Typically, bioturbation's impact on diagenesis comes from a comparison of non-burrowed to burrowed strata, or post-depositional preferential alteration of burrow fabrics (Berner, 1980; Shull, 2001; Gingras et al., 2004; Zorn, 2010; Corlett & Jones, 2012). However, the determination of where carbonate precipitation and dissolution occurs in relation to spatially variable bioturbate textures is not as well previously discussed. This study provides a primary example of how modern burrowing behavior impacts geochemical fluxes within minor geographic changes and in shallow sediments. In this study, we characterize how subsurface lithification is distributed within an intertidal zone, both laterally and vertically. This early marine lithification leads to compartmentalized sections of the intertidal zone that have different permeability. Cementation in Al Qantur lagoon happens very quickly following deposition, and permeability would presumably become enhanced through continued burial and diagenesis. The determination of such processes cannot be evaluated in studies of ancient carbonates, thereby stressing the importance of modern characterizations of these early diagenetic environments. Furthermore, the combination of methods employed here emphasizes the necessity of ichnologists and carbonate sedimentologists to scrutinize examples of modern carbonate environments. First and foremost, developing an understanding of solute behavior in carbonate systems is a crucial step in determining early-diagenetic processes. Bioturbation inherently affects water flow, and so a more integrated approach of ichnology and hydrology must be employed where burrowing organisms are pervasive. Ideally, combining geochemical analyses of modern sediments with locally variable burrow types will reveal more insight to solute variations than previously understood.

## Subsurface firmground and hardground formation: an alternate method for formation and the rock record implication

Hardgrounds are traditionally understood as stratigraphic horizons which form syndepositionally at or near the sediment-water interface during periods of reduced or suspended sedimentation (Christ et al., 2015). Moreover, hardgrounds are defined by a bored, corroded or eroded upper surface with encrusting or other sessile organisms (Bathurst, 1983). Based on the original study of Abu Dhabi coastal sabkha hardgrounds by Shinn (1969) and recent works (Paul & Lokier, 2017; Ge et al., 2020a; Ge et al., 20223), these traditional hardgrounds are observed in exposed tidal channels with little to no sediment accumulation, however no evidence is provided to suggest that they could not have once been covered by sediment. Regardless, the observation of modern firmgrounds and hardgrounds occur at depth within intertidal substrates (Ge et al., 2020a; Vallack, 2021). The firmgrounds and hardgrounds horizons observed in our study lack encrusting organisms or borings on the upper-surfaces, implying a lack of exposure. Therefore, we believe that these subsurface features do not represent conventional seafloor-lithifying hardgrounds, but rather are indicative of complex hydrological and chemical processes that promote lithification.

Ge et al. (2020a) also recognized firmground to hardground formation via peloidal cementation in the intertidal subsurface but refer to both as potential concretionary features. In doing so, the authors propose an alternative naming for these features as "concretionary sub-hardgrounds," which do not represent hiatal intervals, but rather a complex geochemical system. The authors recognize that the hydrogeochemical dynamics that produce these features is not readily apparent, and advocate for spatially-resolved geochemical analyses; one motivation of this study. In recognizing and adding to Ge et al. (2020a), we have highlighted the significance of the upwelling continental brine which drives dissolution, and is responsible for producing the most recent hardground texture, as well as the impact that bioturbation has on providing seawater-derived solutes to the subsurface and preventing early marine cementation.

Therefore, we determine these features are comparable to traditional hardgrounds, but differ by means of lithification, post-depositional alteration, and location of formation. Since hardgrounds are often used as stratigraphic correlative surfaces, the understanding of what environmental parameters are responsible for their formation is crucial in determining stratigraphic position, as well as paleodepositional environment. These subsurface features could be mistaken for depositional marine hiatal hardgrounds in carbonate strata, despite their formation within unlithified sediment. This makes features such as borings (e.g.

*Glossifungites, Trypanites*) even more critical to the recognition of true hiatal marine hargrounds, compared to stratal subsurface concretions.

## SUMMARY

Firmgrounds and hardgrounds in the Abu Dhabi coastal sabkha, specifically Al Qantur lagoon, have been observed forming in the subsurface, which challenges the traditional interpretations of hardground formation as an exposed seafloor. Previous work by Ge et al. (2020a) advocated for spatially-resolved geochemical analyses surrounding the occurrence of these features, which we have presented in this study. By combining porewater characteristics and sediment geochemistry, we have recognized important drivers in the production of these subsurface features.

Firmgrounds and hardgrounds form by means of early marine cementation by primary precipitates (aragonite, high-Mg calcite) and microbial cohesion of sediments. However, firmgrounds contrast hardgrounds in composition. Firmgrounds are dominantly composed of partially lithified peloids, whereas hardgrounds are bioclastic, and dominated by foraminifera and mollusc shells. Additionally, hardgrounds are characterized by a dissolution texture, whereas firmgrounds are more recently cemented, and do not currently present any evidence of diagenesis. Whether firmgrounds are subject to the same dissolution later on in their burial is unclear, however the textural differences suggest their recognition in lithified examples would be different than to hardgrounds. Dissolution in Al Qantur lagoon is driven by advection of continental brines in the upper intertidal zone, which is locally controlled by the porosity and permeability of the basal hardground. Furthermore, dissolution processes are recognized within the laterally extensive bioclastic rudstone layer, which occurs atop the basal hardground in the intertidal zone. The bioclastic rudstone has comparatively enhanced permeability and allows greater brine advection.

Additionally, bioturbation is an essential component determining where solutes, and subsequent precipitation and dissolution, fluctuate in the intertidal zone. In the distal intertidal zone, crustacean-related burrowing throughout the sediment column allows for enhanced permeability of seawaters and mixing of sediments, which results in reduced variability of water and sediment chemistry. In the lower-upper intertidal zone, burrowing is limited to the shallow depths (0-15 cm) and buried microbial mats occur, which leads to significant chemical changes. Conclusively, crustacean activity is responsible for preventing cementation and diagenetic processes.

Groundwater, seawater, bioturbation, and microbial communities together define the diagenetic system in Al Qantur lagoon. The production of firmgrounds and hardgrounds in this locality is dependent on a complex hydrologic regime that supplies solutes via marine and ground waters. Waters are transported into the intertidal substrates via burrow networks and sediment porosity, from both tidal and groundwater advection, alongside microbial mat communities who mediate the microenvironment to produce dolomite and alter transitional metal fluxes. These particular chemical variations support marine primary precipitates and subsequent dissolution within the subsurface, thereby proposing an alternative method of hardground formation. As these subsurface features could be mistaken for the traditionally described “cemented seafloor,” care must be taken when identifying and describing these horizons.

## References


Ahm, A.-S.C., Bjerrum, C.J., Blättler, C.L., Swart, P.K. and Higgins, J.A. (2018) Quantifying early marine diagenesis in shallow-water carbonate sediments. *Geochimica et Cosmochimica Acta*, 236, 140–159.

Al Suwaidi, A.S., Hami, M.E., Hagiwara, H., Aziz, S.K. and Al Habshi, A.R. (2010) Carbonates and evaporites of the Upper Jurassic Arab Formation, Abu Dhabi: a petroleum exploration challenge. *Quaternary carbonate and evaporite sedimentary facies and their ancient analogues*, 1st edn., *Wiley*, 421–429.

Azer, S.R. and Peebles, R.G. (1998) Sequence Stratigraphy of the Arab A to C Members and Hith Formation, Offshore Abu Dhabi. *GeoArabia*, 3, 251–268.

Baker, P.A., Gieskes, J.M. and Elderfield, H. (1982) Diagenesis of carbonates in deep-sea sediments; evidence from Sr/Ca ratios and interstitial dissolved Sr (super 2+) data. *Journal of Sedimentary Research*, 52, 71–82.

Baldermann, A., Deditius, A.P., Dietzel, M., Fichtner, V., Fischer, C., Hippler, D., Leis, A., Baldermann, C., Mavromatis, V., Stickler, C.P. and Strauss, H. (2015) The role of bacterial sulfate reduction during dolomite precipitation: Implications from Upper Jurassic platform carbonates. *Chemical Geology*, 412, 1–14.

Banerjee, I. and Kidwell, S.M. (1991) Significance of molluscan shell beds in sequence stratigraphy: an example from the Lower Cretaceous Mannville Group of Canada1. *Sedimentology*, 38, 913–934.

Baniak, G.M., La Croix, A.D. and Gingras, M.K. (2022) Recent advancements in characterizing permeability and porosity distributions in bioturbated flow media. *Earth-Science Reviews*, 232, 104162.

Bathurst, R.G.C. (1983) Early Diagenesis of Carbonate Sediments. *Sediment Diagenesis*, *Springer Netherlands*, Dordrecht, 115, 349–377.

Berner, R.A. (1966) Chemical diagenesis of some modern carbonate sediments. *American Journal of Science*, 264, 1–36.

Berner, R.A. (1980) Early Diagenesis: A Theoretical Approach. *Princeton University Press*, 260

Bontognali, T.R.R., Vasconcelos, C., Warthmann, R.J., Bernasconi, S.M., Dupraz, C., Strohmenger, C.J. and McKENZIE, J.A. (2010) Dolomite formation within microbial mats in the coastal sabkha of Abu Dhabi (United Arab Emirates). *Sedimentology*, 57, 824–844.

Bontognali, T.R.R., Vasconcelos, C., Warthmann, R.J., Lundberg, R. and McKenzie, J.A. (2012) Dolomite-mediating bacterium isolated from the sabkha of Abu Dhabi (UAE). *Terra Nova*, 24, 248–254.

Butler, G.P. (1969) Modern Evaporite Deposition and Geochemistry of Coexisting Brines, the Sabkha, Trucial Coast, Arabian Gulf. *Journal of Sedimentary Research*, 39, 70-89.

Calvert, S.E. and Pedersen, T.F. (1993) Geochemistry of Recent oxic and anoxic marine sediments: Implications for the geological record. *Marine Geology*, 113, 67–88.

Campbell, M.A., Grice, K., Visscher, P.T., Morris, T., Wong, H.L., White, R.A., Burns, B.P. and Coolen, M.J.L. (2020) Functional Gene Expression in Shark Bay Hypersaline Microbial Mats: Adaptive Responses. *Frontiers in Microbiology*, 11, 1-16.

Christ, N., Immenhauser, A., Wood, R.A., Darwich, K. and Niedermayr, A. (2015) Petrography and environmental controls on the formation of Phanerozoic marine carbonate hardgrounds. *Earth-Science Reviews*, 151, 176–226.

Coimbra, R., Immenhauser, A. and Olóriz, F. (2009) Matrix micrite δ13C and δ18O reveals synsedimentary marine lithification in Upper Jurassic Ammonitico Rosso limestones (Betic Cordillera, SE Spain). *Sedimentary Geology*, 219, 332–348.

Corlett, H.J. and Jones, B. (2012) Petrographic and Geochemical Contrasts Between Calcite- and Dolomite-Filled Burrows In the Middle Devonian Lonely Bay Formation, Northwest Territories, Canada: Implications for Dolomite Formation In Paleozoic Burrows. *Journal of Sedimentary Research*, 82, 648–663.

Curtis, R., Evans, G., Kinsman, D.J.J. and Shearman, D.J. (1963) Association of Dolomite and Anhydrite in the Recent Sediments of the Persian Gulf. *Nature*, 197, 679–680.

Declet, A., Reyes, E. and Suárez, O.M. (2016) Calcium Carbonate Precipitation: A Review of the Carbonate Crystallization Process and Applications in Bioinspired Composites. *Reviews on Advanced Materials Science*, 44, 87–107.

Diaz, M.R. and Eberli, G.P. (2022) Microbial contribution to early marine cementation. *Sedimentology*, 69, 798–822.

Diaz, M.R., Link to external site, this link will open in a new tab, Eberli, G.P. and Weger, R.J. (2023) Indigenous microbial communities as catalysts for early marine cements: An in vitro study. *The Depositional Record*, 9, 437–456.

DiLoreto, Z.A., Bontognali, T.R.R., Al Disi, Z.A., Al-Kuwari, H.A.S., Williford, K.H., Strohmenger, C.J., Sadooni, F., Palermo, C., Rivers, J.M., McKenzie, J.A., Tuite, M. and Dittrich, M. (2019) Microbial community composition and dolomite formation in the hypersaline microbial mats of the Khor Al-Adaid sabkhas, Qatar. *Extremophiles*, 23, 201–218.

Dittrich, M. and Sibler, S. (2010) Calcium carbonate precipitation by cyanobacterial polysaccharides. *Geological Society, London, Special Publications*, 336, 51–63.

Dravis, J. (1979) Rapid and widespread generation of Recent oolitic hardgrounds on a high energy Bahamian platform, Eleuthera Bank, Bahamas. *Journal of Sedimentary Research*, 49, 195–207.

Dupraz, C., Reid, R.P., Braissant, O., Decho, A.W., Norman, R.S. and Visscher, P.T. (2009) Processes of carbonate precipitation in modern microbial mats. *Earth-Science Reviews*, 96, 141–162.

Dupraz, C. and Visscher, P.T. (2005) Microbial lithification in marine stromatolites and hypersaline mats. *Trends in Microbiology*, 13, 429–438.

Ekdale, A.A., Bromley, R.G. and Pemberton, S.G. (1984) SEPM Short Course: Ichnology: The Use of Trace Fossils in Sedimentology and Stratigraphy.

Elicki, O., Schneider, J. and Shinaq, R. (2002) Prominent facies from the Lower/Middle Cambrian of the Dead Sea area (Jordan) and their palaeodepositional significance. *Bulletin de la Société Géologique de France*, 173, 547–552.

El-Sayed, M.I. (1999) Sedimentological characteristics and morphology of the aeolian sand dunes in the eastern part of the UAE, a case study from Ar Rub'Al Khali: *Sedimentary Geology*, 123, 219-238.

Evamy, B.D. (1973) The Precipitation of Aragonite and Its Alteration to Calcite on the Trucial Coast of the Persian Gulf. *The Persian Gulf*, Conference paper: Berlin, Heidelberg, 329–341.

Evans, G. The Recent Sedimentary Facies of the Persian Gulf Region. *Philosophical Transactions of the Royal Society of London. Series A, Mathematical and Physical Sciences*, 259, 291-298.

Evans, G., Kendall, C.G.St.C. and Skipwith, P. (1964) Origin of the Coastal Flats, the Sabkha, of the Trucial Coast, Persian Gulf. *Nature*, 202, 759–761.

Evans, G., Schmidt, V., Bush, P. and Nelson, H. (1969) stratigraphy and geologic history of the sabkha, abu dhabi, persian gulf. *Sedimentology*, 12, 145–159.

Folk, R.L. (1974) The natural history of crystalline calcium carbonate; effect of magnesium content and salinity. *Journal of Sedimentary Research*, 44, 40–53.

Folk, R.L. and Lynch, L. (2001) Organic matter, putative nannobacteria and the formation of ooids and hardgrounds. *Sedimentology*, 48, 215–229.

Friedman, G.M. (1964) Early diagenesis and lithification in carbonate sediments. *Journal of Sedimentary Research*, 34, 777–813.

Garrison, R.E., Luternauer, J.L., Grill, E.V., Macdonald, R.D. and Murray, J.W. (1969) Early Diagenetic Cementation of Recent Sands, Fraser River Delta, British Columbia. *Sedimentology*, 12, 27–46.

Ge, Y., Lokier, S.W., Hoffmann, R., Pederson, C.L., Neuser, R.D. and Immenhauser, A. (2020a) Composite micrite envelopes in the lagoon of Abu Dhabi and their application for the recognition of ancient firm- to hardgrounds. *Marine Geology*, 423, 106141.

Ge, Y., Pederson, C.L., Lokier, S.W., Strauss, H. and Immenhauser, A. (2023) Radiaxial fibrous calcite forms via early marine-diagenetic alteration of micritic magnesium calcite. *Sedimentology*, 70, 434–450.

Ge, Y., Pederson, C.L., Lokier, S.W., Traas, J.P., Nehrke, G., Neuser, R.D., Goetschl, K.E. and Immenhauser, A. (2020b) Late Holocene to Recent aragonite-cemented transgressive lag deposits in the Abu Dhabi lagoon and intertidal sabkha. *Sedimentology*, 67, 2426–2454.

Gerbersdorf, S.U. and Wieprecht, S. (2015) Biostabilization of cohesive sediments: revisiting the role of abiotic conditions, physiology and diversity of microbes, polymeric secretion, and biofilm architecture. *Geobiology*, 13, 68–97.

Geske, A., Lokier, S., Dietzel, M., Richter, D.K., Buhl, D. and Immenhauser, A. (2015) Magnesium isotope composition of sabkha porewater and related (Sub-)Recent stoichiometric dolomites, Abu Dhabi (UAE). *Chemical Geology*, 393–394, 112–124.

Gingras, M.K., Baniak, Greg., Gordon, John., Hovikoski, Jussi., Konhauser, K.O., La Croix, Andrew., Lemiski, Ryan., Mendoza, Carl., Pemberton, S.G., Polo, Camilo. and Zonneveld, J.-Paul. (2012) Chapter 27 - Porosity and Permeability in Bioturbated Sediments. *Developments in Sedimentology*, 64, 837–868.

Gingras, M.K., Pemberton, S.G., Muelenbachs, K. and Machel, H. (2004) Conceptual models for burrow-related, selective dolomitization with textural and isotopic evidence from the Tyndall Stone, Canada. *Geobiology*, 2, 21–30.

Halbertsma, H.L., Mossop, G.D. and Shetsen, I. (1994) Devonian Wabamun Group of the western Canada sedimentary basin. *Geological Atlas of the Western Canada Sedimentary Basin*, 4, 203-220.

Hiatt, E. and Pufahl, P. (2014) Cathodoluminescence petrography of carbonate rocks: application to understanding diagenesis, reservoir quality, and pore system evolution. 45, 75–96.

Hippler, D., Buhl, D., Witbaard, R., Richter, D.K. and Immenhauser, A. (2009) Towards a better understanding of magnesium-isotope ratios from marine skeletal carbonates. *Geochimica et Cosmochimica Acta*, 73, 6134–6146.

Hope, J.A., Paterson, D.M. and Thrush, S.F. (2020) The role of microphytobenthos in soft-sediment ecological networks and their contribution to the delivery of multiple ecosystem services. *Journal of Ecology*, 108, 815–830.

Hubas, C., Passarelli, C. and Paterson, D.M. (2018) Microphytobenthic Biofilms: Composition and Interactions: *Mudflat Ecology*, 7, 63–90.

Katz, A., Sass, E., Starinsky, A. and Holland, H.D. (1972) Strontium behavior in the aragonite-calcite transformation: An experimental study at 40–98°C. *Geochimica et Cosmochimica Acta*, 36, 481–496.

Kendall, C. and Skipwith, P. (1968) Recent Algal Mats of a Persian Gulf Lagoon: *Journal of Sedimentary Research*, 38, 1040-1058.

Kennedy, W.J. and Garrison, R.E. (1975) Morphology and genesis of nodular chalks and hardgrounds in the Upper Cretaceous of southern England. *Sedimentology*, 22, 311–386.

Kidwell, S.M. (1989) Stratigraphic Condensation of Marine Transgressive Records: Origin of Major Shell Deposits in the Miocene of Maryland. *The Journal of Geology*, 97, 1–24.

Kinsman, D.J.J. (1969) Modes of Formation, Sedimentary Associations, and Diagnostic Features of Shallow-Water and Supratidal Evaporites. *AAPG Bulletin*, 53, 830–840.

Kirkham, A. (1998) A Quaternary proximal foreland ramp and its continental fringe, Arabian Gulf, UAE. *SP*, 149, 15–41.

Knaust, D. (2007) Meiobenthic Trace Fossils as Keys to the Taphonomic History of Shallow-Marine Epicontinental Carbonates. *Trace Fossils*, *Elsevier*, Amsterdam, 502–517.

Kumar, A. (2017) Recent biogenic traces from the coastal environments of the southern Red Sea coast of Saudi Arabia. *Arab J Geosci*, 10, 1-11.

LaGrange, M.T., Konhauser, K.O., Catuneanu, O., Harris, B.S., Playter, T.L. and Gingras, M.K. (2020) Sequence stratigraphy in organic-rich marine mudstone successions using chemostratigraphic datasets. *Earth-Science Reviews*, 203, 103137.

Land, L.S., and Hoops, G.K. (1973) Sodium in carbonate sediments and rocks; a possible index to the salinity of diagenetic solutions. *Journal of Sedimentary Research*, 43, 614-617.

Liu, Y., Jiao, J.J. and Luo, X. (2016) Effects of inland water level oscillation on groundwater dynamics and land-sourced solute transport in a coastal aquifer. *Coastal Engineering*, 114, 347–360.

Lokier, S. and Steuber, T. (2009) Large-scale intertidal polygonal features of the Abu Dhabi coastline. *Sedimentology*, 56, 609–621.

Lokier, S.W., Bateman, M.D., Larkin, N.R., Rye, P. and Stewart, J.R. (2015) Late Quaternary sea-level changes of the Persian Gulf. *Quaternary Research*, 84, 69–81.

Lokier, S.W., Knaf, A. and Kimiagar, S. (2013) A quantitative analysis of Recent arid coastal sedimentary facies from the Arabian Gulf Coastline of Abu Dhabi, United Arab Emirates. *Marine Geology*, 346, 141–152.

Lundkvist, M., Grue, M., Friend, P.L. and Flindt, M.R. (2007) The relative contributions of physical and microbiological factors to cohesive sediment stability. *Continental Shelf Research*, 27, 1143–1152.

Machel, H.G. (2001) Bacterial and thermochemical sulfate reduction in diagenetic settings — old and new insights. *Sedimentary Geology*, 140, 143–175.

Mandal, A., Dutta, A., Das, R. and Mukherjee, J. (2021) Role of intertidal microbial communities in carbon dioxide sequestration and pollutant removal: A review. *Marine Pollution Bulletin*, 170, 112626.

Melim, L.A. and Scholle, P.A. (2002) Dolomitization of the Capitan Formation forereef facies (Permian, west Texas and New Mexico): seepage reflux revisited. *Sedimentology*, 49, 1207–1227.

Meysman, F.J.R., Galaktionov, O.S., Gribsholt, B. and Middelburg, J.J. (2006) Bioirrigation in permeable sediments: Advective pore-water transport induced by burrow ventilation. *Limnology and Oceanography*, 51, 142–156.

Milliman, J.D. (1993) Production and accumulation of calcium carbonate in the ocean: Budget of a nonsteady state. *Global Biogeochemical Cycles*, 7, 927–957.

Moore, C.H. (ed) (2001) Chapter 6 - Evaporative Marine Diagenetic Environments. *Developments in Sedimentology*, *Elsevier*, 55, 145–183.

Morse, J.W., Arvidson, R.S. and Lüttge, A. (2007) Calcium Carbonate Formation and Dissolution. *Chem. Rev.*, 107, 342–381.

Morse, J.W., Wang, Q. and Tsio, M.Y. (1997) Influences of temperature and Mg:Ca ratio on CaCO3 precipitates from seawater. *Geology*, 25, 85–87.

Paterson, D.M. (1994) Microbiological mediation of sediment structure and behaviour. *Microbial Mats*, *Springer*, Berlin, Heidelberg, 35, 97–109.

Paul, A. and Lokier, S.W. (2017) Holocene marine hardground formation in the Arabian Gulf: Shoreline stabilisation, sea level and early diagenesis in the coastal sabkha of Abu Dhabi. *Sedimentary Geology*, 352, 1–13.

Pederson, C.L., Ge, Y., Lokier, S.W., Swart, P.K., Vonhof, H., Strauss, H., Schurr, S., Fiorini, F., Riechelmann, S., Licha, T. and Immenhauser, A. (2021) Seawater chemistry of a modern subtropical 'epeiric' sea: Spatial variability and effects of organic decomposition. *Geochimica et Cosmochimica Acta*, 314, 159–177.

Pfeifer, K., Kasten, S., Hensen, C. and Schulz, H.D. (2001) Reconstruction of primary productivity from the barium contents in surface sediments of the South Atlantic Ocean. *Marine Geology*, 177, 13–24.

Rasmussen, B., Krapež, B. and Muhling, J.R. (2015) Seafloor silicification and hardground development during deposition of 2.5 Ga banded iron formations. *Geology*, 43, 235–238.

Sadooni, F.N., Howari, F. and El-Saiy, A. (2010) Microbial Dolomites from Carbonate-Evaporite Sediments of the Coastal Sabkha of Abu Dhabi and Their Exploration Implications. *Journal of Petroleum Geology*, 33, 289–298.

Saller, A.H. (1986) Radiaxial calcite in lower Miocene strata, subsurface Enewetak Atoll. *Journal of Sedimentary Research*, 56, 743–762.

Saller, A.H. and Henderson, N. (1998) Distribution of Porosity and Permeability in Platform Dolomites: Insight from the Permian of West Texas1. *AAPG Bulletin*, 82, 1528–1550.

Sarg, J.F. (1988) Carbonate sequence stratigraphy. Sea-level Changes: An Integral Approach. Wilgus, B.S.H.C.K., Kendall, C.G.S.C., Posamentier, H.W., Ross, C.A., van Wagoner, J.C. (Eds.), SEPM Special Publication 42, 155–181.

Schlanger, S.O. (1988) Strontium Storage and Release During Deposition and Diagenesis of Marine Carbonates Related to Sea-Level Variations. *Physical and Chemical Weathering in Geochemical Cycles*, *Springer Netherlands*, Dordrecht, 251, 323–339.

Schroeder, J.H. (1969) Experimental Dissolution of Calcium, Magnesium, and Strontium from Recent Biogenic Carbonates: A Model of Diagenesis, 39, 1057-1073

Shinn, E.A. (1969) Submarine Lithification of Holocene Carbonate Sediments in the Persian Gulf. *Sedimentology*, 12, 109–144.

Shull, D.H. (2001) Transition-matrix model of bioturbation and radionuclide diagenesis. *Limnology and Oceanography*, 46, 905–916.

Søndergaard, M. (2009) Redox Potential. *Encyclopedia of Inland Waters*, *Academic Press*, Oxford, 852–859.

Stehli, F.G. and Hower, J. (1961) Mineralogy and early diagenesis of carbonate sediments. *Journal of Sedimentary Research*, 31, 358–371.

Steiner, Z., Lazar, B., Torfstein, A. and Erez, J. (2017) Testing the utility of geochemical proxies for paleoproductivity in oxic sedimentary marine settings of the Gulf of Aqaba, Red Sea. *Chemical Geology*, 473, 40–49.

Strohmenger, C.J., Al-Mansoori, A., Al-Jeelani, O., Al-Shamry, A., Al-Hosani, I., Al-Mehsin, K. and Shebl, H. (2010) The sabkha sequence at Mussafah Channel (Abu Dhabi, United Arab Emirates): Facies stacking patterns, microbial-mediated dolomite and evaporite overprint. *GeoArabia*, 15, 49–90.

Sumner, D.Y. and Grotzinger, J.P. (2004) Implications for Neoarchaean ocean chemistry from primary carbonate mineralogy of the Campbellrand-Malmani Platform, South Africa. *Sedimentology*, 51, 1273–1299.

Sunagawa, I., Takahashi, Y. and Imai, H. (2007) Strontium and aragonite-calcite precipitation. *Journal of Mineralogical and Petrological Sciences*, 102, 174–181.

Swart, P.K. (1981) The strontium, magnesium and sodium composition of recent scleractinian coral skeletons as standards for palaeoenvironmental analysis. *Palaeogeography, Palaeoclimatology, Palaeoecology*, 34, 115–136.

Swart, P.K. (2015) The geochemistry of carbonate diagenesis: The past, present and future. *Sedimentology*, 62, 1233–1304.

Taylor, P.D. and Wilson, M.A. (2003) Palaeoecology and evolution of marine hard substrate communities. *Earth-Science Reviews*, 62, 1–103.

Tribovillard, N., Algeo, T.J., Lyons, T. and Riboulleau, A. (2006) Trace metals as paleoredox and paleoproductivity proxies: An update. *Chemical Geology*, 232, 12–32.

Vallack, H.L. (2021) Physical and biogeochemical drivers of Modern carbonate diagenesis in intertidal sediments of Abu Dhabi. Ph.D., University of Bristol

Vasconcelos, C. and McKenzie, J.A. (1997) Microbial mediation of modern dolomite precipitation and diagenesis under anoxic conditions (Lagoa Vermelha, Rio de Janeiro, Brazil). *Journal of Sedimentary Research*, 67, 378–390.

Vasconcelos, C., McKenzie, J.A., Bernasconi, S., Grujic, D. and Tiens, A.J. (1995) Microbial mediation as a possible mechanism for natural dolomite formation at low temperatures. *Nature*, 377, 220–222.

Wanty, R.B. and Goldhaber, M.B. (1992) Thermodynamics and kinetics of reactions involving vanadium in natural systems: Accumulation of vanadium in sedimentary rocks. *Geochimica et Cosmochimica Acta*, 56, 1471–1483.

Warren, J. (2000) Dolomite: occurrence, evolution and economically important associations. *Earth-Science Reviews*, 52, 1–81.

Wong, H.L., Smith, D.-L., Visscher, P.T. and Burns, B.P. (2015) Niche differentiation of bacterial communities at a millimeter scale in Shark Bay microbial mats. *Sci Rep*, 5, 15607.

Wood, W.W., Sanford, W.E. and Habshi, A.R.S.A. (2002) Source of solutes to the coastal sabkha of Abu Dhabi. *GSA Bulletin*, 114, 259–268.

Yallop, M.L., Paterson, D.M. and Wellsbury, P. (2000) Interrelationships between Rates of Microbial Production, Exopolymer Production, Microbial Biomass, and Sediment Stability in Biofilms of Intertidal Sediments. *Microb Ecol*, 39, 116–127.

Zorn, M.E., Gingras, M.K. and Pemberton, S.G. (2010) Variation in burrow-wall micromorphologies of select intertidal invertebrates along the pacific northwest coast, usa: behavioral and diagenetic implications. *PALAIOS*, 25, 59–72.

## Chapter 4: Conclusions

Carbonate ramps are prevalent in the rock record, and observations of modern analogues help us to understand stratal successions. The southwestern Arabian Gulf provides one of the best localities to assess ramp characteristics, as the homoclinal ramp extends over a large geographic area and is relatively easy to access (Lokier, 2013). Additionally, the modern setting is analogous to the world's largest oil-bearing reservoir, the Arab Formation (Alsharhan, 1989; Azer & Peebles, 1998). Particularly, the Abu Dhabi coastal sabkha has become one of the most frequently visited and cited study areas for sedimentologists following oil initiatives in the '60s and onward (Purser, 1973; Lokier, 2013). With this is in mind, it is surprising that no neoichnological studies have been produced out of this locale, considering the sedimentological and hydrological information that can be gained from biogenic sedimentary structures. Additionally, current research in the area has improved our understanding of carbonate precipitation and diagenesis, however the formation of early marine firmgrounds and hardground within the intertidal zone is still ambiguous.

This thesis recognizes that the formation and dissolution of firmgrounds and hardgrounds in the subsurface is a product of specific chemical interactions that are influenced by spatially variable infaunal communities and locally variable groundwater leakage. The previous lack of ichnological and hydrological discussion is perhaps one reason why the genesis of these features has remained clouded. Additionally, this thesis is one of few studies to analyze porewater and sediment geochemistry together, further progressing our knowledge of the entire geochemical system.

Chapter 2 has accomplished characterizing a carbonate ramps intertidal zone using a neoichnological framework, the first study to do so. By combining observations of carbonate sedimentology and bioturbation textures, we have detailed how sediment fabrics are spatially variable within the intertidal zone. In doing so, we have recognized how burrowers influence solute distributions. Bioirrigation, sediment mixing, and enhanced burrow-permeability leads to increasing amounts of seawater permeation within intertidal substrates. The heightened flux of seawaters via burrow fabrics has proven to be significant in controlling the precipitation and diagenesis of carbonate material (Fig. 3.8; 3.9). Considering this, we have recognized how bioturbation prohibits diagenetic processes in this locale.

Chapter 3 has integrated the works of Chapter 2 and further detailed spatially resolved chemical analyses of both porewaters and sediments. In doing so, Chapter 3 has achieved one of the more thorough geochemical characterizations of the Abu Dhabi intertidal zone to date. Chapter 3 has recognized that early marine cements are precipitated out of porewaters, and that these cements together with microbial cohesion are responsible for the lithification of subsurface firmground and hardgrounds horizons. This observation presents an alternative method to hardground formation, challenging conventional interpretations. In addition to recognizing the impact of bioturbation in reducing diagenesis, Chapter 3 has also detailed how an advecting continental brine drives dissolution. Additionally, Chapter 3 combines the geochemistry of both porewaters and sediments. More often, porewater chemistry is inferred in carbonate studies, and so the combination of methods removes hypotheses, and provides quantitative comparisons.

These chapters together provide the basis for future works detailing early marine subsurface features and encourage future carbonate studies to involve more ichnologic discussion. Carbonate studies inherently incorporate some biologic discussion, and indeed the current discourse related to the microbial influence on carbonate precipitation is substantial (Vasconcelos & McKenzie, 1997; Bontognali et al. 2010; Declet et al. 2016; Diaz et al. 2022; Diaz & Eberli, 2022). However, little dialogue exists pertaining to the role of infaunal communities on carbonate precipitation and diagenesis. Here, we have provided one example of how bioturbators prohibit cement formation and enhance solute movement within shallow substrates. Presumably, this interaction exists, yet varies, within other modern carbonate environments. What if there is increased meteoric input? No continental brine? Undersaturated seawaters? Protected versus open marine? Different infaunal communities? So many variables influence solute distributions, yet little to no modern carbonate studies integrate descriptions of biogenic sedimentary structures, which inevitably change substrate permeability.

Dolomite and Mg fluxes in the proximal study sites of this thesis are another interesting topic of the Abu Dhabi coastal sabkha. These chapters did not dwell on the logistics of dolomite precipitation, as the delineation of the primary processes responsible for dolomitization and dedolomitization exceeded the scope of this project. Likely, the complex geochemistry of the Site 4 microenvironment is related to spatial variability in microbial communities. Further research should compare buried mat characteristics to the more landward, surficial mat environments.

Furthermore, modern firmground and hardground horizons are currently found in the Bahamas, the Bermudas, the Arabian Gulf, the Red Sea, the Gulf of Mexico, USA, Australia, Northern Europe, the Mediterranean and Canada (see Christ et al. 2015 for review). As we have detailed another method for hardground formation, alongside Ge et al. (2020), there now exists a demand for caution when encountering such horizons in the subsurface, as hardgrounds are stratigraphically important. Additionally, we have presented one of few studies which compares both porewater and sediment chemistry and have exhibited how effective this combination can be in identifying early marine carbonate precipitation and alteration. The information gained by detailing both the carbonate and porewater composition quantitatively defines elemental distributions, which lends to source identification. We encourage future carbonate studies to approach their research with this framework.

## References

Alsharhan, A.S. (1989) Petroleum Geology of the United Arab Emirates. *Journal of Petroleum Geology*, 12, 253–288.

Azer, S.R. and Peebles, R.G. (1998) Sequence Stratigraphy of the Arab A to C Members and Hith Formation, Offshore Abu Dhabi. *GeoArabia*, 3, 251–268.

Bontognali, T.R.R., Vasconcelos, C., Warthmann, R.J., Bernasconi, S.M., Dupraz, C., Strohmenger, C.J. and McKENZIE, J.A. (2010) Dolomite formation within microbial mats in the coastal sabkha of Abu Dhabi (United Arab Emirates). *Sedimentology*, 57, 824–844.

Christ, N., Immenhauser, A., Wood, R.A., Darwich, K. and Niedermayr, A. (2015) Petrography and environmental controls on the formation of Phanerozoic marine carbonate hardgrounds. *Earth-Science Reviews*, 151, 176–226.

Declet, A., Reyes, E. and Suárez, O.M. (2016) Calcium Carbonate Precipitation: A Review of the Carbonate Crystallization Process and Applications in Bioinspired Composites. *Reviews on Advanced Materials Science*, 44, 87–107.

Diaz, M.R. and Eberli, G.P. (2022) Microbial contribution to early marine cementation. *Sedimentology*, 69, 798–822.

Diaz, M.R., Link to external site, this link will open in a new tab, Eberli, G.P. and Weger, R.J. (2023) Indigenous microbial communities as catalysts for early marine cements: An in vitro study. *The Depositional Record*, 9, 437–456.

Ge, Y., Pederson, C.L., Lokier, S.W., Traas, J.P., Nehrke, G., Neuser, R.D., Goetschl, K.E. and Immenhauser, A. (2020) Late Holocene to Recent aragonite-cemented transgressive lag deposits in the Abu Dhabi lagoon and intertidal sabkha. *Sedimentology*, 67, 2426–2454.

Lokier, S.W. (2013) Coastal Sabkha Preservation in the Arabian Gulf. *Geoheritage*, 5, 11–22.

Purser, B.H. (2012) The Persian Gulf: Holocene Carbonate Sedimentation and Diagenesis in a Shallow Epicontinental Sea. *Springer Science & Business Media*, 470 pp.

Vasconcelos, C. and McKenzie, J.A. (1997) Microbial mediation of modern dolomite precipitation and diagenesis under anoxic conditions (Lagoa Vermelha, Rio de Janeiro, Brazil). *Journal of Sedimentary Research*, 67, 378–390.

## Bibliography

Ahm, A.-S.C., Bjerrum, C.J., Blättler, C.L., Swart, P.K. and Higgins, J.A. (2018) Quantifying early marine diagenesis in shallow-water carbonate sediments. *Geochimica et Cosmochimica Acta*, 236, 140–159.

Al Suwaidi, A.S., Hami, M.E., Hagiwara, H., Aziz, S.K. and Al Habshi, A.R. (2010) Carbonates and evaporites of the Upper Jurassic Arab Formation, Abu Dhabi: a petroleum exploration challenge. *Quaternary carbonate and evaporite sedimentary facies and their ancient analogues*, 1st edn., *Wiley*, 421–429.

Alexander, R.R., Stanton, R.J., and Dodd, J.R. (1993) Influence of Sediment Grain Size on the Burrowing of Bivalves: Correlation with Distribution and Stratigraphic Persistence of Selected Neogene Clams: *PALAIOS*, 8, 289–303.

Alsharhan, A.S., and Kendall, C.G.St.C. (2003) Holocene coastal carbonates and evaporites of the southern Arabian Gulf and their ancient analogues: *Earth-Science Reviews*, 61, 191–243.

Arribas, J., Alonso, Á., Pagés, J.L., and González-Acebrón, L. (2010) Holocene transgression recorded by sand composition in the mesotidal Galician coastline (NW Spain): *The Holocene*, 20, 375–393.

Azer, S.R. and Peebles, R.G. (1998) Sequence Stratigraphy of the Arab A to C Members and Hith Formation, Offshore Abu Dhabi. *GeoArabia*, 3, 251–268.

Azer, S.R., Peebles, R. G. (1995) Sequence Stratigraphy of the Hith I Upper Arab Formations Offshore Abu Dhabi, U.A.E. *SPE Middle East Oil and Gas Show and Conference, Bahrain*, SPE-29799-MS.

Baker, P.A., Gieskes, J.M. and Elderfield, H. (1982) Diagenesis of carbonates in deep-sea sediments; evidence from Sr/Ca ratios and interstitial dissolved Sr (super 2+) data. *Journal of Sedimentary Research*, 52, 71–82.

Baldermann, A., Deditius, A.P., Dietzel, M., Fichtner, V., Fischer, C., Hippler, D., Leis, A., Baldermann, C., Mavromatis, V., Stickler, C.P. and Strauss, H. (2015) The role of bacterial sulfate reduction during dolomite precipitation: Implications from Upper Jurassic platform carbonates. *Chemical Geology*, 412, 1–14.

Banerjee, I. and Kidwell, S.M. (1991) Significance of molluscan shell beds in sequence stratigraphy: an example from the Lower Cretaceous Mannville Group of Canada1. *Sedimentology*, 38, 913–934.

Baniak, G.M., La Croix, A.D. and Gingras, M.K. (2022) Recent advancements in characterizing permeability and porosity distributions in bioturbated flow media. *Earth-Science Reviews*, 232, 104162.

Bathurst, R.G.C. (1983) Early Diagenesis of Carbonate Sediments. *Sediment Diagenesis*, *Springer Netherlands*, Dordrecht, 115, 349–377.

Beadle, L.C. (1937) Adaptation to Changes of Salinity in the Polychaetes: *Journal of Experimental Biology*, 14, 56–70.

Berner, R.A. (1966) Chemical diagenesis of some modern carbonate sediments. *American Journal of Science*, 264, 1–36.

Berner, R.A. (1980) Early Diagenesis: A Theoretical Approach. *Princeton University Press*, 260

Bontognali, T.R.R., Vasconcelos, C., Warthmann, R.J., Bernasconi, S.M., Dupraz, C., Strohmenger, C.J. and McKENZIE, J.A. (2010) Dolomite formation within microbial mats in the coastal sabkha of Abu Dhabi (United Arab Emirates). *Sedimentology*, 57, 824–844.

Bontognali, T.R.R., Vasconcelos, C., Warthmann, R.J., Lundberg, R. and McKenzie, J.A. (2012) Dolomite-mediating bacterium isolated from the sabkha of Abu Dhabi (UAE). *Terra Nova*, 24, 248–254.

Brush, L.M., Jr. (1965) Sediment Sorting in Alluvial Channels: *SEPM Special Publication*, 12, 25-33.

Buatois, L.A., and Mángano, M.G. (2011) Ichnology: Organism-Substrate Interactions in Space and Time: *Cambridge University Press*, 371.

Butler, G.P. (1969) Modern Evaporite Deposition and Geochemistry of Coexisting Brines, the Sabkha, Trucial Coast, Arabian Gulf. *Journal of Sedimentary Research*, 39, 70-89.

Button, A., and Vos, R.G. (1977) Subtidal and intertidal clastic and carbonate sedimentation in a macrotidal environment: an example from the lower proterozoic of South Africa: *Sedimentary Geology*, 18, 175–200.

Calvert, S.E. and Pedersen, T.F. (1993) Geochemistry of Recent oxic and anoxic marine sediments: Implications for the geological record. *Marine Geology*, 113, 67–88.

Campbell, M.A., Grice, K., Visscher, P.T., Morris, T., Wong, H.L., White, R.A., Burns, B.P. and Coolen, M.J.L. (2020) Functional Gene Expression in Shark Bay Hypersaline Microbial Mats: Adaptive Responses. *Frontiers in Microbiology*, 11, 1-16.

Chakrabarti, A., Chakrabarti, R., and Hertweck, G. (2006) Surface traces and bioturbate textures from bubbler crabs: an indicator of subtropical to tropical tidal flat environments*: Senckenbergiana maritima*, 36, 19–27.

Christ, N., Immenhauser, A., Wood, R.A., Darwich, K. and Niedermayr, A. (2015) Petrography and environmental controls on the formation of Phanerozoic marine carbonate hardgrounds. *Earth-Science Reviews*, 151, 176–226.

Coimbra, R., Immenhauser, A. and Olóriz, F. (2009) Matrix micrite δ13C and δ18O reveals synsedimentary marine lithification in Upper Jurassic Ammonitico Rosso limestones (Betic Cordillera, SE Spain). *Sedimentary Geology*, 219, 332–348.

Corlett, H.J. and Jones, B. (2012) Petrographic and Geochemical Contrasts Between Calcite- and Dolomite-Filled Burrows In the Middle Devonian Lonely Bay Formation, Northwest Territories, Canada: Implications for Dolomite Formation In Paleozoic Burrows. *Journal of Sedimentary Research*, 82, 648–663.

Curtis, R., Evans, G., Kinsman, D.J.J. and Shearman, D.J. (1963) Association of Dolomite and Anhydrite in the Recent Sediments of the Persian Gulf. *Nature*, 197, 679–680.

Dashtgard, S.E., and Gingras, M.K. (2012) Marine Invertebrate Neoichnology: *Developments in Sedimentology: Elsevier*, 273–295.

Davenport, J. (1985) Osmotic control in marine animals: *Symposia of the Society for Experimental Biology*, 39, 207–244.

Declet, A., Reyes, E. and Suárez, O.M. (2016) Calcium Carbonate Precipitation: A Review of the Carbonate Crystallization Process and Applications in Bioinspired Composites. *Reviews on Advanced Materials Science*, 44, 87–107.

Desjardins, P.R., Buatois, L.A., and Mángano, M.G. (2012) Tidal Flats and Subtidal Sand Bodies: *Developments in Sedimentology: Elsevier*, 529–561.

Diaz, M.R. and Eberli, G.P. (2022) Microbial contribution to early marine cementation. *Sedimentology*, 69, 798–822.

Diaz, M.R., Link to external site, this link will open in a new tab, Eberli, G.P. and Weger, R.J. (2023) Indigenous microbial communities as catalysts for early marine cements: An in vitro study. *The Depositional Record*, 9, 437–456.

DiLoreto, Z.A., Bontognali, T.R.R., Al Disi, Z.A., Al-Kuwari, H.A.S., Williford, K.H., Strohmenger, C.J., Sadooni, F., Palermo, C., Rivers, J.M., McKenzie, J.A., Tuite, M. and Dittrich, M. (2019) Microbial community composition and dolomite formation in the hypersaline microbial mats of the Khor Al-Adaid sabkhas, Qatar. *Extremophiles*, 23, 201–218.

Dittrich, M. and Sibler, S. (2010) Calcium carbonate precipitation by cyanobacterial polysaccharides. *Geological Society, London, Special Publications*, 336, 51–63.

Dravis, J. (1979) Rapid and widespread generation of Recent oolitic hardgrounds on a high energy Bahamian platform, Eleuthera Bank, Bahamas. *Journal of Sedimentary Research*, 49, 195–207.

Dupraz, C. and Visscher, P.T. (2005) Microbial lithification in marine stromatolites and hypersaline mats. *Trends in Microbiology*, 13, 429–438.

Dupraz, C., Reid, R.P., Braissant, O., Decho, A.W., Norman, R.S. and Visscher, P.T. (2009) Processes of carbonate precipitation in modern microbial mats. *Earth-Science Reviews*, 96, 141–162.

Ekdale, A.A., Bromley, R.G., and Pemberton, S.G. (1984) *SEPM Short Course: Ichnology: The Use of Trace Fossils in Sedimentology and Stratigraphy: SEPM (Society for Sedimentary Geology).*

Elicki, O., Schneider, J. and Shinaq, R. (2002) Prominent facies from the Lower/Middle Cambrian of the Dead Sea area (Jordan) and their palaeodepositional significance. *Bulletin de la Société Géologique de France*, 173, 547–552.

El-Sayed M.I. (1999) Sedimentological characteristics and morphology of the aeolian sand dunes in the eastern part of the UAE, a case study from Ar Rub'Al Khali: *Sedimentary Geology*, 123(3-4), 219-238.

Evamy, B.D. (1973) The Precipitation of Aragonite and Its Alteration to Calcite on the Trucial Coast of the Persian Gulf. *The Persian Gulf*, Conference paper: Berlin, Heidelberg, 329–341.

Evans, G. (1966) The Recent Sedimentary Facies of the Persian Gulf Region: *Philosophical Transactions of the Royal Society of London. Series A, Mathematical and Physical Sciences*, 259(1099), 291-298.

Evans, G. (2005) Douglas James Shearman, 1918–2003: *Proceedings of the Geologists' Association*, 116, 191–205.

Evans, G. (1966) The Recent Sedimentary Facies of the Persian Gulf Region. *Philosophical Transactions of the Royal Society of London. Series A, Mathematical and Physical Sciences*, 259, 291-298.

Evans, G., Kendall, C.G.St.C. and Skipwith, P. (1964) Origin of the Coastal Flats, the Sabkha, of the Trucial Coast, Persian Gulf. *Nature*, 202, 759–761.

Evans, G., Schmidt, V., Bush, P. and Nelson, H. (1969) stratigraphy and geologic history of the sabkha, abu dhabi, persian gulf. *Sedimentology*, 12, 145–159.

Folk, R.L. (1974) The natural history of crystalline calcium carbonate; effect of magnesium content and salinity. *Journal of Sedimentary Research*, 44, 40–53.

Folk, R.L. and Lynch, L. (2001) Organic matter, putative nannobacteria and the formation of ooids and hardgrounds. *Sedimentology*, 48, 215–229.

Friedman, G.M. (1964) Early diagenesis and lithification in carbonate sediments. *Journal of Sedimentary Research*, 34, 777–813.

Furlong, C.M., Gingras, M.K. and Zonneveld, J.P. (2015) Trypanites-Type Ichnofacies at the Bay of Fundy, Nova Scotia, Canada. *Palaios*, 30, 258-271.

Garrison, J., Henk, B., and Creel, R. (2007) Neoichnology of the Micro-Tidal Gulf Coast of Texas: Implications for Paleoecological and Paleoenvironmental Interpretations of Ancient Micro-Tidal Clastic Shoreline Systems: *Gulf Coast Association of Geological Societies Transactions*, 57, 319-330.

Garrison, R.E., Luternauer, J.L., Grill, E.V., Macdonald, R.D. and Murray, J.W. (1969) Early Diagenetic Cementation of Recent Sands, Fraser River Delta, British Columbia. *Sedimentology*, 12, 27–46.

Ge, Y., Lokier, S.W., Hoffmann, R., Pederson, C.L., Neuser, R.D. and Immenhauser, A. (2020a) Composite micrite envelopes in the lagoon of Abu Dhabi and their application for the recognition of ancient firm- to hardgrounds. *Marine Geology*, 423, 106141.

Ge, Y., Pederson, C.L., Lokier, S.W., Strauss, H. and Immenhauser, A. (2023) Radiaxial fibrous calcite forms via early marine-diagenetic alteration of micritic magnesium calcite. *Sedimentology*, 70, 434–450.

Ge, Y., Pederson, C.L., Lokier, S.W., Traas, J.P., Nehrke, G., Neuser, R.D., Goetschl, K.E., and Immenhauser, A. (2020b) Late Holocene to Recent aragonite-cemented transgressive lag deposits in the Abu Dhabi lagoon and intertidal sabkha: *Sedimentology*, 67, 2426–2454.

Gerbersdorf, S.U. and Wieprecht, S. (2015) Biostabilization of cohesive sediments: revisiting the role of abiotic conditions, physiology and diversity of microbes, polymeric secretion, and biofilm architecture. *Geobiology*, 13, 68–97.

Geske, A., Lokier, S., Dietzel, M., Richter, D.K., Buhl, D. and Immenhauser, A. (2015) Magnesium isotope composition of sabkha porewater and related (Sub-)Recent stoichiometric dolomites, Abu Dhabi (UAE). *Chemical Geology*, 393–394, 112–124.

Gingras, M.K., and MacEachern, J.A. (2012) Tidal Ichnology of Shallow-Water Clastic Settings, *Principles of Tidal Sedimentology: Springer Netherlands, Dordrecht*, 57–77.

Gingras, M.K., and Zonneveld, J.P. (2015) Tubular Tidalites: A Biogenic Sedimentary Structure Indicative of Tidally Influenced Sedimentation: *Journal of Sedimentary Research*, 85, 845–854.

Gingras, M.K., Baniak, Greg., Gordon, John., Hovikoski, Jussi., Konhauser, K.O., La Croix, Andrew., Lemiski, Ryan., Mendoza, Carl., Pemberton, S.G., Polo, Camilo. and Zonneveld, J.-Paul. (2012) Chapter 27 - Porosity and Permeability in Bioturbated Sediments. *Developments in Sedimentology*, 64, 837–868.

Gingras, M.K., MacEachern, J.A., and Dashtgard, S.E. (2011) Process ichnology and the elucidation of physico-chemical stress: *Sedimentary Geology*, 237, 115–134.

Gingras, M.K., Pemberton, S.G., and Saunders, T. (2000) Firmness Profiles Associated with Tidal-Creek Deposits: The Temporal Significance of Glossifungites Assemblages: *Journal of Sedimentary Research*, 70, 1017–1025.

Gingras, M.K., Pemberton, S.G., Muelenbachs, K. and Machel, H. (2004) Conceptual models for burrow-related, selective dolomitization with textural and isotopic evidence from the Tyndall Stone, Canada. *Geobiology*, 2, 21–30.

Gingras, M.K., Pemberton, S.G. and Saunders, T. (2001) Bathymetry, sediment texture, and substrate cohesiveness; their impact on modern Glossifungites trace assemblages at Willapa Bay, Washington. *Palaeogeography, Palaeoclimatology, Palaeoecology*, *169*, 1-21.

Gingras, M.K., Pemberton, S.G., Saunders, T., and Clifton, H.E. (1999) The Ichnology of Modern and Pleistocene Brackish-Water Deposits at Willapa Bay, Washington: Variability in Estuarine Settings: *PALAIOS*, 14, 352.

Goldring, R. (1995) Organisms and the substrate: response and effect: *Geological Society, London, Special Publications*, 83, 151–180.

Grizzle, R.E., Bricelj, V.M., AlShihi, R.M., Ward, K.M., and Anderson, D.M. (2018) Marine Molluscs in Nearshore Habitats of the United Arab Emirates: Decadal Changes and Species of Public Health Significance: *Journal of Coastal Research*, 345, 1157–1175.

Halbertsma, H.L., Mossop, G.D. and Shetsen, I. (1994) Devonian Wabamun Group of the western Canada sedimentary basin. *Geological Atlas of the Western Canada Sedimentary Basin*, 4, 203-220.

Hamza, W., Al Hameli, S., Ramadan, G., and Hameli, M.A. (2018) Coastal Alterations and Its Impact on Diversity of Macrobenthic Fauna in the Intertidal Zone of Abu Dhabi Western Coast (UAE): *Journal of Marine Biology & Oceanography*, 7, 2-11.

Hauck, T.E., Dashtgard, S.E., Pemberton, S.G., and Gingras, M.K. (2009) Brackish-Water Ichnological Trends in a Microtidal Barrier Island Embayment System, Kouchibouguac National Park, New Brunswick, Canada: *PALAIOS*, 24, 478–496.

Hazzouri, K.M., Sudalaimuthuasari, N., Saeed, E.E., Kundu, B., Al-Maskari, R.S., Nelson, D., AlShehhi, A.A., Aldhuhoori, M.A., Almutawa, D.S., Alshehhi, F.R., Balan, J., Mundra, S., Alam, M., Salehi-Ashtiani, K., et al. (2022) Salt flat microbial diversity and dynamics across salinity gradient: *Scientific Reports*, 12, 11293.

Hiatt, E. and Pufahl, P. (2014) Cathodoluminescence petrography of carbonate rocks: application to understanding diagenesis, reservoir quality, and pore system evolution. 45, 75–96.

Hilton, M.J., and Loke Ming, C. (1999) Sediment Facies of a Low-Energy, Meso-Tidal, Fringing Reef, Singapore: *Singapore Journal of Tropical Geography*, 20, 111–130.

Hippler, D., Buhl, D., Witbaard, R., Richter, D.K. and Immenhauser, A. (2009) Towards a better understanding of magnesium-isotope ratios from marine skeletal carbonates. *Geochimica et Cosmochimica Acta*, 73, 6134–6146.

Hodgson, C.A. (2013) Sedimentology and Neoichnology of a Wave-Dominated, Tidally-Influenced, Fully Marine Bay, Oregon, USA, unpublished M.S. thesis, University of Alberta, Edmonton, 312

Hope, J.A., Paterson, D.M. and Thrush, S.F. (2020) The role of microphytobenthos in soft-sediment ecological networks and their contribution to the delivery of multiple ecosystem services. *Journal of Ecology*, 108, 815–830.

Hubas, C., Passarelli, C. and Paterson, D.M. (2018) Microphytobenthic Biofilms: Composition and Interactions: *Mudflat Ecology*, 7, 63–90.

John, D., and George, J. (2004) Intertidal and subtidal benthic communities in Abu Dhabi: *Marine Atlas of Abu Dhabi*, 94–123.

Katz, A., Sass, E., Starinsky, A. and Holland, H.D. (1972) Strontium behavior in the aragonite-calcite transformation: An experimental study at 40–98°C. *Geochimica et Cosmochimica Acta*, 36, 481–496.

Kendall, C. and Skipwith, P. (1968) Recent Algal Mats of a Persian Gulf Lagoon: *Journal of Sedimentary Research*, 38, 1040-1058.

Kendall, C., and Alsharhan, A. (2010) Quaternary carbonate and evaporite sedimentary facies and their ancient analogues: *A Tribute to Douglas James Shearman: John Wiley & Sons, Hoboken, NJ*, 496.

Kendall, C.S.C., Alsharhan, A. S., Cohen, A. (2002) The Holocene tidal flat complex of the Arabian Gulf coast of Abu Dhabi: *Sabkha Ecosystems*: *The Arabian Peninsula and Adjacent Countries*, 1, 21.

Kennedy, W.J. and Garrison, R.E. (1975) Morphology and genesis of nodular chalks and hardgrounds in the Upper Cretaceous of southern England. *Sedimentology*, 22, 311–386.

Kidwell, S.M. (1989) Stratigraphic Condensation of Marine Transgressive Records: Origin of Major Shell Deposits in the Miocene of Maryland. *The Journal of Geology*, 97, 1–24.

Kidwell, S.M., Fursich, F.T., and Aigner, T. (1986) Conceptual Framework for the Analysis and Classification of Fossil Concentrations: *PALAIOS*, 1, 228.

Kinsman, D.J.J. (1969) Modes of Formation, Sedimentary Associations, and Diagnostic Features of Shallow-Water and Supratidal Evaporites. *AAPG Bulletin*, 53, 830–840.

Kirkham, A., (1998) A Quaternary proximal foreland ramp and its continental fringe, Arabian Gulf, UAE: *Geological Society, London, Special Publications*, 149, 15–41.

Knaust, D. (2007) Meiobenthic Trace Fossils as Keys to the Taphonomic History of Shallow-Marine Epicontinental Carbonates. *Trace Fossils*, *Elsevier*, Amsterdam, 502–517.

Knaust, D., and Costamagna, L.G. (2012) Ichnology and sedimentology of the Triassic carbonates of North-west Sardinia, Italy: *Sedimentology*, 59, 1190–1207.

Kopcznski, K., Buynevich, I., Curran, H.A., Caris, J., and Nyquist, J. (2017) Imaging Bioturbation in Supratidal Carbonates: Non-Invasive Field Techniques Enhance Neoichnological and Zoogeomorphological Research, San Salvador, The Bahamas: Bollettino della Società *Paleontologica Italiana*, 56, 289–297.

Kristensen, E., and Kostka, J.E. (2005) Macrofaunal Burrows and Irrigation in Marine Sediment: Microbiological and Biogeochemical Interactions, in Interactions Between Macro- and Microorganisms in Marine Sediments: *American Geophysical Union*, 60, 125–157.

Kulkarni, K.G., and Panchang, R. (2015) New Insights into Polychaete Traces and Fecal Pellets: Another Complex Ichnotaxon? *PLOS ONE*, 10, e0139933.

Kumar, A. (2017) Recent biogenic traces from the coastal environments of the southern Red Sea coast of Saudi Arabia. *Arab J Geosci*, 10, 1-11.

LaGrange, M.T., Konhauser, K.O., Catuneanu, O., Harris, B.S., Playter, T.L. and Gingras, M.K. (2020) Sequence stratigraphy in organic-rich marine mudstone successions using chemostratigraphic datasets. *Earth-Science Reviews*, 203, 103137.

Lambeck, K. (1996) Shoreline reconstructions for the Persian Gulf since the last glacial maximum: *Earth and Planetary Science Letters*, 142, 43–57.

Lambiase, J.J., Damit, A.R., Simmons, M.D., Abdoerrias, R., and Hussin, A. (2003) A Depositional Model and the Stratigraphic Development of Modern and Ancient Tide-Dominated Deltas in NW Borneo: *Sedimentology, Stratigraphy, and Petroleum Geology, Special Publication–Society for Sedimentary Geology*, 76, 109–123.

Land, L.S., and Hoops, G.K. (1973) Sodium in carbonate sediments and rocks; a possible index to the salinity of diagenetic solutions. *Journal of Sedimentary Research*, 43, 614-617.

Liu, Y., Jiao, J.J. and Luo, X. (2016) Effects of inland water level oscillation on groundwater dynamics and land-sourced solute transport in a coastal aquifer. *Coastal Engineering*, 114, 347–360.

Lokier, S. and Steuber, T. (2009) Large-scale intertidal polygonal features of the Abu Dhabi coastline. *Sedimentology*, 56, 609–621.

Lokier, S.W., Bateman, M.D., Larkin, N.R., Rye, P. and Stewart, J.R. (2015) Late Quaternary sea-level changes of the Persian Gulf. *Quaternary Research*, 84, 69–81.

Lokier, S.W., Knaf, A. and Kimiagar, S. (2013) A quantitative analysis of Recent arid coastal sedimentary facies from the Arabian Gulf Coastline of Abu Dhabi, United Arab Emirates. *Marine Geology*, 346, 141–152.

Lucrezi, S. (2010) Ghost crabs as ecological indicators of human stressors on sandy beaches: Ph.D dissertation, University of the Sunshine Coast, Queensland, 360.

Lundkvist, M., Grue, M., Friend, P.L. and Flindt, M.R. (2007) The relative contributions of physical and microbiological factors to cohesive sediment stability. *Continental Shelf Research*, 27, 1143–1152.

Lyster, I.H.J. (1965) The Salinity Tolerance of Polychaete Larvae: *Journal of Animal Ecology*, 34, 517–527.

MacEachern, J.A., and Burton, J.A. (2000) Firmground Zoophycos in the Lower Cretaceous Viking Formation, Alberta: A Distal Expression of the Glossifungites Ichnofacies: *PALAIOS*, 15, 387–398.

MacEachern, J.A., Bann, K.L., Gingras, M.K., Zonneveld, J.-Paul., Dashtgard, S.E., and Pemberton, S.G. (2012) The Ichnofacies Paradigm, Developments in Sedimentology: *Trace Fossils as Indicators of Sedimentary Environments, Elsevier*, 103–138.

MacEachern, J.A., Bann, K.L., Pemberton, S.G., and Gingras, M.K. (2007a) The Ichnofacies Paradigm: High-Resolution Paleoenvironmental Interpretation of the Rock Record, Applied Ichnology: *SEPM Society for Sedimentary Geology*, 0

MacEachern, J.A., Gingras, M.K., Bann, K., Dafoe, L.T., and Pemberton, S.G. (2007b) Applications of Ichnology to High-Resolution Genetic Stratigraphic Paradigms, Applied Ichnology: *SEPM Society for Sedimentary Geology*, 0

Machel, H.G. (2001) Bacterial and thermochemical sulfate reduction in diagenetic settings — old and new insights. *Sedimentary Geology*, 140, 143–175.

Mandal, A., Dutta, A., Das, R. and Mukherjee, J. (2021) Role of intertidal microbial communities in carbon dioxide sequestration and pollutant removal: A review. *Marine Pollution Bulletin*, 170, 112626.

Mángano, M.G., and Buatois, L.A. (2004a) Ichnology of Carboniferous tide-influenced environments and tidal flat variability in the North American Midcontinent: *Geological Society, London, Special Publications*, 228, 157–178.

Mángano, M.G., and Buatois, L.A. (2004b) Reconstructing Early Phanerozoic intertidal ecosystems: ichnology of the Cambrian Campanario Formation in northwest Argentina, Trace Fossils in Evolutionary Palaeoecology: *Fossils and Strata*, Taylor & Francis, 17–38.

Melim, L.A. and Scholle, P.A. (2002) Dolomitization of the Capitan Formation forereef facies (Permian, west Texas and New Mexico): seepage reflux revisited. *Sedimentology*, 49, 1207–1227.

Meysman, F.J.R., Galaktionov, O.S., Gribsholt, B. and Middelburg, J.J. (2006) Bioirrigation in permeable sediments: Advective pore-water transport induced by burrow ventilation. *Limnology and Oceanography*, 51, 142–156.

Milliman, J.D. (1993) Production and accumulation of calcium carbonate in the ocean: Budget of a nonsteady state. *Global Biogeochemical Cycles*, 7, 927–957.

Moore, C.H. (ed) (2001) Chapter 6 - Evaporative Marine Diagenetic Environments. *Developments in Sedimentology*, *Elsevier*, 55, 145–183.

Morse, J.W., Arvidson, R.S. and Lüttge, A. (2007) Calcium Carbonate Formation and Dissolution. *Chem. Rev.*, 107, 342–381.

Morse, J.W., Wang, Q. and Tsio, M.Y. (1997) Influences of temperature and Mg:Ca ratio on CaCO3 precipitates from seawater. *Geology*, 25, 85–87.

Nombela, M.A., Vilas, F., and Evans, G. (1995) Sedimentation in the Mesotidal Rías Bajas of Galicia (North-Western Spain): *Ensenada De San Simón, Inner Ría De Vigo, Tidal Signatures in Modern and Ancient Sediments: John Wiley & Sons, Ltd*, 133–149.

Paterson, D.M. (1994) Microbiological mediation of sediment structure and behaviour. *Microbial Mats*, *Springer*, Berlin, Heidelberg, 35, 97–109.

Paterson, D.M., Hope, J.A., Kenworthy, J., Biles, C.L., and Gerbersdorf, S.U. (2018) Form, function and physics: the ecology of biogenic stabilisation: *Journal of Soils and Sediments*, 18, 3044–3054.

Paul, A. and Lokier, S.W. (2017) Holocene marine hardground formation in the Arabian Gulf: Shoreline stabilisation, sea level and early diagenesis in the coastal sabkha of Abu Dhabi. *Sedimentary Geology*, 352, 1–13.

Pederson, C.L., Ge, Y., Lokier, S.W., Swart, P.K., Vonhof, H., Strauss, H., Schurr, S., Fiorini, F., Riechelmann, S., Licha, T. and Immenhauser, A. (2021) Seawater chemistry of a modern subtropical ‘epeiric’ sea: Spatial variability and effects of organic decomposition. *Geochimica et Cosmochimica Acta*, 314, 159–177.

Pemberton, S.G., and Maceachern, J.A. (2005) Significance of Ichnofossils to Applied Stratigraphy, in Koutsoukos, E.A.M., Applied Stratigraphy: *Topics in Geobiology, Springer, Netherlands*, 279–300.

Pemberton, S.G., and Wightman (1992) Applications of ichnology to petroleum exploration—A core workshop: *Society of Economic Paleontologists and Mineralogists, Core Workshop*, 17, 141–67.

Pemberton, S.G., MacEachern, J.A., Dashtgard, S.E., Bann, K.L., Gingras, M.K., and Zonneveld, J.P. (2012) Shorefaces, Developments in Sedimentology: *Trace Fossils as Indicators of Sedimentary Environments, Elsevier*, 563–603.

Pfeifer, K., Kasten, S., Hensen, C. and Schulz, H.D. (2001) Reconstruction of primary productivity from the barium contents in surface sediments of the South Atlantic Ocean. *Marine Geology*, 177, 13–24.

Rasmussen, B., Krapež, B. and Muhling, J.R. (2015) Seafloor silicification and hardground development during deposition of 2.5 Ga banded iron formations. *Geology*, 43, 235–238.

Reineck, H., and IB, S. (1980) Depositional Sedimentary Environments with Reference to Terrigenous Clastics, 2, 430–456.

Richter, R. (1936) Marken und Spruren im Hunsriick-Schiefer. II: *Schichtung und Grund-Leben. Senckenbergiana*, 18, 215-244.

Rodríguez-Tovar, F.J., Seike, K., and Allen Curran, H. (2014) Characteristics, Distribution Patterns, and Implications for Ichnology of Modern Burrows of Uca (Leptuca) Speciosa, San Salvador Island, Bahamas: *Journal of Crustacean Biology*, 34, 565–572.

Rollet, N., Logan, G.A., Kennard, J.M., O'Brien, P.E., Jones, A.T., and Sexton, M. (2006) Characterisation and correlation of active hydrocarbon seepage using geophysical data sets: An example from the tropical, carbonate Yampi Shelf, Northwest Australia: *Marine and Petroleum Geology*, 23, 145–164.

Sadooni, F.N., Howari, F. and El-Saiy, A. (2010) Microbial Dolomites from Carbonate-Evaporite Sediments of the Coastal Sabkha of Abu Dhabi and Their Exploration Implications. *Journal of Petroleum Geology*, 33, 289–298.

Saller, A.H. (1986) Radiaxial calcite in lower Miocene strata, subsurface Enewetak Atoll. *Journal of Sedimentary Research*, 56, 743–762.

Saller, A.H. and Henderson, N. (1998) Distribution of Porosity and Permeability in Platform Dolomites: Insight from the Permian of West Texas1. *AAPG Bulletin*, 82, 1528–1550.

Sanders, H. L., Mangelsdorf Jr, P. C., & Hampson, G. R., (1965) Salinity and faunal distribution in the Pocasset River, Massachusetts: *Limnology and Oceanography*, 10, 216-229.

Sarg, J.F. (1988) Carbonate sequence stratigraphy. Sea-level Changes: An Integral Approach. Wilgus, B.S.H.C.K., Kendall, C.G.S.C., Posamentier, H.W., Ross, C.A., van Wagoner, J.C. (Eds.), SEPM Special Publication 42, 155–181.

Savrda, C.E. (1991) Ichnology in Sequence Stratigraphic Studies: An Example from the Lower Paleocene of Alabama: *PALAIOS*, 6, 39–53.

Scannell P.W.,, Jacobs, L.L. (2001) Effects of total dissolved solids on aquatic organisms*: Alaska Department of Fish and Game: Division of habitat and restoration*, 01-06

Schlanger, S.O. (1988) Strontium Storage and Release During Deposition and Diagenesis of Marine Carbonates Related to Sea-Level Variations. *Physical and Chemical Weathering in Geochemical Cycles*, *Springer Netherlands*, Dordrecht, 251, 323–339.

Schroeder, J.H. (1969) Experimental Dissolution of Calcium, Magnesium, and Strontium from Recent Biogenic Carbonates: A Model of Diagenesis, 39, 1057-1073

Serk, H. (2008) Community Structures of Microbial Mats in the Sabkha Environment of Abu Dhabi, UAE: unpublished Ph.D dissertation, Newcastle University, Newcastle, 82

Shearman, D.J. (1963) Recent anhydrite, gypsum, dolomite and halite from the coastal flats of the Arabian shore of the Persian Gulf: *Proc. Geol. Soc. London*, 1607(63), 5.

Shearman, D.J. (1980) Sabkha facies evaporites: *Evaporite Deposits.-Editions Technip*, 19, 96-109.

Shearman, D.J.(1978) Evaporites of Coastal Sabkhas: *Evaporites of Coastal Sabkhas*

Shinn, E.A. (1969) Submarine Lithification of Holocene Carbonate Sediments in the Persian Gulf. *Sedimentology*, 12, 109–144.

Shull, D.H. (2001) Transition-matrix model of bioturbation and radionuclide diagenesis. *Limnology and Oceanography*, 46, 905–916.

Smith, C.R., A. Levin, L., Hoover, D.J., McMurtry, G., and Gage, J.D. (2000) Variations in bioturbation across the oxygen minimum zone in the northwest Arabian Sea: Deep Sea Research Part II: *Topical Studies in Oceanography*, 47, 227–257

Smythe, K. R. (1979) The marine Mollusca of the United Arab Emirates, Arabian Gulf*: Journal of Conchology*, 30, 57.

Søndergaard, M. (2009) Redox Potential. *Encyclopedia of Inland Waters*, *Academic Press*, Oxford, 852–859.

Stehli, F.G. and Hower, J. (1961) Mineralogy and early diagenesis of carbonate sediments. *Journal of Sedimentary Research*, 31, 358–371.

Steiner, Z., Lazar, B., Torfstein, A. and Erez, J. (2017) Testing the utility of geochemical proxies for paleoproductivity in oxic sedimentary marine settings of the Gulf of Aqaba, Red Sea. *Chemical Geology*, 473, 40–49.

Strohmenger, C.J., Al-Mansoori, A., Al-Jeelani, O., Al-Shamry, A., Al-Hosani, I., Al-Mehsin, K. and Shebl, H. (2010) The sabkha sequence at Mussafah Channel (Abu Dhabi, United Arab Emirates): Facies stacking patterns, microbial-mediated dolomite and evaporite overprint. *GeoArabia*, 15, 49–90.

Sumner, D.Y. and Grotzinger, J.P. (2004) Implications for Neoarchaean ocean chemistry from primary carbonate mineralogy of the Campbellrand-Malmani Platform, South Africa. *Sedimentology*, 51, 1273–1299.

Sunagawa, I., Takahashi, Y. and Imai, H. (2007) Strontium and aragonite-calcite precipitation. *Journal of Mineralogical and Petrological Sciences*, 102, 174–181.

Swart, P.K. (1981) The strontium, magnesium and sodium composition of recent scleractinian coral skeletons as standards for palaeoenvironmental analysis. *Palaeogeography, Palaeoclimatology, Palaeoecology*, 34, 115–136.

Swart, P.K. (2015) The geochemistry of carbonate diagenesis: The past, present and future. *Sedimentology*, 62, 1233–1304.

Taylor, P.D. and Wilson, M.A. (2003) Palaeoecology and evolution of marine hard substrate communities. *Earth-Science Reviews*, 62, 1–103.

Tedesco, L.P., and Wanless, H.R. (1991) Generation of Sedimentary Fabrics and Facies by Repetitive Excavation and Storm Infilling of Burrow Networks, Holocene of South Florida and Caicos Platform, B.W.I.: *PALAIOS*, 6, 326–343

Tribovillard, N., Algeo, T.J., Lyons, T. and Riboulleau, A. (2006) Trace metals as paleoredox and paleoproductivity proxies: An update. *Chemical Geology*, 232, 12–32.

Vallack, H.L. (2021) Physical and biogeochemical drivers of Modern carbonate diagenesis in intertidal sediments of Abu Dhabi: Ph.D. dissertation, University of Bristol, Bristol, 309

Vasconcelos, C. and McKenzie, J.A. (1997) Microbial mediation of modern dolomite precipitation and diagenesis under anoxic conditions (Lagoa Vermelha, Rio de Janeiro, Brazil). *Journal of Sedimentary Research*, 67, 378–390.

Vasconcelos, C., McKenzie, J.A., Bernasconi, S., Grujic, D. and Tiens, A.J. (1995) Microbial mediation as a possible mechanism for natural dolomite formation at low temperatures. *Nature*, 377, 220–222.

Wanty, R.B. and Goldhaber, M.B. (1992) Thermodynamics and kinetics of reactions involving vanadium in natural systems: Accumulation of vanadium in sedimentary rocks. *Geochimica et Cosmochimica Acta*, 56, 1471–1483.

Warren, J. (2000) Dolomite: occurrence, evolution and economically important associations. *Earth-Science Reviews*, 52, 1–81.

Wong, H.L., Smith, D.-L., Visscher, P.T. and Burns, B.P. (2015) Niche differentiation of bacterial communities at a millimeter scale in Shark Bay microbial mats. *Sci Rep*, 5, 15607.

Wood, W.W., Sanford, W.E. and Habshi, A.R.S.A. (2002) Source of solutes to the coastal sabkha of Abu Dhabi. *GSA Bulletin*, 114, 259–268.

Yallop, M.L., Paterson, D.M. and Wellsbury, P. (2000) Interrelationships between Rates of Microbial Production, Exopolymer Production, Microbial Biomass, and Sediment Stability in Biofilms of Intertidal Sediments. *Microb Ecol*, 39, 116–127.

Yang, B.C., and Chang, T.S. (2018) Integrated sedimentological and ichnological characteristics of a wave-dominated, macrotidal coast: a case study from the intertidal shoreface of the Dongho coast, southwest Korea: *Geo-Marine Letters*, 38, 139–151.

Zonneveld, J.P., Gingras, M.K., Hodgson, C.A., McHugh, L.P., Myers, R.A., Schoengut, J.A., and Wetthuhn, B. (2014) Biotic Segregation in an Upper Mesotidal Dissipative Ridge and Runnel Succession, West Salish Sea, Vancouver Island, British Columbia, Experimental Approaches to Understanding Fossil Organisms: *Lessons from the Living: Topics in Geobiology, Springer Netherlands, Dordrecht*, 169–194.

Zonneveld, J.P., Zaim, Y., Rizal, Y., Ciochon, R.L., Bettis, E.A., Aswan, and Gunnell, G.F. (2012) Ichnological constraints on the depositional environment of the Sawahlunto Formation, Kandi, northwest Ombilin Basin, west Sumatra, Indonesia: *Journal of Asian Earth Sciences*, 45, 106–113.

Zorn, M.E., Gingras, M.K. and Pemberton, S.G. (2010) Variation in burrow-wall micromorphologies of select intertidal invertebrates along the pacific northwest coast, usa: behavioral and diagenetic implications. *PALAIOS*, 25, 59–72.